

A Survey of Representation Learning, Optimization Strategies, and Applications for Omnidirectional Vision

Hao Ai¹ · Zidong Cao¹ · Lin Wang^{1,2}, ✉

the date of receipt and acceptance should be inserted later

Abstract Omnidirectional image (ODI) data is captured with a field-of-view of $360^\circ \times 180^\circ$, which is much wider than the pinhole cameras and captures richer surrounding environment details than the conventional perspective images. In recent years, the availability of customer-level 360° cameras has made omnidirectional vision more popular, and the advance of deep learning (DL) has significantly sparked its research and applications. This paper presents a systematic and comprehensive review and analysis of the recent progress of DL for omnidirectional vision. It delineates the distinct challenges and complexities encountered in applying DL to omnidirectional images as opposed to traditional perspective imagery. Our work covers four main contents: (i) A thorough introduction to the principles of omnidirectional imaging and commonly explored projections of ODI; (ii) A methodical review of varied representation learning approaches tailored for ODI; (iii) An in-depth investigation of optimization strategies specific to omnidirectional vision; (iv) A structural and hierarchical taxonomy of the DL methods for the representative omnidirectional vision tasks, from visual enhancement (*e.g.*, image generation and super-resolution) to 3D geometry and motion estimation (*e.g.*, depth and optical flow estimation), alongside the discussions on emergent research directions; (v) An overview of cutting-edge applications (*e.g.*, autonomous driving and virtual reality), coupled with a critical discussion on prevailing challenges and open questions, to trigger more research in the community.

Keywords Omnidirectional vision · Deep neural networks · Survey · Representation learning · Optimization strategies · Applications

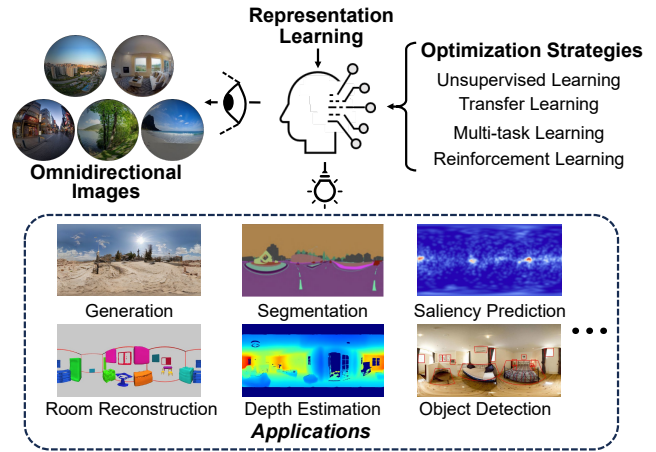


Fig. 1: Overview of representation learning, optimization strategies, and applications for omnidirectional vision.

1 Introduction

With the rapid development of 3D technology and the pursuit of realistic visual experience, research interest in computer vision has gradually shifted from traditional 2D perspective images to omnidirectional images (ODIs) [175], also known as the 360° images, panoramas¹, or spherical images. ODIs captured by the 360° cameras yield a $360^\circ \times 180^\circ$ field-of-view (FoV), which is much wider than the pinhole cameras (maximum $180^\circ \times 180^\circ$) and fisheye cameras [163] (about $220^\circ \times 180^\circ$); therefore, it can capture the entire surrounding environment by reflecting richer spatial information than the conventional perspective images and fisheye images. Due to the complete view and immersive viewing experience, ODIs have been widely applied to numerous applications, *e.g.*, augmented reality (AR)/virtual

¹ In this survey, panorama specifically refers to the equirectangular projection (ERP) format ODI.

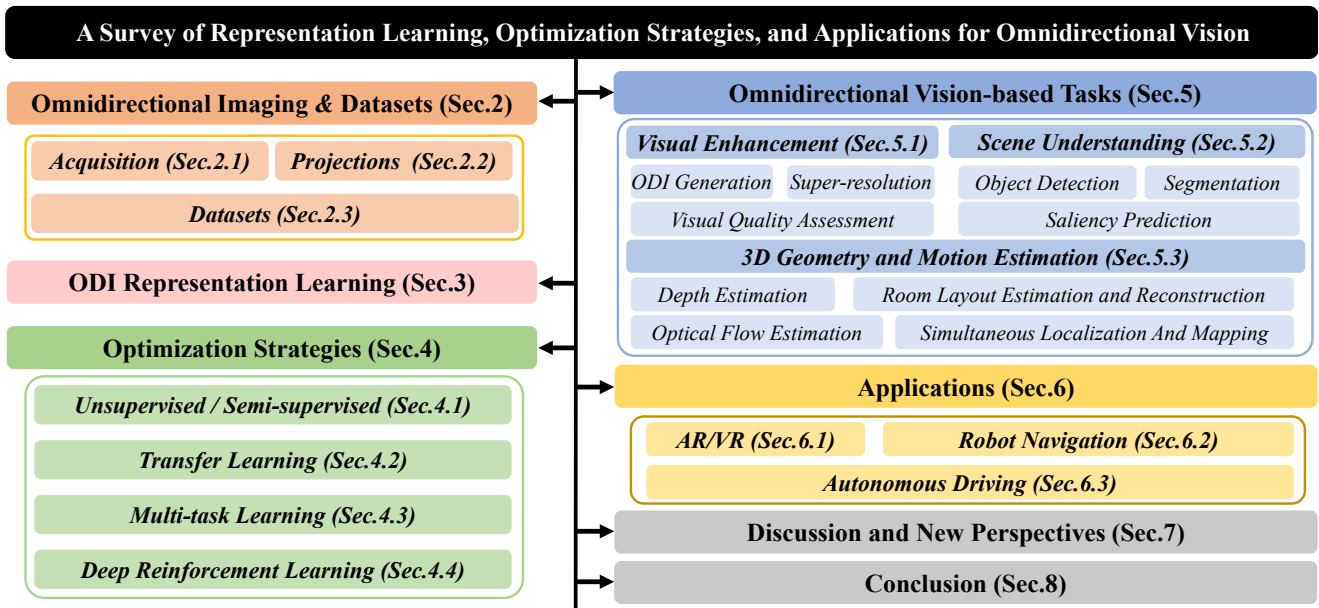


Fig. 2: Hierarchical and structural taxonomy of omnidirectional vision with deep learning.



Fig. 3: Examples of 360° cameras: (a) RICOH Theta Z1, and (b) GoPro Omni.

reality (VR), autonomous driving, and robot navigation. As raw ODIs are captured on the sphere (Fig. 1 Left), the two-dimensional (2D) projection formats of ODIs are required for coding, compression, transmitting, and analysis. Common 2D projection formats include Equirectangular projection (ERP), Cubemap projection (CP), and so on [38], [234]. As a novel data domain, ODIs have both domain-unique advantages (ultra-wide FoV of spherical imaging, comprehensive structural information of surrounding environments, multiple projection formats with distinctive advantages) and challenges (the demand for large receptive fields, robust rotation equivariance for spherical rotation, undeniable flaws in each projection format). These render the research on omnidirectional vision valuable yet challenging.

Recently, popular customer-level 360° cameras (See Fig. 3) have made omnidirectional vision more attractive, and the advance of deep learning (DL) has significantly promoted its research and applications, (See Fig. 1). In particular, the continual release of public datasets, *e.g.*, Stanford2D3D [8], Matterport3D [25] and PanoContext [312], have rapidly enabled the data-driven DL methods to accomplish remarkable breakthroughs and

often achieve the state-of-the-art (SoTA) performances on various vision tasks. Moreover, various deep neural network (DNN) models have been developed based on diverse architectures, ranging from convolutional neural networks (CNNs) [84], recurrent neural networks (RNNs) [161], to vision transformers (ViTs) [61]. In general, SoTA DL methods for ODI focus on three major aspects: **(i)** learning effective representations from diverse projections, **(ii)** novel learning strategies to utilize powerful knowledge of perspective images, **(iii)** customizing task-specific network architectures.

In the past decade, several survey papers and reviews have been published in the omnidirectional vision community, including works by [346], [48], [290], [108], [340], [261], [285], [74]. Zink *et al.* [340] and Yaqoob *et al.* [285] have focused on techniques for 360° video streaming systems, particularly on transmission and compression. Similarly, Xu *et al.* [261] concentrated on the transmission, compression, and quality assessment of ODIs and omnidirectional videos (ODVs). Specializing on room layout estimation based on indoor ODIs, Zou *et al.* [346] reviewed and evaluated previous methods on numerous benchmark datasets, analyzing the design differences among various approaches. Subsequently, Gao *et al.* [74] introduced the details of omnidirectional imaging systems and related optical technologies. With an emphasis on robotic applications, Gao *et al.* introduced and summarized various scene understanding tasks based on ODIs, such as depth estimation, semantic segmentation, and simultaneous localization and mapping (SLAM). By contrast, Recent surveys [346, 48, 290, 108] collect and analyse approaches designed for 3D vision tasks, covering fields such as

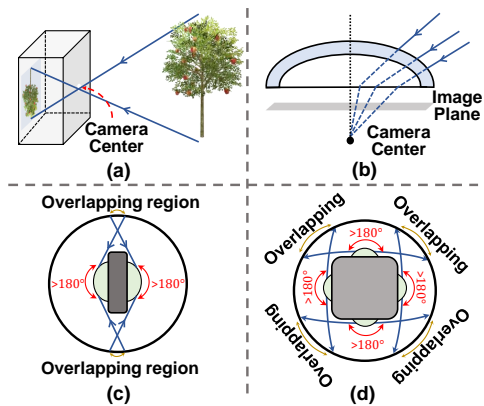


Fig. 4: Imaging principles of several cameras: (a) Pinhole camera; (b) Fisheye camera; (c) 360° camera (dual-fisheye); (d) 360° camera (multi-fisheye).

stereo matching, 3D reconstruction, and so on. Despite the extensive focus on how DL-based methods can effectively process ODIs or ODVs, there is a relative lack of exploration into the broader impact of DL’s development on omnidirectional vision.

It can be observed that existing surveys mainly focus on specific domains. However, with the advent of deep learning, its impact on the entire omnidirectional vision community has been substantial. Systematically synthesizing, analyzing, and summarizing deep learning methods across a wide range of vision tasks is highly valuable. Therefore, compared to previous surveys, we provide a more thorough review, investigating how to collect and process ODIs for deep learning (Sec. 2), how to learn representations (Sec. 3) from ODIs, and how to optimize the models (Sec. 4) for omnidirectional vision. Furthermore, while we review DL methods for appealing vision tasks in Sec. 5, we go beyond simply compiling and summarizing algorithms; we critically analyze their foundations to categorize them and scrutinize the differences between methods tailored for ODIs versus those for perspective images. Fig. 2 shows the structural and hierarchical taxonomy of this study.

In summary, the major contributions of this study can be summarized as follows: **(I)** To the best of our knowledge, this is the **first** survey to comprehensively review and analyze the development of DL techniques for omnidirectional vision, including the omnidirectional imaging principle, diverse projection formats, datasets, representation learning, optimization strategies, a taxonomy, and applications, especially highlighting the differences and difficulties compared with 2D perspective images. **(II)** We summarize, if not all but representative, published top-tier conference/journal works (over 200 papers) in the last five years and conduct an analytical study of recent trends of DL on omnidirectional vision, both hierarchically and structurally. Moreover, we offer

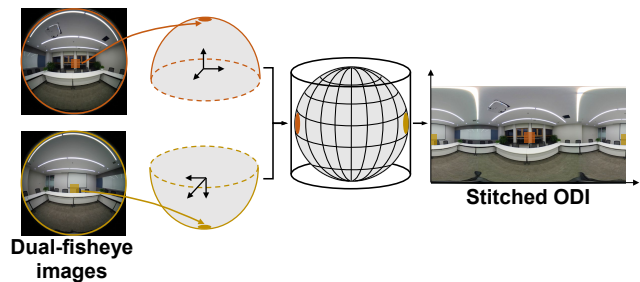


Fig. 5: Illustration of the process for stitching a pair of dual-fisheye images into an ERP format ODI.

insights into the discussions for popular directions. **(III)** We have not only summarized representative methods and their key strategies for some popular omnidirectional vision tasks, *e.g.*, Fig. 16, Fig. 18, Fig. 19, Fig. 22, Fig. 23, Fig. 24, but also presented some representative methods’ quantitative and qualitative results on benchmark datasets for better intra-task comparisons, *e.g.*, Tab. 2, Tab. 3, Tab. 5, Tab. 8, Tab. 7. **(IV)** We provide insightful discussions of the practical applications and challenges yet to be solved and propose the potential of future directions to spur more in-depth research by the community. **(V)** We create an open-source repository that provides a taxonomy of all the mentioned works and code links. We will keep updating our open-source repository with new works in this area and hope it can shed light on future research. The repository link is https://github.com/vlislabs22/360_Survey.

2 Omnidirectional Imaging and Projection

2.1 Acquisition

As shown in Fig. 4(a) and (b), a normal pinhole camera has a FoV less than 180° and thus captures a view at most a hemisphere, while a single fisheye camera usually has a wide FoV but less than 360°, capturing a panoramic hemispherical image. In contrast, an ideal 360° camera can capture lights falling on the focal point from all directions, making the projection plane a whole spherical surface. According to the number of lenses, 360° cameras can be categorized into two types: (i) Cameras with back-to-back dual-fisheye lenses (Fig. 4(c)); (ii) Cameras with more than two lenses (Fig. 4(d)).

The first type of 360° cameras requires a minimal number of lenses, making them cost-effective and user-friendly, which has led to widespread adoption in both industrial and consumer markets, *e.g.*, RICOH Theta² (Fig. 3(a)). However, stitching two back-to-back fisheye images into a seamless omnidirectional image (ODI) presents significant challenges. These challenges arise primarily from (1) the displacement of the optical centers

² <https://www.ricoh360.com/theta>

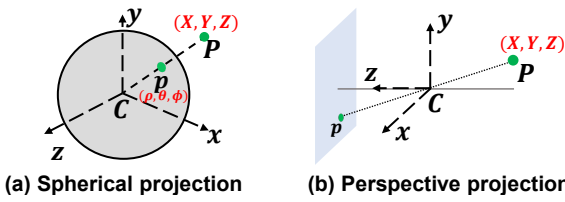


Fig. 6: Spherical projection *v.s.* perspective projection.

of the two fisheye cameras, and (2) limited information and severe distortions in the overlapping regions between the two cameras (Fig. 4(c)). To address these challenges and generate high-quality ODIs, considerable efforts have been dedicated [153], [190], [71], [131], [151], [152]. Typically, the stitching process, as illustrated in Fig. 5, involves three key steps: (1) transforming fisheye images into spherical coordinates, (2) aligning the spherical views within a unified spherical coordinate system, and (3) blending the aligned views while resolving inconsistencies to obtain the final ODI. For the second type, more lenses bring higher precision and less inconsistency for the final stitched results. This type of 360° cameras are professional-level and expensive, *e.g.*, GoPro Omni (six lenses)³ (Fig. 3(b)). In addition, some studies [232], [339] have mounted multiple fisheye cameras on the wings of drones, directly generating high-quality ODIs using the captured fisheye images and corresponding camera parameters. Meanwhile, stitching multiple fisheye images to produce ODIs has also been applied in SLAM systems [101]. In this work, we place greater emphasis on the representation and applications of ODIs. To gain a better understanding of the imaging principles of ODIs, we recommend readers refer to [74], [268].

2.2 Projections of ODI

Spherical Projection. A 360° camera can be modeled as a camera center with a surrounding unit sphere, which projects all visible points in the surroundings onto the sphere surface. Therefore, for a 360° camera, intrinsic parameters such as focal length or distortion values are not required to consider [124], [48], [136]. As shown in Fig. 6(b), given a point $P = [x, y, z]^T$ in space, the spherical projection of P is the intersection p of the sphere surface with the line \overline{CP} joining point P and the sphere center C . To obtain the spherical coordinate of p , we first define that a 360° camera coordinate system is set at the center of a unit sphere with $f = 1$ (radius), and the direction of \overline{CP} is determined by θ (polar angle) and ϕ (azimuth angle). Accordingly, the spherical coordinate of p can be represented as $p = [\sin \theta \cos \phi, \sin \theta \sin \phi, \cos \theta]^T$. Following the relationships between P and p , we can obtain the

spherical projection as follows:

$$\begin{cases} \rho \\ \theta \\ \phi \end{cases} = \begin{cases} (x^2 + y^2 + z^2)^{1/2} \\ \arctan(x/z) \\ \arccos(y/\rho) \end{cases}, \quad \begin{cases} x \\ y \\ z \end{cases} = \begin{cases} \rho \sin(\theta) \sin(\phi) \\ \rho \cos(\phi) \\ \rho \cos(\theta) \sin(\phi) \end{cases}. \quad (1)$$

Equirectangular Projection (ERP). In the industry, there lack the efficient image encoding and storage techniques for the images represented in the spherical space. Therefore, for processing and storing ODIs, the raw spherical data is always projected from the sphere to the 2D plane, as shown in Fig. 7(a). Equirectangular projection (ERP) is the most popular projection format, which uniformly samples grids from the spherical surface. The horizontal unit angle is $\Delta\theta = 2\pi/w$ and the vertical unit angle is $\Delta\varphi = \pi/h$. In particular, if the horizontal and vertical unit angles are equal, the width w is twice of height h . In a word, each pixel coordinate (u, v) in ERP can be mapped to the spherical coordinate $(\theta, \phi) = (u \cdot \Delta\theta, v \cdot \Delta\varphi)$ and vice versa. It is notable that ERP introduces unavoidable shortcomings such as redundant samples and horizontal stretching, which can result in geometric distortions, especially in regions near the two poles [118, 320].

Cubemap Projection (CP). To alleviate the distortion problem in ERP, cubemap projection (CP) is proposed to project the sphere surface to six cube faces with the FoV of $90^\circ \times 90^\circ$. As depicted in Fig. 7(b), each face has the equal-side length w and the distance between the face center and sphere center is $\frac{w}{2}$. The cube faces are denoted as $f_i, i \in \{B, D, F, L, R, U\}$, representing back, down, front, left, right, and up, respectively. By setting the cube center as the origin, the extrinsic matrix of each face can be simplified into 90° or 180° rotation and zero translation matrices [237]. Given a plane pixel f_i , we transform f_i to the front plane (identical to the Cartesian coordinates) and calculate (θ, ϕ) via Eq. 1.

Tangent Projection (TP). To preserve the performance of perspective models on high-resolution spherical data, [64] proposes rendering the omnidirectional image as a set of local planar image grids tangent to the subdivided icosahedron, called tangent projection (TP). Specifically, TP is the gnomonic projection [168], a non-conformal projection from point P_s on the sphere surface with the sphere center O to point P_t in a tangent plane with center P_c ⁴, as shown in Fig. 7(c). For a pixel on the ERP image $P_e(u_e, v_e)$, we first calculate its corresponding point $P_s(\theta = u_e \cdot \vartheta, \phi = v_e \cdot \varphi)$ on the unit sphere, following the transformation in ERP format.

³ <https://gopro.com/en/us/news/omni-is-here>

⁴ <https://mathworld.wolfram.com/GnomonicProjection.html>

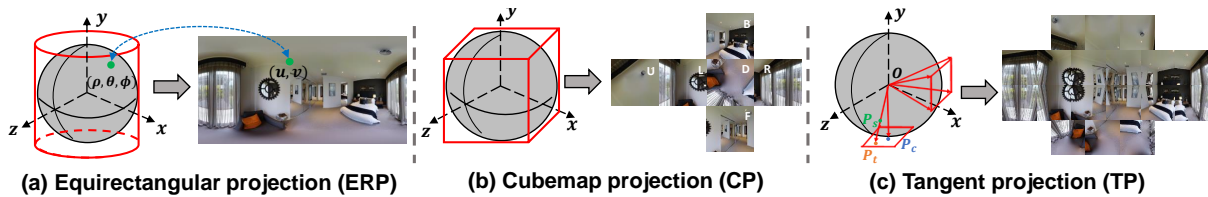


Fig. 7: Illustration of several representative projections: (a) ERP; (b) CP; (c) TP.

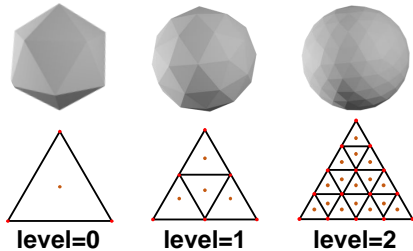


Fig. 8: **Top:** Icosahedron projection; **Bottom:** Subdivision of an icosahedron’s face.

The projection from $P_s(\theta, \phi)$ to $P_t(u_t, v_t)$ is defined as:

$$u_t = \frac{\cos(\phi) \sin(\theta - \theta_c)}{\cos c},$$

$$v_t = \frac{\cos(\phi_c) \sin(\phi) - \sin(\phi_c) \cos(\phi) \cos(\theta - \theta_c)}{\cos(c)}, \quad (2)$$

$$\cos(c) = \sin(\phi_c) \sin(\phi) + \cos(\phi_c) \cos(\phi) \cos(\theta - \theta_c),$$

where (θ_c, ϕ_c) is the spherical coordinate of the tangent plane center P_c , and (u_t, v_t) is the intersection coordinate of the tangent plane and the extension line of $\overrightarrow{OP_s}$. The inverse transformations are formulated as:

$$\theta = \theta_c + \tan^{-1}\left(\frac{u_t \sin(c)}{\gamma \cos(\phi_c) \cos(c) - v_t \sin(\phi_c) \sin(c)}\right), \quad (3)$$

$$\phi = \sin^{-1}\left(\cos(c) \sin(\phi_c) + \frac{1}{\gamma} v_t \sin(c) \cos(\phi_c)\right),$$

where $\gamma = \sqrt{u_t^2 + v_t^2}$ and $c = \tan^{-1} \gamma$. With Eqs. 2 and 3, we can build one-to-one forward and inverse mapping functions between the spherical coordinates and pixels on the tangent patches [140].

Polyhedron Projection. To mitigate the distortions from projecting the spherical images into the planar representations and maintain the continuity of spherical images, polyhedron projection (PP) [129] is proposed to approximate the spherical geometry based on successive divisions of spherical polyhedrons, *e.g.*, octahedron projection, icosahedron projection. Specifically, each face in a spherical polyhedron can be subdivided into four smaller faces to achieve higher resolution and less distortion [129]. Using the icosahedron projection as an example, we can derive 20×4^l faces for an icosahedron mesh at the default subdivision level l (See Fig. 8).

Other projections. Apart from the aforementioned popular projection formats, there are several other formats supported by the 360Lib software package for

coding and processing [234]. They include adjusted equal-area projection (AEP), truncated square pyramid projection (TSP), adjusted cubemap (ACP), rotated sphere projection (RSP), equatorial cylindrical projection (ECP), equiangular cubemap (EAC), and hybrid equiangular cubemap (HEC). Especially, as the map-based projection, AEP adaptively decreases the sampling rate in vertical coordinates and avoids the oversampling problem in ERP. Equi-Angular Cubemap (EAC) projection [38] keeps spatial sampling rates for different sampling locations on the cube faces to alleviate the distortions in CP.

2.3 ODI datasets

As DL is data-driven, the performance of DL-based methods is intricately linked to the qualities and quantities of available data. In other words, ODI and omnidirectional video (ODV) datasets are critical for the development of DL methods on omnidirectional vision. Therefore, we have collected popular datasets for various tasks from the existing literature, listed in Tab. 1. We provide information on the scale and maximum resolution of the datasets. Furthermore, we delineate whether each dataset originates from real-world sources. Notably, synthetic datasets are crafted using computer graphics and rendering technologies. We provide details of several widely used benchmark datasets below.

- SUN360 [253]: A large-scale ODI dataset that contains 80 categories and 67,583 real-world ERP format ODIs. Notably, all ODIs are collected from the Internet⁵. Notably, despite its widespread use, the official download link is presently unavailable online.
- Matterport3D [25]: A large-scale RGB-D ODI dataset comprising 90 building-scale scenes, encompassing 10,800 panoramas, depth maps, and associated annotations for surface reconstructions, camera poses, and 2D and 3D semantic segmentation labels. Notably, each panorama is constructed from 18 RGB-D images captured using a Matterport camera⁶, albeit with a limitation in coverage of the north and south poles. The dataset is split into 61 scenes for training, 11 for validation, and 18 for testing.

⁵ www.360cities.net

⁶ <https://matterport.com/>

Table 1: The summary of ODI image and video datasets. * indicates ‘not available’, ‘Ref.’ indicates ‘Reference image’, and ‘Dist.’ indicates ‘Distorted image’. For the purposes of datasets, **G**: Image Generation, **SR**: Image Super-resolution, **QA**: Image Quality Assessment, **OD**: Object Detection, **SS**: Semantic Segmentation, **DE**: Depth Estimation, **SP**: Saliency Prediction, **RL**: Room Layout Estimation and Reconstruction.

Task	Dataset	Data size	Resolution	Source
G	360SP [26]	15,730	512×256	Real-world
	HDR360-UHD [37]	4,392	8192×4096	Real-world
	Laval Indoor HDR [76]	2,100	2048×1024	Real-world
	Laval Outdoor HDR [87]	205	2048×1024	Real-world
SR	ODI-SR [58]	1,000	2408×1024	Real-world
	Flickr360 [21]	3,150	2408×1024	Real-world
	ODV360 (Video) [21]	250	2160×1080	Real-world
QA	Upenik [233]	6 (Ref.) & 54 (Dist.)	3000×1500	Real-world
	CVIQD [221]	16 (Ref.) & 528 (Dist.)	4096×2048	Real-world
	OIQA [62]	16 (Ref.) & 320 (Dist.)	13320×6660	Real-world
	IQA-ODI [277]	120 (Ref.) & 960 (Dist.)	7680×3840	Real-world
	JUFE-VRIQA [149]	258 (Ref.) & 1032 (Dist.)	8192×4096	Real-world
OD	360-Indoor [42]	3,000	1920×960	Real-world
	ERA [282]	903	3840×1920	Real-world
	OVS [287]	600	2000×1000	Real-world
	PANDORA [257]	3,000	1920×960	Real-world
	VOC360 [318]	21,755	1024×512	Synthetic
	COCO-Men [318]	7,000	1024×512	Synthetic
	FlyingCars [45]	6000	512×256	Synthetic
SS	WildPASS [276]	2,500	2048×400	Real-world
	DensePASS [157]	100	2048×400	Real-world
	SynPASS [305]	9,080	1024×512	Synthetic
	Omni-SYNTHIA [301]	2,269	4192×2096	Synthetic
DE	Deep360 [135]	1,200 (RGB) & 3,000 (Depth)	1024×512	Synthetic
	Depth360 [68]	30,000	1.03Mpx	Synthetic
	Pano3D [6]	29,900	1024×512	Synthetic
	PanoSUNCG [236]	25k	1024×512	Synthetic
	360D [344]	35,977	1024×512	Synthetic
SP	Salient360! [185]	85	18332×9166	Real-world
	AOI [265]	600	8000×4000	Real-world
	Wild-360 (Video) [40]	85	7680×3840	Real-world
	PVS-HM (Video) [262]	76	7680×3840	Real-world
	SVR [208]	22	8192×4096	Synthetic
RL	ZInD [47]	71,474	2048×1024	Synthetic
	Pano3DLayout [178]	107	1024×512	Synthetic
SS, DE	Gibson [252]	572 scenes	–	Synthetic
DE, RL	Shanghaitech-Kujiale Indoor 360 [111]	3,550	1024×512	Synthetic
OD, RL	PanoContext [312]	700	9104×4552	Real-world
G, SR, QA	SUN360* [253]	67,538	9104×4552	Real-world
DE, RL, SS	Matterport3D [25]	10,800	2048×1024	Real-world
G, SR, SS	360+x (Video) [32]	28 scenes	5760×2880	Real-world
OD, DE, RL	Stanford2D3D [8]	1,413	4096×2048	Real-world
SS, DE, RL	Replica [212]	18 scenes	–	Synthetic
OD, SS, DE, G, RL	Structured3D [322]	196,515	1024×512	Synthetic

- Stanford2D3D [8]: A RGB-D dataset consisting of 1,413 RGB panoramas from six real-world areas. Besides, the panoramas are coupled with corresponding depth maps, surface normal information, and semantic annotations. Each panorama is also stitched by 18 perspective images using the Matterport camera; therefore, Poles’ color information is missing.
- PanoContext [312]: This dataset has 700 panoramas of room environment from SUN360, including 418 bedrooms and 282 living rooms. The annotations of cuboid room layout and object bounding boxes are manually annotated by a self-designed WebGL annotation tool in the browser.

Due to space constraints, we do not provide detailed descriptions for each dataset. However, we have included the source of each dataset, allowing researchers in the field to quickly understand the relevant datasets. Additionally, in our open-source repository, we have provided download links for each open dataset, making it easier for researchers to access the datasets they want.

3 ODI Representation Learning

In this section, we mainly focus on how to extract powerful and general representations from ODIs, thus we will not discuss networks specifically designed for down-

Table 2: State-of-the-art Results for spherical image classification on SPH-MNIST and SPH-CIFAR10.

	Method	# Para.	Acc (%) \uparrow
SPH-MNIST	VGG [206]+KTN [215]	294M	97.94
	SphereNet [45]	196k	94.41
	SpherePHD [129]	57K	94.08
	Spherical GCN [279]	60k	94.42
	PanoSwin-Tiny [144]	30M	99.85
	SPHTR [41]	60k	95.01
SPH-CIFAR10	SpherePHD [129]	57K	59.20
	Spherical GCN [279]	60k	60.72
	PanoSwin-Tiny [144]	30M	75.01
	SPHTR [41]	60k	58.21

stream vision tasks. In particular, based on the input projection format, we categorize these methods into: 1) *Euclidean space-based methods* for planar projections, *e.g.*, ERP, and 2) *Non-Euclidean space-based methods* for Non-Euclidean projections, *e.g.*, icosahedron meshes.

3.1 Euclidean space

The most popular planar projection, ERP, supports the networks designed for perspective images. However, the equal spacing of longitudes and latitudes in ERP introduces severe distortions, especially at the two poles. These distortions lead to a degradation in performance when 2D-designed networks are directly applied to ERP images. Therefore, there exist numerous specific representation learning methods for ERP images.

Spherical Convolution [214], as shown in Fig. 10(a), which proposes to leverage the knowledge of networks trained on perspective images to guide the ERP representation learning. Specifically, Spherical Convolution dynamically modifies the shapes of convolutional kernels, promoting alignment between the learned features from ERP data and the perspective features extracted from the associated tangent plane. Furthermore, besides the constraints of feature alignment, KTN [215], [216] introduces a trainable network to adapt source CNNs trained on perspective images to ERP images, focusing on the transformation of convolution kernels, as illustrated in Fig. 10(b). GA-CNN [115] (Fig. 10(c)) proposes the graph-based convolution filters, whose size and shape adaptively depend on the position in ERP image. Meanwhile, SphereNet [45] (Fig. 10(d)) wraps the convolution filters to convert the sampling locations on ERP images into tangent plane around the sphere, effectively improving the distortion invariance. Recently, inspired by the success of vision transformers [61], [150], PanoSwin [144] proposes a transformer-based representation learning method for ERP images, as depicted in Fig. 10(e). Based on Swin Transformer [150], PanoSwin introduces the pano-style shift windowing scheme and

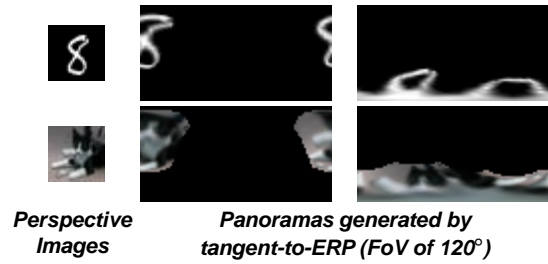


Fig. 9: SPH-MNIST (top) & SPH-CIFAR10 (down). pitch attention to address the edge discontinuity and distortions of ERP images.

3.2 Non-Euclidean space

As the raw spherical data possesses a non-Euclidean spherical data structure, some methods have explored the Non-Euclidean convolution filters in the spherical domain. They represent spherical images as icosahedron meshes [146] or Hierarchical Equal Area iso-Latitude Pixelation (HEALPix) grids [79] for processing. However, standard convolution filters are not applicable to Non-Euclidean representations. Therefore, [43], [300] (Fig. 11(a)) propose similar solutions that are to unfold icosahedron meshes and align its components to the standard image grids. Similarly, SpherePHD [129] and SPHTR [41] also employed the unfolded icosahedron meshes as the input of the proposed CNN and Transformer, respectively. However, as illustrated in Fig. 11(b), the CNN implementation of SpherePHD, *i.e.*, convolution and pooling layers, and the patch embedding of SPHTR, are applied onto the adjacent triangle. By contrast, [103], [279], [197], [200] directly employ the icosahedron meshes as the input without unfolding. Especially, [103], [200] parameterize convolution kernels as a linear combination of differential operators for processing the meshes (Fig. 11(d)), while [279] converts the icosahedron mesh into a spherical graph and designs a rotation-equivariant graph convolution network (GCN) to extract features (Fig. 11(e)). In addition, [64] verifies that it is effective to extract features from less-distorted tangent planes of a subdivided icosahedron through the standard CNNs. For learning ODI representations from the HEALPix grid input, as shown in Fig. 11(c), DeepSphere [54] constructs a rotation equivariant graph convolution network while DISCO [169] proposes a novel equivariant and scalable group convolution based on the spherical coordinates.

3.3 Discussion and Potential

In Tab. 2, we show the benchmark classification results of representative spherical representation learning methods. Since there are currently no dedicated classification datasets designed for spherical image classification, existing methods treat perspective image datasets, such

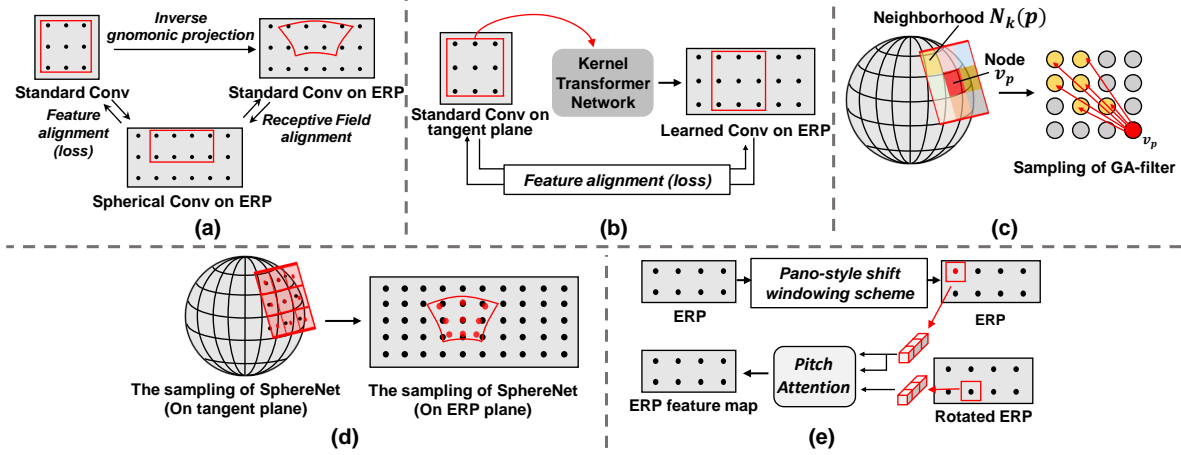


Fig. 10: Illustrations of representative representations on Euclidean space: (a) Spherical convolution [214]; (b) Kernel transformer network [215]; (c) Geometry-aware convolution [115]; (d) SphereNet [45]; (e) PanoSwin [144].

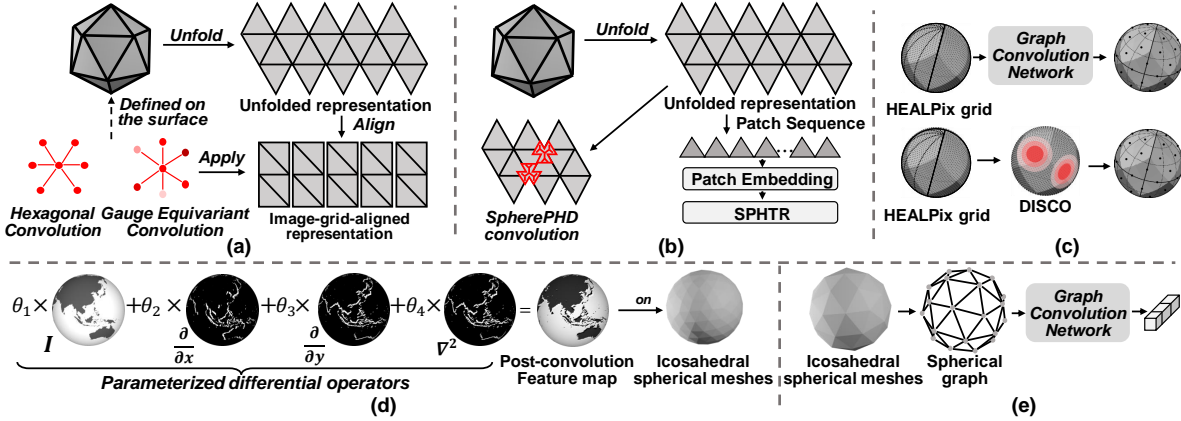


Fig. 11: Illustrations of representative ODI representation learning methods on non-Euclidean space: (a) HexNet [300] and Gauge CNN [43]; (b) SpherePHD [129] and SPHTR [41]; (c) DeepSphere [54] and DISCO [169]; (d) Parameterized differential operators [103, 200]; (e) Spherical GCN [279].

as MNIST [55] and CIFAR10 [123], as tangent patches, and then convert them into panoramas through inverse gnomonic projection. Data augmentation is then performed through rotation, as depicted in Fig. 9. To the best of our knowledge, the tiny version of PanoSwin [144] has attained the best results up to now.

From the aforementioned analysis, most existing Euclidean space-based methods [214], [45], [215], [216] have explored the potential of connecting ERP and perspective images. They propose distortion-aware convolutions based on the geometric relationship in the inverse sphere-to-plane projection to alleviate the issue of 2D off-the-shelf network failure caused by ERP distortion. However, these distortion-aware convolution filters bring substantial computational costs and suffer from the local receptive field. Inspired by the success of PanoSwin [144], the desired direction for Euclidean space-based methods is to specifically design distortion-aware attention mechanisms. For the non-Euclidean space-based methods, existing methods primarily fo-

cus on hand-crafted CNNs for unfolded icosahedron meshes or applying rotation equivariant graph convolution networks on the graphs constructed from icosahedron meshes. As transformer-based graph models have shown their power [36], [28], [333], it could be beneficial to infer these transformer-based graph models and customize spherical graph Transformers for non-Euclidean ODI representation learning.

4 Optimization Strategies

In this section, we will introduce essential optimization strategies applied to omnidirectional vision beyond the supervised learning strategy. To demonstrate the evolution of optimization strategies, we will conduct analyses across multiple tasks.

4.1 Unsupervised/Semi-supervised Learning

Data scarcity problem occurs on ODIs due to the insufficient yet costly panorama annotations. This problem is

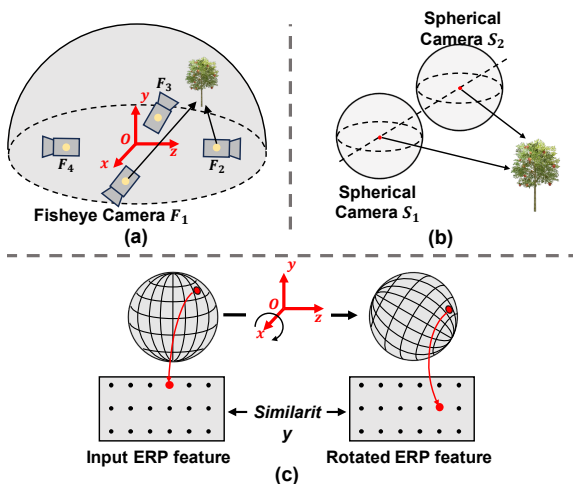


Fig. 12: The input in unsupervised or semi-supervised optimization strategy: (a) Four wide-FoV fisheye images; (b) Two spherical images captured with the horizontal baseline; (c) One spherical image and rotated one.

commonly addressed by semi-supervised learning or unsupervised learning that can take advantage of abundant unlabeled data to enhance the generalization capacity. In existing unsupervised⁷ and semi-supervised learning methods for ODI data, as shown in Fig. 12, there can be divided into three main categories according to the input data: 1) The input is multiple wide field-of-view (wide-FoV) fisheye images (Fig. 12(a)); 2) The input is a pair of panoramas captured from different view positions (Fig. 12(b)); 3) The input is a panorama and its rotated one (Fig. 12(c)). For the first category, representative works are [128], [39]. [128] calculates the unsupervised photometric loss according to the overlapping areas of any two fisheye cameras. In U-OmniMVS [39], four wide-FoV fisheye images with the FoV of 220° are split into two back-to-back pairs and projected into two ERP images. After that, the pseudo-stereo supervision is established on two ERP images following the spherical pseudo-stereo matching. The pipeline of second category is to synthesize novel views from a single input RGB image combined with the estimated depth map or depth ground truth, and then employ the corresponding areas between input view and generated view, calculated by spherical geometry constraint, as the supervision [343], [145], [231], [125], [92], [82]. The third category, [17], [1] aims to maximize the correlations between the representations from original input panoramas and corresponding rotated panoramas.

4.2 Transfer Learning

Transfer learning strategy can leverage the wealthy resource of perspective images to facilitate rapid progress in the field of omnidirectional vision. Meanwhile, transfer

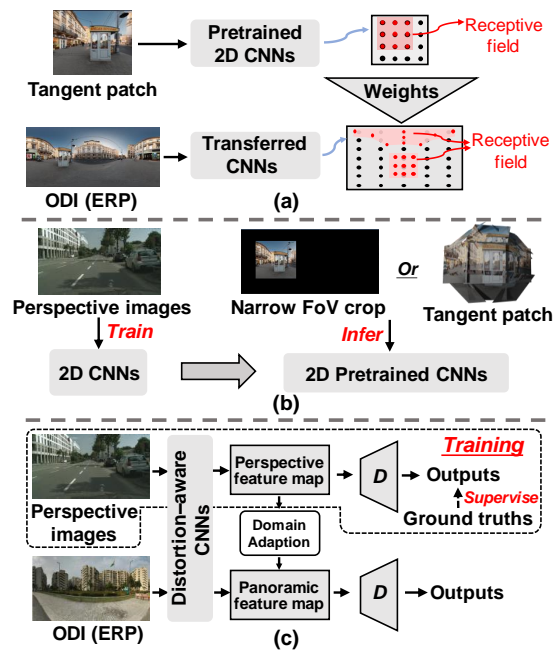


Fig. 13: The illustrations of three directions of transfer learning optimization strategy: (a) kernel-level, (b) data-level (with TP as the example); (c) feature-level.

learning enables the adaptation of knowledge from perspective image domain to the ODI domain, thereby mitigating the challenges posed by limited annotated data and high data acquisition costs in omnidirectional vision. Transfer learning on ODIs can be divided into three major directions: kernel-level transfer, data-level transfer, and feature-level transfer. For kernel-level transfer, the representative works [45], [226], [215], [18], [216], [9] follow the idea of training a standard CNN on the abundant perspective images, and then performing a sampling grid transformation on the convolution kernel based on the geometric relationship between ERP and perspective projection (Fig. 13(a)). Using kernel-level transfer, it is possible to use the weights of pre-trained standard CNNs and make the networks distortion-aware. Data-level transfer methods, as visualized in Fig. 13(b), first convert distorted ERP images into narrow FoV slices [289], [274] or less-distorted patches [324], [64], [315]. Subsequently, networks pre-trained on perspective images are directly employed on slices or patches. Compared with the above two directions, feature-level transfer learning strategy is more popular and mainly seen in unsupervised domain adaptation methods for panoramic semantic segmentation [276], [303], [157], [304], [325]. Following Fig. 13(c), they adapt extracted semantic features in the labeled pinhole image domain to the unlabeled panoramic image domain with several shared classes.

⁷ Also called self-supervised.

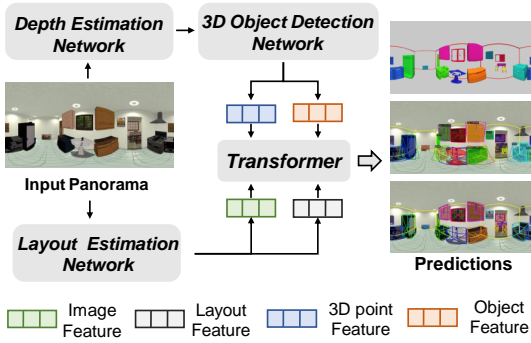


Fig. 14: The representative multi-task learning approach: PanoContext-Former [60].

4.3 Multi-task Learning

Multi-task learning strategy emphasizes sharing representations between the related tasks can increase the generalization capacity of the models and improve the performance on all involved tasks. V-CNN [259] handles four tasks: camera motion detection, viewport proposal, saliency prediction, and visual quality assessment score rating to investigate the correlations between videos’ visual quality and the head movement and eye movement of subjects on watching omnidirectional videos. Similar to V-CNN, [328] proposes an interesting direction that employs an auxiliary distortion discrimination task to reduce the impact of distortions on the quality assessment task learning. This provides a good inspiration for mitigating the distortion issues. Pano-SfMLearner [145] shares the information between three related tasks, *i.e.*, depth estimation, camera motion estimation, and semantic segmentation, to mutually promote each other. Similarly, for scene understanding based on ODIs, there exist several methods [302, 60] that improve the performance on each sub-task by sufficient exploitation of contextual information and geometric relationships between scene objects. In particular, we provide an illustrative diagram of [60] (Fig. 14) to better understand the advantages of multi-task learning. It can be seen that integrating feature representations obtained from different tasks can utilize the rich context information and better understand the components of the scene.

4.4 Deep Reinforcement Learning

Reinforcement learning (RL) aims to computationally determine the states of a specific system and execute an action to optimize an accumulated reward for the system. Deep reinforcement learning (DRL) strategy leverages the deep learning approaches to enhance reinforcement learning’s ability to tackle decision-making challenges previously deemed unsolvable, particularly those involving high-dimensional state and action spaces. As omnidirectional videos (ODVs) are always with high

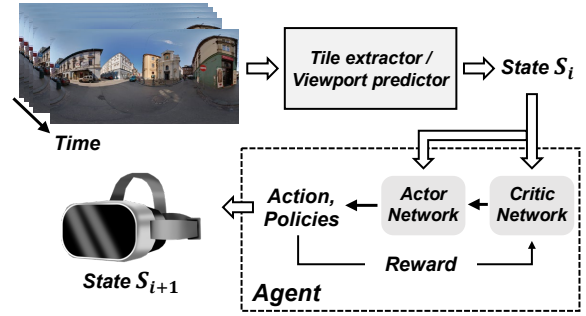


Fig. 15: The common framework of DRL-based rate adaptation for 360° video streaming.

resolution, limited network bandwidth is challenging for transmitting ODVs and proving high Quality of Experience (QoE) of users. Thus, it is to valuable to explore how to effectively allocate the bit-rates for different content of ODVs using DRL strategy. To better understand how it works, we present a common framework in Fig. 15. As a natural sequential decision-making problem, bit-rate allocation can be naturally optimized with the DRL strategy. Specially, due to the limited FoV of human eyes, an individual can only see a single viewport of each ODV frame at any given time. Therefore, existing DRL-based ODV streaming and caching methods [11, 313, 174, 110, 112, 158, 142] adaptively allocate bit-rates based on the viewports. Specifically, they first predicting a user’s viewport, then assigning tile granularities according to this viewport, and subsequently allocate higher or lower bit-rates to different tiles. Ultimately, through DRL strategies based on QoE metrics, the reward of executing actions is calculated, facilitating the adjustment of allocation. Moreover, for saliency prediction, [266] predicts head fixation through DRL strategy by interpreting the trajectories of head movements as discrete actions. Meanwhile, [58] employs the DRL strategy to select up-scaling factors of super-resolution adaptively based on unevenly distributed pixel density in the ERP images.

5 Omnidirectional Vision Tasks

In this work, we primarily focus on three key aspects of prevailing DL techniques for omnidirectional vision: visual enhancement (Sec. 5.1), scene understanding (Sec. 5.2), and 3D geometry and motion estimation (Sec. 5.3). For each aspect, we select some of the most influential research fields, as introduced in Fig. 2. We aim to facilitate a quick understanding of the development for newcomers through a summary and analysis of representative methods mostly published in top-tier conferences or journals.

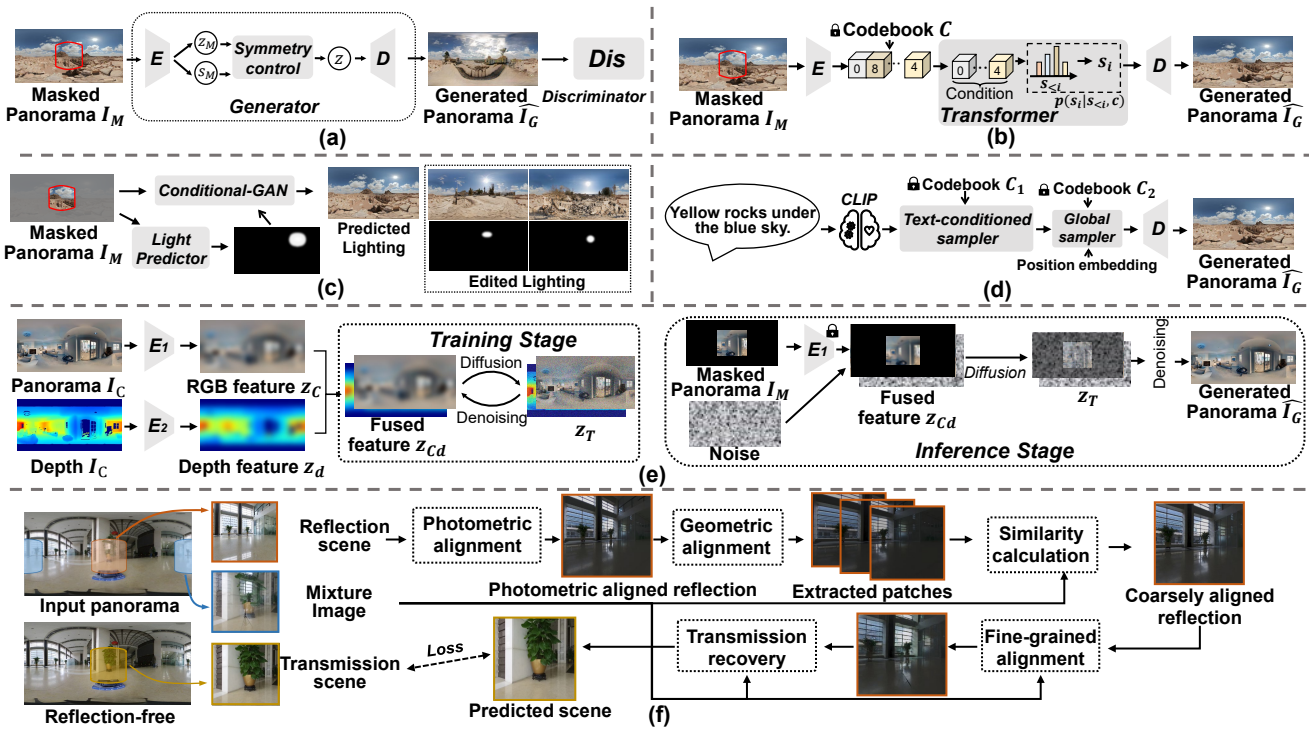


Fig. 16: The illustrations of representative networks for ODI Generation: (a) GAN-based outpainting [83]; (b) Transformer-based outpainting [5]; (c) GAN-based lighting estimation [51]; (d) Transformer-based text-guided generation [37]; (e) Diffusion-based outpainting [250]; (f) Matching-based reflection removal [89]. Not all details of the architecture are depicted.

5.1 Visual Enhancement

5.1.1 ODI Generation

ODI inpainting/outpainting: Image inpainting and outpainting are conceptually opposite, where inpainting aims to fill missing or damaged parts of an image while outpainting requires extending an image beyond its original boundaries. Especially, current efforts on ODI generation are primarily focused on outpainting, which extrapolates a complete high-quality panorama from the given narrow FoV (NFoV) images (typically masked panoramas). Notably, compared to perspective images, ODI outpainting faces the challenge, that is the continuity at the left and right sides of panoramas.

The pioneering work, 360IC [4] introduces an insightful approach. By harnessing the cylinder projection property of ERP and exploiting continuity on both ends, 360IC shifts the given NFoV content from the center towards the edges and employs two-stage conditional GANs [165] to generate the missing area. This innovative technique effectively transforms the outpainting challenge into an easier inpainting task. Furthermore, as only given content on both sides is continuous in 360IC, SIG-SS [83] proposes circular shift and circular padding to control kinds of scene symmetries and maintain conti-

nunity on whole regions of both sides. Especially, circular padding strategy is popular in panorama outpainting methods to ensure the wraparound consistency of generated panoramas [50], [143], [242], [205], [37], [240]. For instance, [250] applies circular padding as data augmentation. Moreover, circular inference [5], [3] are common in transformer-based methods. Besides, Cylin-Painting [143] constructs a GAN-based framework with the cylinder-style convolution layers and exploits collaborations between inpainting and outpainting, which are geometrically related within a seamless cylinder.

Inspired by recent advancements in generative models based on perspective images, numerous panorama outpainting works also strive to generate more diverse plausible panoramas based on given NFoV images, as shown in Fig. 16. Based on conditional VAE [209], SIG-SS [83] utilizes the scene symmetry intensity of global structure to control the generated content (Fig. 16(a)). Omnidreamer [5] and Dream360 [3] (Fig. 16(b)), based on Taming transformer [66], generate high-resolution, diverse and semantically consistent results with autoregressive transformers. To improve the generation quality and control the generation styles, ImmerseGAN [50] introduces a class-driven discriminative network into CoModGAN [321] for editing the scene classes. Meanwhile, built on the latest latent diffusion model [192],

PanoDiffusion [250] takes panoramic depths and N FoV images as the joint inputs and presents the rotation-augmented diffusion process to generate well-structured results (Fig. 16(e)).

For the inpainting task, whether based on regular masks or free-form masks, existing methods [81], [198], [291] focus on N FoV viewports of ODIs. [81], [291] convert a single panorama into six CP patches and directly apply the perspective inpainting network on these less-distorted CP patches. Differently, [198] perform generative adversarial inpainting on both panorama and the set of less-distorted N FoV viewports and fuse the features from ERP and viewports to improve the generation performance.

Text-Guided Generation: Text guidance can provide a more interactive experience, which is crucial for practical applications such as AR/VR. Text2Light [37] utilizes the pre-trained Contrastive Language-Image Pre-training (CLIP) model [184] and auto-regressive transformer-based generative models [66] to learn the text-conditioned samplers for modeling the ODI data distributions and synthesizing panoramas patch-by-patch (Fig. 16(d)). Similarly, PanoGen [132] first converts an ODI into multiple tangent patches and uses the vision-language model BLIP-2 [133] to generate text captions for each patch. Subsequently, these annotations, along with a SoTA text-to-image diffusion model [192], are recursively used to generate new tangent patches while ensuring semantic consistency across patches. Finally, the generated tangent patches are integrated through stitching to produce the final ERP-format ODI. [240] fine-tunes MultiDiffusion [12] based on the Low-Rank Adaptation (LoRA) [93] for customizing panoramas according to the text. Differently, built on the latent diffusion model, AOG-Net [154] and PanoDiff [242] focus on the text-guided panorama outpainting task, which generate the complete panoramas with the guidance of N FoV images and text prompts. Notably, both AOG-Net and PanoDiff support input from multiple N FoV images. Particularly, the N FoV images in AOG-Net are registered, while in PanoDiff the N FoV images can be unregistered. This owes to PanoDiff introduces an angle prediction branch to predict the shooting positions of multiple N FoV images.

Lighting Estimation: It is to estimate the high dynamic range (HDR) illumination of the surrounding environment and approximate realistic lighting effects while inserting virtual objects. Specifically, the most popular lighting representation is environment maps, which are ERP format ODIs with promising realistic reflections. For lighting estimation with the environment maps, there exist numerous learning-based works [76, 87, 211, 210, 239, 51] to directly generate the HDR panora-

mas from the given low dynamic range (LDR), limited field-of-view (LFoV) images. As the pioneer work, Gardner *et al.* [76] presented an end-to-end training approach with a two-stage network to predict the HDR environment maps. In the first stage, a deep convolution network is trained to anticipate the spatial arrangement of light sources within a complete scene from a given LDR LFoV input. By fine-tuning the model on the HDR panorama dataset, this network can predict the HDR environment map with the light intensities from the given LDR LFoV image. Differently from the fine-tuning strategy for mitigating task difficulty in [76], [87] proposes a step-by-step sky modeling approach. This method sequentially learns the latent code for HDR sky panorama reconstruction, trains the network for LDR-to-HDR sky panorama conversion, and predicts HDR sky panorama from LDR LFoV images using the previous latent codes and conversion network. In contrast, Neural Illumination [211] provides a universal procedure for the lighting estimation with three steps: 1) converting LDR LFoV inputs into partial LDR panoramas, 2) completing partial LDR panoramas, and 3) performing LDR-to-HDR estimation. With the strong GANs for scene completion [78], EnvMapNet [210] directly synthesizes complete HDR panorama from the partial LDR panoramas. Recently, editable lighting estimation with an HDR environment map has been attractive, allowing for flexible control over light intensity. For instance, StyleLight [239] utilizes dual-StyleGAN [281] to predict HDR environment maps from partial LDR panoramas and achieves editable lighting through GAN inversion. To avoid expensive GAN inversion techniques, EverLight [51] generates HDR environment maps via combining GAN and parametric lighting models, and controls the illumination based on predicted lighting parameters (See Fig. 16(c)).

Besides the HDR environment map-based lighting estimation works, other lighting representations have also been well explored, *e.g.*, parametric light sources [88], [75], [307], spatially-varying spherical harmonics [77], [334], and spherical gaussians [141], [299], [298], etc. These methods aim to employ deep networks to predict a compact set of lighting parameters (*e.g.*, sun position, lighting intensities, sun shape, sky turbidity) or spherical harmonics coefficients, which are used to reconstruct HDR illumination maps with the ERP format. From the aforementioned analysis, it is evident that many methods related to lighting estimation share overlaps with panorama outpainting. However, pure panorama outpainting methods primarily focus on generating complete LDR panoramas from masked LDR panorama images, emphasizing diversity and realism in the generated regions. By contrast, lighting estimation concerns

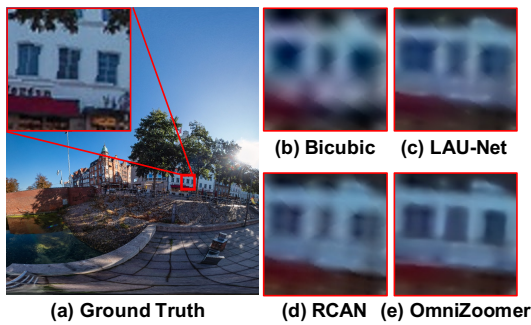


Fig. 17: Quantitative results on the SUN360 dataset. (a) High-resolution ground truth ODI. (b) Result of Bicubic interpolation. (3) Result of LAU-Net [58]. (d) Result of RCAN [314]. (e) Result of OmniZoomer [22].

itself with producing HDR results. In addition to plausible textures, it also places emphasis on shading and strong cast shadow.

Reflection removal: It aims to analyze reflection content and recover the transmission scene from reflection-contaminated images (commonly referred to as mixed images). As ODIs capture the surrounding environment in a single shot, they inherently provide the reflection scene and mixed scene simultaneously, which can solve the challenge of *content ambiguity*. Recent studies [89], [90], [80], [173] have demonstrated the potential of ODIs for reflection removal. The pioneering work [89] introduced a representative pipeline, as shown in Fig. 16(f), which consists of identifying the mixed image (an NFOV region of ODI) based on user interactions, locating corresponding glass reflection image, and learning to recover the transmission scene through matching cropped reflection and mixed images. Recently, Park *et al.* [173] utilized the similarities among attention windows in transformer blocks [61] to ensure the locations of reflection and mixed regions and achieved fully-automatic end-to-end learning. Additionally, ZS360 [80] employs zero-shot learning, assuming the ODI center aligns with the reflection glass center, to recover the transmission scene without requiring large-scale ground truth labels.

Discussion: As mentioned above, it can be observed that the key directions in existing ODI generation works, compared to planar image generation, focus on ensuring the semantic consistency, content richness, and spherical continuity of generated content at high resolution. Since panoramas can offer high interactivity, especially when applied to head-mounted devices, generating high-resolution and realistic panoramas is of significant research value. Additionally, generating well-decorated indoor panoramas from background photographs, as explored in [205], is with also high practical value. Recently, with the emergence of large-scale image-to-image and text-to-image generation models [245, 308], how to

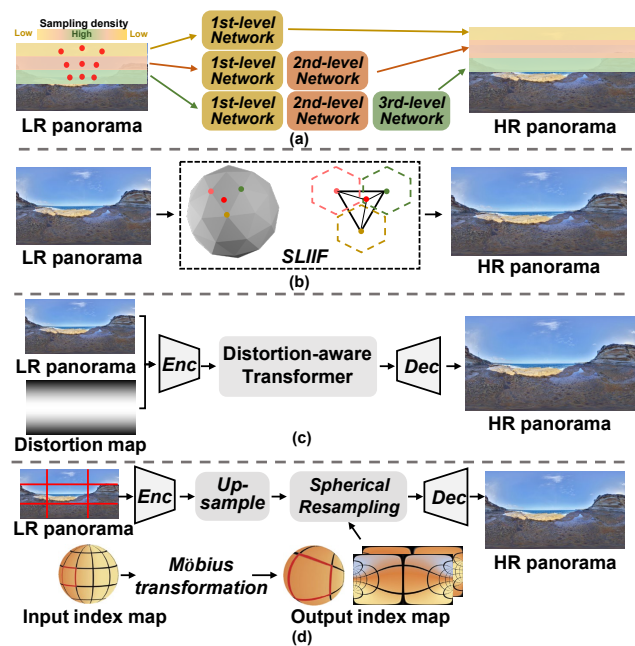


Fig. 18: The illustrations of representative networks for ODI super-resolution: (a) LAU-Net [58], (b) SphereSR [286], (c) OSRT [288], (d) OmniZoomer [22].

efficiently and effectively leverage these powerful models designed for perspective images to advance ODI generation is also meaningful. Furthermore, while most reflection removal studies focus on single regions of an ODI, exploring methods for multi-region reflection detection and removal presents a meaningful challenge. For the ODV generation, it has received limited attention while 360DVD [246] leverages diffusion models for text-guided ODV generation.

5.1.2 Super-Resolution

The Head-Mounted Display (HMD) devices [191] necessitate ODIs with a resolution of at least 21600×10800 for an immersive experience. However, due to the limitation of transmission and storage, such an immersive demand cannot be met by existing camera systems [172]. An alternative approach is to capture low-resolution (LR) ODIs and up-sample them into high-resolution (HR) ODIs effectively. Except for designing effective modules for extracting features, the properties of ODIs, such as different distortion levels in different latitudes, spherical projections, and rotation can be utilized to improve the methods' performance and generalization. LAU-Net [58], pioneering in considering the distortion variance across latitudes for ODI super-resolution (SR), introduces a multi-level network by segmenting an ODI into different latitude bands and upsampling these bands with adaptive factors (See Fig. 18(a)). Extending beyond SR on the ERP, Yoon *et al.* [286] introduced SphereSR to be capable of generating arbitrary projections, *e.g.*, ERP,

CP, and perspective views. As illustrated in Fig. 18(b), the arbitrary projection is accomplished with an implicit function by querying the spherical coordinates. Recently, as shown in Fig. 18(c), OSRT [288] designs a transformer architecture with adaptively sampling according to the distortion level, which can mitigate distortion effects in ERP format ODIs. Additionally, OmniZoomer [22] is designed to super-resolve the ODIs under various transformations, such as zooming in/out and rotation. It utilizes the Möbius transformation, which is the only bijective transformation with preserved shapes on the sphere (See Fig. 18(d)). The quantitative results are provided in Fig. 17. Compared with previous methods, OmniZoomer achieves better visual quality, benefiting from its specific design to address ODIs under various transformations.

5.1.3 Visual Quality Assessment

In today’s era of information explosion, billions of images are generated and used every day. Effective visual quality assessment (VQA) can enhance the quality of experience (QoE) of users. Particularly, since ODIs and ODVs can provide interactive experiences with head-mounted displays (HMD) devices, it is crucial to study the quality of ODIs and ODVs to avoid visually unpleasant experiences caused by low-quality content and guide the optimization of broadcasting systems.

Compared to VQA on conventional 2D images and videos, ODI-VQA and ODV-VQA pose greater challenges due to intrinsic factors such as the all-encompassing field-of-view, ultra-high resolution, and geometric deformation resulting from sphere-to-plane projection. Consequently, numerous works have been specifically designed for ODI- and ODV-VQA, tailored to the characteristics of ODIs and ODVs. Notably, VQA can be categorized based on the source of quality scores into subjective and objective methods. Subjective VQA involves collecting reliable human ratings, while objective VQA automatically measures perceptual quality. In this survey, we focus on learning-based methods, thus primarily analyzing objective VQA techniques.

ODI-VQA. ODI-VQA can be categorized into full-reference (FR) ODI-VQA and no-reference (NR) ODI-VQA (a.k.a. blind ODI-VQA). The goal of FR ODI-VQA is to measure the difference or fidelity between distorted ODIs and the original ones. However, this task is challenging due to the structural characteristics of ODIs and the complexity of the assessment process.

Various methods [292, 297, 223] have been developed, leveraging existing 2D image quality metrics such as peak signal-to-noise ratio (PSNR) and structural similarity index (SSIM)[91]. One of the most representative works is S-PSNR[292], which extends PSNR to

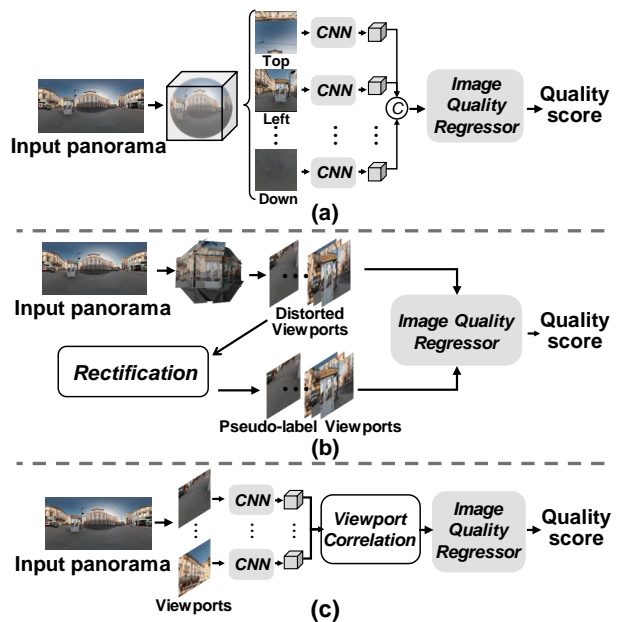


Fig. 19: Typical pipelines of NR ODI-VQA: (a) CP patch-based approach; (b) TP patch-based approach; (c) Sequence-based approach.

the spherical domain. It samples a limited number of points uniformly distributed on the sphere to calculate the mean error. Additionally, L-PSNR [292] assigns larger weights to pixels near the equator. To facilitate quality comparisons across multiple projections, CPP-PSNR [297] converts diverse projections into the craster parabolic projection (CPP) for distortion calculation. In contrast, WS-PSNR [223] proposes an efficient and effective weighted-to-spherically uniform method to generate distortion-aware weights at different locations, avoiding complex re-projection operations. In addition, certain methods utilize saliency maps [230, 171] or head movement maps [260] as weight maps to allocate weights in the calculation of PSNR. Similar to the various versions of PSNR, there are also different versions of SSIM for FR ODI-VQA, such as S-SSIM [34] and WS-SSIM [329]. Besides, [225, 116] accomplish the quality assessment based on the discriminator between distorted and reference panoramas. The approach involves cropping patches from distorted ERP format ODIs and concurrently estimating weights and quality scores for these patches. The quality score of distorted ODI is then predicted by aggregating the weights and scores of all patches. With network predicted scores and human perception scores, discriminator-based human perception guiders are employed to compare both features of reference and distorted images.

In many real-world applications, the original ODIs are often unavailable, rendering previous learning-based NR ODI-VQA methods widely applicable. These methods typically follow two main pipelines: **viewport-**

Table 3: Quantitative comparison of the methods for ODI and ODV VQA task on two popular datasets. The higher the SRCC and PLCC values, the better the performance of the model.

Datasets	Method	Type	SRCC \uparrow	PLCC \uparrow
OIQA [62] (ODI)	WS-PSNR [223]	FR	0.3829	0.3678
	WS-SSIM [329]		0.6020	0.3537
	MC360IQA [222]	NR	0.9071	0.8925
	VGCN [258]		0.9515	0.9584
	AHGCN [72]		0.9647	0.9682
Assessor360 [72]	0.9802		0.9747	
VQA-ODV [259] (ODV)	WS-PSNR [223]	FR	0.6232	0.6069
	OV-PSNR [73]		0.7503	0.7483
	MC360IQA [222]	NR	0.5106	0.5632
	VGCN [258]		0.4092	0.4059
	BOVQA [24]		0.6403	0.5569
	CIQNet [94]		0.9342	0.9333

based, and **sequence-based** approaches, as shown in Fig. 19. Numerous existing works [278, 328, 222, 258, 227, 104, 72, 327, 251] assess the visual quality of ODIs based on viewpoints. Viewports represent the undeformed content seen by human eyes during browsing, akin to CP and TP patches. A notable work in this direction is MC360IQA [222], which employs CP patches as viewport inputs and presents an image quality regressor that concatenates features of the six viewport images for final quality scores. Building upon MC360IQA, Zhou *et al.* [327] incorporated an extra distortion discrimination task while using cubemap patches (Fig. 19(a)) to assess quality scores, facilitating mutual enhancement between the two tasks. In contrast, CPBQA [104] learns human attention behavior to weight the quality scores of cubemap patches rather than direct feature concatenation as in [222, 327]. Furthermore, studies [227, 228] extract tangent viewpoints (Fig. 19(b)) to predict quality scores. Tian *et al.* [227] rectified distorted viewpoints around stitching seams to obtain pseudo-references and calculate quality scores based on differences between distorted and pseudo-reference viewpoints, while Tofighi *et al.* [228] sampled tangent viewpoints from salient parts and directly predict their quality scores.

Recent studies [258], [72], [278], [251], [217] have explored the influence of the observer’s browsing process on ODI-VQA (Fig. 19(c)). These sequence-based works introduce correlations between different viewpoints to improve prediction accuracy. One of the first methods to model interactions among different viewpoints was proposed by Xu *et al.* [258]. They built a spatial viewport graph to model the mutual dependency of viewpoints and developed a global-local mechanism to learn quality features of global ODI and local viewport sequences simultaneously. However, the limitation of VGCN [258] and AHGCN [72] lies in neglecting the dynamic viewport sequence during the browsing process. To address this, TVFormer [278] interpolates the head

trajectory prediction task to ensure viewport locations and models long-range viewport-to-viewport quality correlation via a transformer-based network. The latest state-of-the-art work, Assessor360 [251], estimates multiple pseudo-viewport sequences from a given starting point and models viewport-to-viewport correlation for each sequence. The final quality score is the average of quality scores generated for all generated viewport sequences.

ODV-VQA. In general, assessing ODV quality mirrors ODI quality assessment, especially for FR ODV-VQA. For NR ODV-VQA, Li *et al.* [130] proposed a representative viewport-based CNN approach comprising a viewport proposal network and a viewport quality network. The viewport proposal network generates several potential viewpoints and their error maps, while the viewport quality network rates the VQA score for each proposed viewport. The final score is calculated as the weighted average of all viewport scores. Another notable work is by Azevedo *et al.* [52], which considers temporal changes in spatial distortions in ODVs. They fused a set of spatio-temporal objective quality metrics from multiple viewpoints to learn the final quality score. A similar spatio-temporal consideration strategy is employed in [24], [94]. Gao *et al.* [73] modeled the spatial-temporal distortions of ODVs and integrated three existing ODI-QA objective metrics into a novel objective metric, namely OV-PSNR.

Discussion: Tab. 3 shows the state-of-the-art results for ODI-VQA and ODV-VQA on two popular datasets, *i.e.*, OIQA [62], and VQA-ODV [259]. We report the metrics of Pearson linear correlation coefficient (PLCC) and Spearman rank-order correlation coefficient (SRCC). To the best of our knowledge, Assessor360 [251] attains the best results on the OIQA dataset up to now, while CIQNet [94] outperforms other ODV-VQA methods.

5.2 Scene Understanding

5.2.1 Object Detection

Compared with perspective images, learning-based object detection on ODIs faces two main challenges: 1) traditional convolutional kernels struggle to process the irregular grid structures within ERP; 2) 2D object detection criteria are not well-suited for spherical images.

To tackle the first challenge, some studies have customized network architectures using standard convolution kernels. For example, Tong *et al.* [229] proposed a multi-scale feature pyramid network, Wang *et al.* [243] introduced multi-kernel layers, and Shen *et al.* [199] utilized depth-wise separable convolutions. Additionally, Su *et al.* [214] replaced the standard convolution filters of Faster RCNN [188] with distortion-aware spherical con-

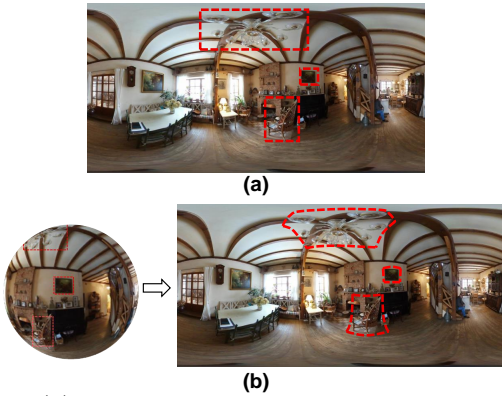


Fig. 20: (a) conventional planar bounding boxes (BBs) and (b) field-of-view bounding boxes (FoV-BBs).

volutions. Notably, Yang *et al.* [282] first converted ERP format ODIs into multiple stereographic sub-projections and then employed the 2D object detector to process these less-distorted patches individually.

For the second challenge, existing methods employ diverse criteria for ODI object detection, *i.e.*, bounding boxes (BBs) and intersection-over-unions (IoUs). In particular, Coors *et al.* [45] predicted unbiased bounding boxes (TanBBs) on the tangent plane instead of regressing rectangular BBs on the ERP format ODI. Furthermore, to better align the criteria with the characteristics of spherical imaging in ODI, Spherical Criteria [318] proposes spherical BB (Sph-BB) and spherical IoU (Sph-IoU), directly defined on the sphere. Notably, the Sph-IoU calculation moves the Sph-BBs to the equator along the longitude, making the intersection calculation more convenient as the adjusted Sph-BBs become rectangular. However, moving the centers of Sph-BBs can improve IoU calculation but also alter the great-circle distance between two centers, which should be preserved. Therefore, Zhao *et al.* [319] and Cao *et al.* [20] calculated unbiased spherical IoUs based on the intersection area between overlapping spherical rectangles on the sphere (referred to as Field of View BBs or FoV-BBs, as shown in Fig. 20(b)). Inspired by objects with arbitrary orientations in ODIs, rotated Field of View BBs (RFoV-BBs) [257] are proposed based on FoV-BBs, incorporating the angle of rotation of the tangent plane of the RFoV-BBs. Furthermore, similar to Sph-BBs, Sph2Pob [148] is proposed to move the arc between the two FoV-BBs' centers to the equator, making it easier to map to planar-oriented boxes. Based on Sph2Pob, a differentiable IoU, Sph2Pob-IoU, is utilized to approximate spherical IoU with IoU for planar-oriented boxes.

Differently, GLDL [256] provides a novel direction by modeling FoV-BBs using Gaussian distributions and calculating the K-L divergence between the two distributions as the sample selection strategy. This distribution-based selection strategy can alleviate the drawback of

the IoU threshold-based strategy, which is weak to the uneven scales of objects from different categories.

Discussion: Through the aforementioned analysis, it is evident that in ODI object detection, the key challenge lies in determining the BBs of objects and computing the IoUs between different BBs, compared to object detection in perspective images. Due to the spherical imaging nature of ODIs, conventional rectangular bounding boxes are often inadequate, particularly for distorted objects in ERP format panoramas. Consequently, several methods have been proposed to introduce spherical BBs for improved representation of objects. Specifically, the ability of ODIs to freely rotate enables the movement of spherical BBs, facilitating the computation of IoU between them. The approach presented in GLDL, utilizing Gaussian distribution to establish differences between various bounding boxes for better positive sample selection, offers an intriguing direction on how to effectively leverage spherical geometry to explore the relationships between different bounding boxes. Concurrently, recent advancements in planar generative models in planar object detection, such as DiffusionDet [33], have spurred an exploration into generating spherical bounding boxes via more flexible ways.

5.2.2 Segmentation

Learning-based panoramic semantic segmentation has attracted significant attention due to the comprehensive information it provides about the surrounding space, which is crucial for scene understanding. However, this field encounters several practical challenges, including distortions in planar projections, object deformations, semantic complexity in wide-FoV scenes, and limited labeled data. In the following sections, we will delve into the development of this field by analyzing some representative works.

Initially, people mostly cover the wide Field of View (FoV) up to 360 degrees by arranging multiple narrow-FoV perspective cameras [57] or connecting fisheye cameras with obvious lens distortion [56]. However, the use of multiple camera systems often led to large processing latency and required complex calibration tasks. In contrast, recent panoramic semantic segmentation methods typically utilize a single panorama as input, following two main approaches: 1) Knowledge transfer from perspective domain to panoramic domain; 2) Direct prediction of panoramic semantic segmentation results while considering the 3D spherical properties.

PASS [271], [272] proposes the first panoramic semantic segmentation framework based on perspective knowledge. Specifically, PASS utilizes a pre-trained segmentation network from pinhole imagery to omnidirectional imagery, thereby bypassing the need for exten-

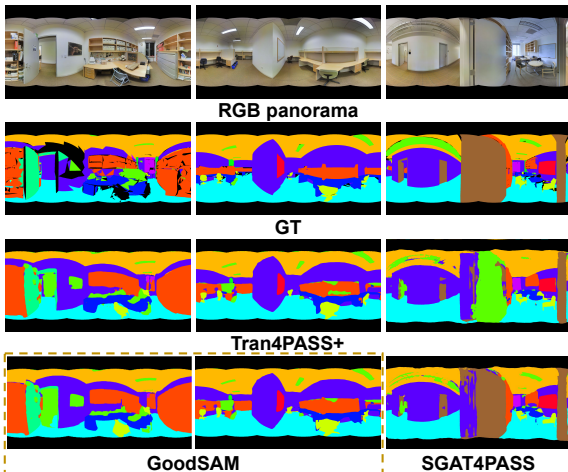


Fig. 21: Performance of SoTA panoramic segmentation methods: Trans4PASS [304], SGAT4PASS [138], and GoodSAM [310], as reported in their original papers.

sive pixel-exact annotations for panoramas. Building on PASS, Yang *et al.* [273] further enhanced the knowledge transfer performance from the 2D domain to the panoramic domain. They introduced attention-based lateral connections to improve sensitivity to spatial details. Both PASS and DS-PASS divide a panorama into segments for semantic predictions using pre-trained 2D segmenters, which are then fused back into a complete panorama. To mitigate computational complexity and capture global scenes, Yang *et al.* [274] employed data distillation between labeled pinhole images and unlabeled panoramas. This approach learns a teacher model from labeled pinhole images and generates semantic labels for training the student network. The data distillation strategy is also utilized in [275], [276], where hand-crafted feature extraction modules are proposed to capture contextual information of wide-FoV panoramas.

Other researchers have explored the concept of unsupervised domain adaptation for panoramic semantic segmentation. A prominent work in this area is DensePASS [157], [303], which introduces a generic pinhole-to-panoramic domain adaptation (P2PDA) pipeline. This pipeline adapts semantic segmentation networks from the label-rich source domain of pinhole camera images to the target domain of unlabeled panoramas. To achieve better cross-domain alignment, DensePASS specifically designs several domain adaptation modules, which can be activated individually or jointly within the P2PDA framework. In addition to the gap caused by different FoVs, spherical distortion also presents a significant domain gap. Addressing this, Trans4PASS [304] and Trans4PASS+ [305] propose a distortion-aware transformer with several deformable components as the semantic segmentation network. Meanwhile, Inspired by [309], Trans4PASS employs a semantic prototypes-

Table 4: Quantitative comparison of the methods for UDA-based panoramic annular semantic segmentation task on DensePASS dataset.

Method	# Para. (M)	mIoU (%)
PASS [272]	–	23.66
Yang <i>et al.</i> [274]	–	23.66
Dense-PASS [303]	–	43.02
Trans4PASS-Small [304]	24.98	55.22
DPPASS-Small [324]	25.40	56.28
DATR-Small [325]	25.76	56.81
GoodSAM-Small [310]	25.40	60.56

based domain adaptation strategy to generate pseudo labels for unlabeled panoramas. DPPASS [324] leverages the geometric correspondence between two types of projections, *i.e.*, less-distorted tangent projection and ERP, for cross-projection domain adaptation. Besides, DPPASS performs cross-style domain adaptation by transforming pinhole images into pseudo ERP and TP formats and aligning the pinhole domain with the panoramic domain. Moreover, Zheng *et al.* [325] exploited the non-uniform sampling density of ERP projection, quantified distortion, and proposed minimizing the receptive field of the segmentation backbone to address the distortion problem. Recently, Zheng *et al.* further investigated a source-free unsupervised panoramic segmentation method, 360SFUDA [323], which leverages the semantic, distortion, and style similarity between ERP slices and tangent patches to achieve knowledge transfer, enabling effective pinhole-to-panoramic adaptation. With the rise of large vision models, Zhang *et al.* [310] evaluated the SAM model [121] on panoramas and introduced GoodSAM, which enhances SAM’s zero-shot segmentation capabilities for panoramic semantic segmentation. By integrating the instance masks from SAM and logits from a teacher-assistant model, GoodSAM generates high-quality guidance to achieve unsupervised panoramic semantic segmentation.

In contrast, supervised panoramic semantic segmentation research based on spherical geometry remains an open field. Zhang *et al.* [301] converted the given spherical panorama into an unfolded icosahedron mesh and utilized a customized orientation-aware CNN for segmentation prediction. Li *et al.* [138] addressed the high sensitivity of existing 2D segmentation models to 3D disturbances and proposed the spherical geometry-aware framework. Specifically, they employed random rotations to the given panoramas and incorporated spherical geometry into deformable patch embedding [304] to construct the transformer.

Discussion: Tab. 4 and Tab. 5 show state-of-the-art results of unsupervised domain adaptation (UDA)-based panoramic semantic segmentation methods and super-

Table 5: Quantitative comparison of the methods for supervised panoramic semantic segmentation task on Stanford2D3D dataset.

Method	Avg mIoU (%)	F1 mIoU
Tangent (ResNet-101) [64]	45.6	-
PanoFormer [201]	48.9	-
HoHoNet (ResNet-101) [219]	52.0	53.9
Trans4PASS-Small [304]	52.1	53.3
SGAT4PASS [138]	55.3	56.4

vised panoramic semantic segmentation methods, respectively. We consider the DensePASS [157] and Stanford2D3D [8] datasets. Especially, for the Stanford2D3D dataset, we listed the performance of official fold 1 and the average performance of all three official folds. To our best knowledge, GoodSAM [310] has achieved the most promising results among the UDA-based methods thus far, while SGAT4PASS [138] has notably enhanced the performance of supervised semantic segmentation. Furthermore, to effectively demonstrate the performance of previous SoTA methods, we provide the visual results of Trans4PASS+[305], SGAT4PASS[138], and GoodSAM [310] on Stanford2D3D dataset (See Fig. 21).

Through the previous analysis, it can be observed that the current focus remains on unsupervised domain adaptation (UDA) for panoramic semantic segmentation. This preference is primarily due to the ease of obtaining accurate annotations for traditional pinhole camera images, which facilitates data-driven learning methods. However, existing UDA-based approaches overlook the spherical geometry of panoramas, such as pitch and roll rotations. Given that 3D robustness presents a significant gap between pinhole and panoramic images, enhancing the 3D robustness of segmentation models in the UDA process is a crucial area for future research. In particular, it is worth noting that, in most current UDA-based methods, the ‘panoramic images’ they use do not strictly adhere to the definition of panoramas but are *panoramic annular images* (as mentioned in PASS [271, 272, 273]). The difference is that panoramic annular images do not have seriously distorted poles like panoramas, so the impact of distortion on UDA-based methods still deserves further exploration.

Additionally, panoramic panoptic segmentation, aiming to simultaneously predict semantic and object instance information, is of significant value for autonomous driving. Nevertheless, this area of research remains relatively unexplored. Mei *et al.* [162] collected a large-scale panoramic video panoptic segmentation dataset with dense, high-quality labels. Similar to unsupervised panoramic semantic segmentation, Jaus *et al.* [98, 99] improved the performance of panoramic panoptic segmentation by leveraging models trained on richly labeled pinhole images. Recent work [120] proposed to predict

segmentation results from multiple less-distorted NFOV regions and stitch them into a panoramic view. However, this method suffers from limited real-time capability. Panoramic panoptic segmentation requires finer-grained scene understanding, making it promising to adapt the feature extraction capabilities of planar vision models to panoramas. Additionally, collecting high-quality real-world annotations can support the development of sphere-specific learning algorithms to advance this field.

5.2.3 Saliency Prediction

As ODIs/ODVs can offer an immersive experience to observers within Head-Mounted Displays (HMDs), it is crucial to predict the most visually significant or attention-grabbing areas in a 360° scene. This not only aids in designing the user interface and eye tracking for future VR systems but also contributes to understanding the visual behaviors of users in virtual environments. In the literature, most methods have focused on two projection formats: ERP and CP. They either use ERP or CP individually as input or combine both as joint inputs. Tab. 6 presents an overview of the reviewed approaches and Fig. 22 concludes some representative types of ODI saliency prediction frameworks.

ODI Saliency Prediction. In Fig. 22(a), with a single panorama as the input, Zhu *et al.* [330] proposed a feature filtering mechanism, which ranks the extracted features and adaptively selects desired feature channels according to the ranking scores, avoiding the redundant information in the features extracted by deep convolutional layers. Some authors employ diverse convolution filters to enhance the feature representation capability. Zhu *et al.* [332] designed a decoupled dynamic group equivariant filter based on group equivariant convolution filter (p4-convolution) [44] to extract content-adaptive features from ERP input. The authors decoupled p4-convolution into spatial and channel dynamic filters which are content-agnostic and efficient for better saliency prediction. Zhu *et al.* [331] proposed a light-weight saliency model using the dynamic convolution [35] and aggregated multiple parallel convolution kernels with the attention weights for extract powerful features from ERP input. Besides, Zhu *et al.* [335] proposed a novel approach in which they employed spherical harmonics to represent the panorama. They utilized this representation to extract features across various frequency bands and orientations, enabling the estimation of saliency. Ma *et al.* [86] built the ODI saliency model, SalGAIL, via generative adversarial imitation learning (GAIL) [264]. SalGAIL predicts the head fixations of users and then estimates the saliency through the predicted head fixations. Based on the consistency between head fixations and subjects in ODIs, SalGAIL

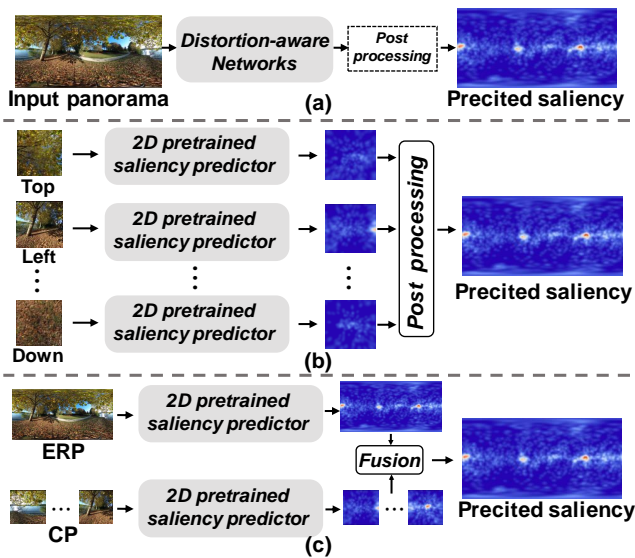


Fig. 22: Typical pipelines of ODI saliency prediction: (a) ERP-based; (b) CP-based; (c) ERP with CP-based.

applies the deep reinforcement learning to predict the head fixations of one subject and use the GAIL to learn the reward of DRL. Recently, MFFPANet [31] takes an ERP as input to predict object-level semantic images, which are taken as joint inputs with the panorama. In MFFPANet, a transformer-based network is proposed to aggregate contextual long-range information. Due to the lack of large-scale ODI/ODV datasets with accurate pixel-accurate annotations, many methods are exploring how to leverage more abundant perspective image datasets to aid in the saliency prediction of ODIs/ODVs. Considering the gap between ERP images and perspective images, *e.g.*, spherical distortion, some methods proposed to use less-distorted cubemap projection patches as input, as illustrated in Fig. 22(b). As the first attempt of the pre-trained 2D saliency model on ODI saliency prediction, SalNet360 [166] splits an ERP into a set of six CP patches as the input via the geometric relationships (See Fig. 7). Then SalNet360 combines predicted saliency maps and per-pixel spherical coordinates of these patches to output a resulting saliency map in ERP format. As CP patches inherently exhibit distortion, some methods are proposed to mitigate this effect. Dai *et al.* [49] proposed the use of dilated convolutional layers to extract features from CP patches, providing a method to address distortion in CP slices. Djemai *et al.* [59] provided a pipeline that random rotates the content of each CP patch before applying 2D saliency methods to CP patches. This can make each CP patch provide a larger context and enhance the performance of 2D saliency methods. In contrast, SalReGCN360 [29] establishes spatial and semantic correlations among the set of CP patches, enabling the saliency model to perceive

global information. Specifically, SalReGCN360 introduces a graph convolutional network (GCN) to enhance spatial and semantic associations among CP features.

Some works take the panorama and CP patches as the joint inputs, as shown in Fig. 22(c). They [53], [30] extend the 2D saliency predictor to omnidirectional imagery and leverage the fusion of saliency results from ERP and CP to generate the final results. [53] employs the equator bias map to adjust the fused result and mimic the viewers' behavior, while SalBiNet360 [30] builds a two-branch local-global bifurcated deep network to process ERP and CP input separately.

In particular, some works explore the potential of other input representations. [224] applies a 2D saliency model on multiple viewports, re-projects all the viewports' results into an ERP format saliency map, and emphasizes the gaze at the equator with equator bias map. Differently from the aforementioned works, [156], [284] propose to represent the ODIs as non-Euclidean spherical graphs and build the graph convolution networks to predict the saliency maps. SalGCN [156] is the pioneer representative work with the spherical graph signals, which are constructed based on the geodesic icosahedral pixelation. Then, using a U-Net structured graph convolutional network, a saliency map in spherical graph format is predicted. Then, through a designed spherical crown-based interpolation module, the spherical graph is transformed into ERP format. While SalGFCN [284] is also based on a spherical graph, unlike SalGCN, the graph construction in SalGFCN is based on Spherical Fibonacci Mapping (SFM) [113]. Additionally, the prediction network of SalGFCN is composed of a residual U-Net architecture incorporating dilated graph convolutions and an attention mechanism in the bottleneck. The process of transforming the graph into ERP format is based on distance-based interpolation.

ODV Saliency Prediction. For the saliency prediction in ODVs, the key points are accurate saliency prediction for each frame and the temporal coherence of the viewing process. As videos with dynamic contents are widely used in real applications, deep ODV saliency prediction has received more attention in the community. Nguyen *et al.* [167] proposed a representative transfer learning framework that fine-tunes existing 2D saliency predictors for ERP input and employs a structure-aware prior filter to enhance the predicted results, targeting specific areas such as the four corners of an input panorama. For cubemap projection format input, customized Cube Padding [40] is an influenced method, whose proposed padding operation can mitigate patch boundaries among CP patches, and be generally applicable to almost all existing 2D CNN architectures. Moreover, they proposed a spatial-temporal network consisting of a static [326]

Table 6: ODI and ODV Saliency prediction methods. EM and HM mean eye and head movement.

	Reference	Publication	Category	Input	Technology	Contribution
Image	Monroy <i>et al.</i> [166]	SPIC'18	HM&EM	CP	CNN	Transfer learning
	Dedhia <i>et al.</i> [53]	ICASSP'19	HM&EM	ERP&CP	CNN	Transfer learning
	Zhu <i>et al.</i> [330]	ICME'20	HM	ERP	CNN & Attention	Specific attention modules
	Djemai <i>et al.</i> [59]	ICME'20	HM	CP	CNN	Rotations on input
	Chen <i>et al.</i> [30]	VR'20	HM&EM	ERP&CP	CNN	Bi-projection fusion
	Lv <i>et al.</i> [156]	ACM MM'20	HM&EM	spherical graph	GCN	Graph saliency prediction
	Dai <i>et al.</i> [49]	ICASSP'20	HM&EM	CP	CNN	Dilated convolution
	Zhu <i>et al.</i> [335]	TMM'20	HM&EM	ERP	CNN	Spherical harmonics
	Zhu <i>et al.</i> [331]	ICME'21	EM	ERP	CNN & Attention	Dynamic convolution
	Chen <i>et al.</i> [29]	TVSVT'22	EM	CP	GCN	Intra- and Inter-graph inference
Chen <i>et al.</i> [31]	TETCF'24	HM&EM	ERP	CNN	Feature fusion	
Video	Nguyen <i>et al.</i> [167]	ACM MM'18	HM	ERP	CNN & LSTM	Transfer learning
	Chen <i>et al.</i> [40]	CVPR'18	EM	CP	CNN&ConvLSTM	Cube padding
	Zhang <i>et al.</i> [317]	ECCV'18	EM	ERP	CNN	spherical CNN
	Xu <i>et al.</i> [263]	TPAMI'19	HM	ERP&TP	CNN&LSTM	Deep reinforcement learning
	Qiao <i>et al.</i> [183]	TMM'21	HM&EM	ERP&TP	CNN&ConvLSTM	Multi-task learning
	Zhu <i>et al.</i> [336]	TCSVT'21	HM&EM	ERP&TP	CNN&GCN	Visual attention

model and a ConvLSTM [204] module. Similar to [224], a viewport saliency prediction model is proposed in [183] which first studies human attention to detect the desired viewports of the ODV and then predict the fixations based on the viewport content. One more representative is proposed by [317], in which the convolution kernel is defined on a spherical crown and the convolution operation corresponds to the rotation of kernel on the sphere. Considering the common planar ERP format, Zhang *et al.* [317] re-sampled the kernel based on the position of the sampled patches on ERP. There also exist some works based on novel learning strategies. Xu *et al.* [263] developed the saliency prediction network of head movement (HM) based on deep reinforcement learning (DRL). The proposed DRL-based head movement prediction approach owns offline and online versions. In offline version, multiple DRL workflows determines potential HM positions at each panoramic frame and generate a heat map of the potential HM positions. In online version, the DRL model will estimate the next HM position of one subject according to the currently observed HM position. Zhu *et al.* [336] proposed a graph-based CNN model to estimate the fraction of the visual saliency via Markov Chains. The edge weights of the chains represent the characteristics of viewing behaviors, and the nodes are feature vectors from the spatial-temporal units.

5.3 3D Geometry and Motion Estimation

5.3.1 Depth Estimation

The commonly used ERP format of ODIs exhibits horizontal distortion. Consequently, ERP images often exhibit increased curves compared to perspective images. It would also result in neighboring points on the sphere becoming more distant. Considering that the number of monocular methods for ODIs is larger than stereophonic methods by a great deal, we mainly focus on monocular methods in this subsection. For the task

of monocular depth estimation task, 2D methods typically apply regular convolutional kernels (*e.g.*, 3×3) to extract geometric information. However, the direct application of planar designs struggles to capture effective geometric structures due to the increased curves and distant neighbors, leading to sub-optimal results. To address this issue, recent trends can be grouped into five directions: (i) Tailored networks, such as distortion-aware convolution filters [226] and attentions [296]; (ii) Exploring more projection types of ODIs with less distortion [237], [68], [140] (Fig. 23(a)); (iii) Developing 2D representations specifically for ERP [179] (Fig. 23(b)); (iv) Leveraging inherent geometric priors contained in ODI [63], [111] (Fig. 23(c)); (v) Employing multiple views of ODIs [342] (Fig. 23(d)). We further provide a detailed accuracy comparison of these methods in Tab. 7, which will be discussed subsequently. Finally, we introduce the ODI depth completion with additional sparse depth input, and stereo matching within two paired ODIs.

Tailored networks: This category can be divided into two subsets: specialized CNN design and attention design. In terms of CNN design, the main emphasis is on the shape and sampling positions of the CNN kernel. To mitigate the effects of stretch distortion, Zioulis *et al.* [344] building on [214], transformed regular square convolution filters into row-wise rectangles and adjusted filter sizes across latitudes to compensate for distortions near the poles. Tateno *et al.* [226] introduced a deformable convolution filter that samples the pixel grids on the tangent planes and then projects them back to the unit sphere coordinates. More recently, Zhuang *et al.* [337] developed an approach combining a series of dilated convolutions with varying dilation rates, which adaptively enlarges the receptive field in the ERP images. In the realm of attention design, PanoFormer [201] introduces pixel-wise deformable attention, echoing the principles of [45]. However, PanoFormer further incorpo-

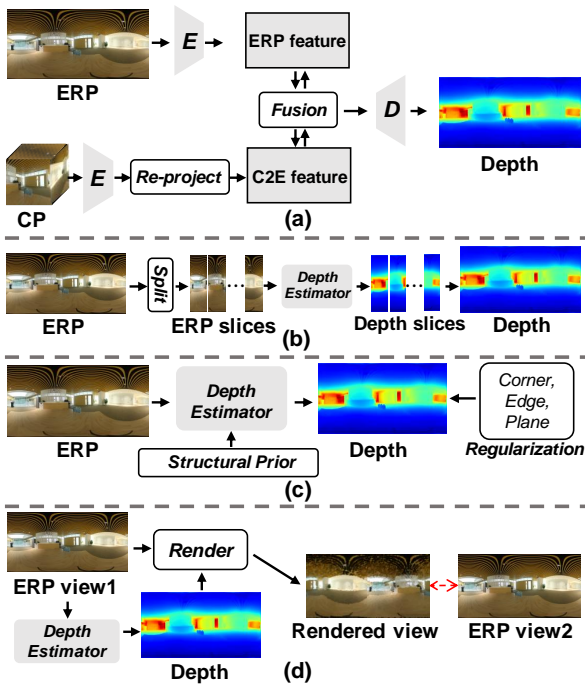


Fig. 23: Representative monocular depth estimation methods: (a) Multi-projection input; (b) 2D representations (e.g., vertical slices of ERP); (c) Extra geometric prior knowledge; (d) View synthesis.

rates a learnable token flow to ensure that the sampled positions of the attention mechanism align closely with the geometric structures in the scene. EGFormer [296] introduces a relative position embedding that calculates the distances between pixels in spherical coordinates, which is then utilized to re-weight the attention scores.

Different Projection Formats: Efforts have been made to mitigate the distortion in ERP by exploring other projection formats with less distortion, e.g., Cube-map Projection (CP), and tangent projection, as shown in Fig. 23(a). BiFuse [237], a notable study, introduces a dual-branch architecture in which one branch processes the ERP input, while the other extracts features from CP to mimic the human peripheral and foveal vision. A fusion model is then proposed to process the semantic and geometric information from both branches. Drawing inspiration from BiFuse, UniFuse [105] proposes a more efficient fusion module to combine the features from two branches, in which the CP features are passed exclusively to the ERP branch during the decoding phase. To enhance the global context extraction, GLPanoDepth [10] transforms the ERP input into a collection of CP images and employs a Vision Transformer (ViT) model to learn long-range dependencies. Given that tangent projection yields less distortion than CP, 360MonoDepth [189] employs state-of-the-art 2D depth estimation models [187] to predict depths from

tangent images, which are then readjusted and merged to ERP depths with alignment and blending techniques. Nevertheless, directly re-projecting tangent images back to ERP can lead to overlapping and discontinuities. To ensure global consistency, Peng *et al.* [176] proposed to employ a pre-computed ERP depth map from the pre-trained depth estimator to support other patch-wise depth predictions’ registrations. Additionally, OmniFusion [140] introduces additional 3D geometric embeddings to lessen the discrepancy in patch-wise features and aggregate such information with a transformer. Considering that tangent projection is limited to local regions, HRDFuse [2] unveils a dual-branch strategy, comprising an ERP branch and a TP branch. The integration of the two branches is facilitated by learnable feature alignment, which offers benefits in both efficiency and accuracy compared to geometric fusion. Recently, S2Net [134] introduces to project ERP features onto the sphere with HEALPix [79], which achieves uniform sampling on the sphere. Especially, HEALPix transforms an ERP into a point set and S2Net processes the point set with a cross-attention block.

2D Representations: This approach pertains to the ERP representation which is vertically captured or aligned with gravity. To exploit the gravity-aligned features in ERP, Pintore *et al.* [179] developed a framework called SliceNet, which deconstructs the ERP into vertical slices and reduces the input tensor along the vertical (gravity) dimension to assemble a sequence of such slices, as shown in Fig. 23(b). It then utilizes a Long Short-Term Memory (LSTM) network [204] to restore the spatial relationships among the slices, both in the short and long term. HoHoNet [219] squeezes ERP features along the vertical direction and unsqueezes the compressed features for dense depth prediction, which is fast and accurate. More recently, PanelNet [289] introduces to segment the ERP into panels. PanelNet employs window attention to extract local geometric information and applies a specially designed panel attention mechanism to capture global geometric information.

Geometric Information Prior: With large FoV, ODI provides rich and complete geometric information in the scene. Exploiting the geometric information in the ODI, e.g., edge and surface normal, can improve the performance effectively, as shown in Fig. 23(c). Eder *et al.* [63] proposed a plane-aware learning scheme that jointly predicts depth, surface normal, and boundaries. Similar to [63], Feng *et al.* [67] proposed a framework to refine ODI depth estimation using the surface normal and uncertainty scores. Moreover, Jin *et al.* [111] demonstrated that the representations of geometric structure, i.e., corners, boundaries, and planes, can provide useful regularization for ODI depth estimation.

Table 7: Quantitative comparison for monocular ODI depth estimation task on two popular datasets.

Datasets	Method	Publication	Backbone	Input Format	Abs Rel ↓	Sq Rel ↓	RMSE ↓	δ_1 ↑	δ_2 ↑	δ_3 ↑
Stanford2D3D	BiFuse [237]	CVPR'20	Res-50	ERP+CP	0.1209	–	0.4142	0.8660	0.9580	0.9860
	UniFuse [105]	RAL'21	ResNet-18	ERP+CP	0.1114	–	0.3691	0.8711	0.9664	0.9882
	HoHoNet [219]	CVPR'21	ResNet-50	ERP	0.1014	–	0.3834	0.9054	0.9693	0.9886
	OmniFusion [140]	CVPR'22	ResNet-34	TP	0.0950	0.0491	0.3474	0.8988	0.9769	0.9924
	PanoFormer [201]	ECCV'22	–	ERP	0.1131	0.0723	0.3557	0.8808	0.9623	0.9855
	PanelNet [289]	CVPR'23	ResNet-34	ERP	–	0.0829	0.2933	0.9242	0.9796	0.9915
	HRDFuse [2]	CVPR'23	ResNet-34	ERP+TP	0.0935	0.0508	0.3106	0.9140	0.9798	0.9927
	S2Net [134]	RAL'23	Swin-Base	ERP+HEALPix	0.0903	–	0.3383	0.9191	0.9782	0.9912
Matterport3D	BiFuse [237]	CVPR'20	ResNet-50	ERP+CP	0.2048	–	0.6259	0.8452	0.9319	0.9632
	UniFuse [105]	RAL'21	ResNet-18	ERP+CP	0.1063	–	0.4941	0.8897	0.9623	0.9831
	HoHoNet [219]	CVPR'21	ResNet-50	ERP	0.1488	–	0.5138	0.8786	0.9519	0.9771
	OmniFusion [140]	CVPR'22	ResNet-34	TP	0.1007	0.0969	0.4435	0.9143	0.9666	0.9844
	PanoFormer [201]	ECCV'22	–	ERP	0.0904	0.0764	0.4470	0.8816	0.9661	0.9878
	HRDFuse [2]	CVPR'23	ResNet-34	ERP+TP	0.0967	0.0936	0.4433	0.9162	0.9669	0.9844
	PanelNet [289]	CVPR'23	ResNet-34	ERP	0.1150	–	0.4528	0.9123	0.9703	0.9856
	S2Net [134]	RAL'23	Swin-Base	ERP+HEALPix	0.0865	–	0.4052	0.9264	0.9768	0.9911

Multiple Views: Given that depth annotations for ODIs are costly, several studies have focused on multiple viewpoints to synthesize data and achieve competitive results. Zioulis *et al.* [342] investigated spherical view synthesis for self-supervised ODI monocular depth estimation. In their work, upon predicting the depth map in ERP format, stereo viewpoints with vertical and horizontal baselines are generated using depth-image-based rendering, as shown in Fig. 23(d). These synthesized images are then aligned with real images sharing the same viewpoints, employing a photometric image reconstruction loss for supervision. To enhance both accuracy and stability, Yun *et al.* [295] introduced a joint learning framework that estimates ODI depth through supervised learning while concurrently estimating poses from adjacent ODI frames through self-supervised learning. Zhuang *et al.* [338] proposed a transformer-based self-supervised depth prediction model, namely SPDET. In detail, SPDET first predicts a depth map from the source-view panorama, then introduces the spherical geometry feature to learn the target-view panorama from the source-view panorama, and finally achieves self-supervised depth prediction via supervising the target-view panorama generation. Similarly, Chang *et al.* [27] proposed to utilize the Neural Radiance Field (NeRF) [164] to achieve unsupervised panoramic depth estimation. They re-projected the pixels of panoramas onto the unit sphere to get the camera rays and then supervised the generation of novel-view ODIs, based on the predicted depth maps, to achieve unsupervised depth estimation.

Depth Completion: Due to the scarcity of real-world sparse-to-dense panoramic depth maps, this task mainly utilizes simulation techniques to generate artificially sparse depth maps as training data. Liu *et al.* [147] proposed a representative two-stage framework to achieve panoramic depth completion. In the first stage, a spherical normalized convolution network is proposed to predict the initial dense depth maps and confidence maps

from the sparse depth inputs. Then the output of the first stage is combined with corresponding ODIs to generate the final panoramic dense depth maps through a cross-modal depth completion network. Especially, BIPS [170] proposes a GAN framework to synthesize RGB-D indoor panoramas from the limited input information about a scene captured by the camera and depth sensors in arbitrary configurations. However, BIPS ignores a large distribution gap between synthesized and real LIDAR scanners, which could be better addressed with domain adaptation techniques. Moreover, there are several methods which design depth pre-training [270] and spherical uncertainty loss [269], respectively.

Stereophonic Depth Estimation: Li *et al.* [137] used a pair of ODIs as input for estimating the depth in the scene, as the pioneering work in this field, who . They utilized the Lucas-Kanade [155] method to construct the relationships between the paired ODIs. As for deep learning-based methods, Wang *et al.* [244] extracted features from ODIs with top and bottom views and calculated the cost volume from the features with two views. Finally, the disparity is regressed from the cost volume with stacked CNNs. Lai *et al.* [126] outputted both disparity and normal maps, in which the multi-task learning constrained the rationality of both types of outputs. However, as non-overlapped regions between paired ODIs are limited, this direction is scarce.

Discussion: In Table 7, we evaluate the performance of monocular depth estimation methods for ODIs across two datasets. Our findings indicate that: 1) Utilizing projection types with less distortion proves to be an effective strategy for enhancing performance. Specifically, TP incurs less distortion compared to CP, resulting in TP-based methods outperforming those based on CP. 2) Incorporating an attention mechanism shows superiority over traditional CNN-based methods, primarily because attention mechanisms are expert at capturing global structural information, which is particularly advantageous for ODIs that contain abundant structural scene

details. 3) The choice of network backbone is crucial. For instance, S2Net [134] utilizes the Swin Transformer [150] as its backbone, yielding significantly better performance than other methods on the Matterport3D dataset.

Moreover, based on the aforementioned analysis, we think some directions are also worth exploring, except for improving the depth estimation performance. For example, as the ODI application requires extremely high spatial resolution, especially for mobile devices, *e.g.*, VR headsets. Current methods often output depths with 512×1024 spatial resolution, which can not support immersive experience. It is interesting to investigate how to improve the computational efficiency, and simultaneously improve the output resolution.

5.3.2 Optical Flow Estimation

Optical flow estimation analyzes pixel-level motion between two consecutive video frames, offering valuable insights for dynamic scene understanding. ODIs, with their ultra-wide field of view (FoV), provide a comprehensive perspective of the surrounding environment, making optical flow estimation based on ODIs particularly important for practical applications such as autonomous driving. However, existing optical flow methods designed for perspective images have been shown to perform poorly on ODIs [7]. To address this, Xie *et al.* [254] introduced a diagnostic dataset, FlowCLEVR, to evaluate the performance of tailored convolutional filters—namely, correlation, coordinate, and deformable convolutions—for estimating optical flow in ERP format. Given the scarcity of panoramic optical flow datasets, other studies [194], [18], [9] have utilized domain adaptation strategies to leverage the wealth of perspective image datasets. Drawing inspiration from representation learning methods [215], [45], these studies exploit the geometric relationship between tangent planes and the spherical surface to re-project square convolutional filter weights learned from perspective images onto the spherical surface of ODIs. Li *et al.* [139] and Yuan *et al.* [293] further addressed distortion challenges by employing less-distorted projection formats. They first applied perspective-based methods to predict optical flow in these projections and then integrated the patch-based results into ERP format. More recently, PanoFlow [203] leveraged the cyclic nature of ODIs, similar to [143], to reduce large displacements into smaller ones, simplifying the estimation process.

Discussion: Despite these advancements, panoramic optical flow remains a largely underexplored area, presenting abundant opportunities for future research. Key directions include, but are not limited to, the collection of large-scale real-world datasets, the development of specialized network architectures to enhance prediction

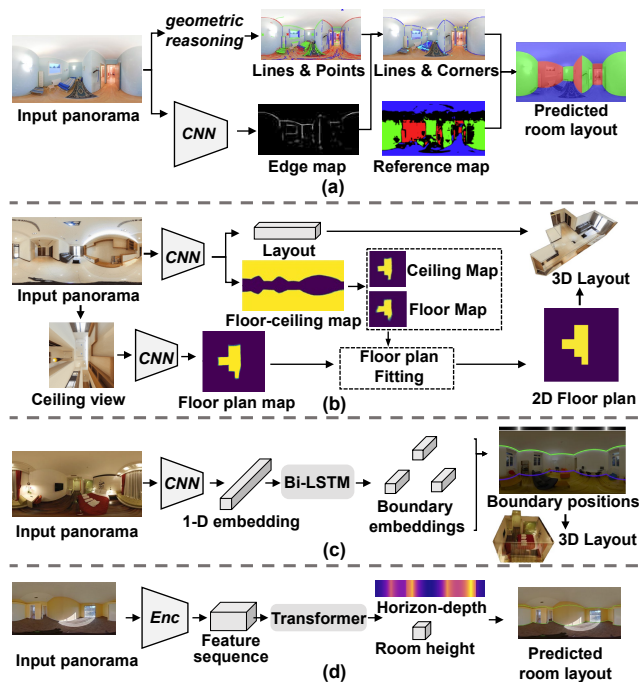


Fig. 24: Representative room layout estimation methods: (a) Based on the combination of geometric reasoning and deep patterns [70]; (b) Based on panorama-view and ceiling-view inputs [280]; (c) Based on three 1D boundary embeddings [218]; (d) Based on predicting the depth of the horizon line and room height [238].

accuracy, and the integration of powerful large-scale vision models to push the boundaries of this field further.

5.3.3 Room Layout Estimation and reconstruction

Room layout estimation and reconstruction aims to learn the sparse 3D representation of an indoor scene. Specifically, to reduce the difficulty, rooms are often modeled as cuboids, or with either the Manhattan World [46] or Atlanta World [193]. Manhattan World assumes that there exist three mutually orthogonal vanishing directions in the scene, while there is one additional degree of freedom in the Atlanta World assumption. For room layout estimation and reconstruction methods on perspective images, they face two limitations: 1) the limited field of view prevents the reconstruction of the complete closed geometry of the room; 2) the ceiling does not usually appear in perspective images, which is essential for detecting the main structure of the room. Therefore, ODIs are naturally suitable for this task as they can capture the entire surroundings in a single shot.

Fernandez-Labrador *et al.* [70] proposed the first deep learning-based framework for recovering room layouts from ODIs (See Fig. 24(a)). They integrated geometric reasoning (lines and vanishing points) with extracted deep patterns, *i.e.* edge maps, to predict struc-

Table 8: Quantitative comparison of the methods for cuboid room layout estimation on PanoContext.

Datasets	Method	Publication	Backbone	3D IoU (%) \uparrow	Corner error (%) \downarrow	Pixel error (%) \downarrow
PanoContext [312]	LayoutNet [345]	CVPR'18	-	74.48	1.06	3.34
	DuLaNet [280]	CVPR'19	ResNet-18	77.42	-	-
	CFL [69]	RAL'20	ResNet-50	78.87	0.75	2.6
	HorizonNet [218]	CVPR'19	ResNet-50	82.17	0.76	2.20
	LayoutNet v2 [346]	IJCV'21	ResNet-34	85.02	0.63	1.79
	DuLa-Net v2 [346]	IJCV'21	ResNet-50	83.77	0.81	2.43
	SSC [341]	-	-	83.97	0.63	1.78
	LED ² -Net [238]	CVPR'21	ResNet-50	82.75	-	-
	LGT-Net [109]	CVPR'22	ResNet-50	84.94	0.69	2.07
	DOP [202]	CVPR'23	ResNet	85.00	0.69	2.13

tural corners. After obtaining the ceiling-wall and floor-wall corners, the authors estimated room height based on Manhattan World constraints and refined layout results using learned surface normal maps for the final output. To accurately predict edge maps of ODIs and mitigate distortions, they initially divided an ODI into 60 overlapping narrow-FoV perspective patches. Subsequently, they fused the edge maps of all patches, predicted by a pre-trained 2D edge detector, back into the ERP format. Differing from [70], LayoutNet [345] directly learns rooms' boundary and corner maps simultaneously through a two-branch network, consisting of one encoder and two decoders. The network takes joint ERP format inputs from ODIs and Manhattan line segments. Additionally, Manhattan line segments, serving as geometrical cues, are re-projected into the ERP format from detected line segments [235] of overlapping perspective patches and also utilized to align the input panorama upright. Finally, following Manhattan World constraints, LayoutNet further refines the estimations and obtain the final layouts.

As geometric reasoning brings extra computation cost and inference time, some approaches propose end-to-end trainable pipelines without no additional geometric reasoning. As illustrated in Fig. 24(b), DuLa-Net [280] leverages the complementary room layout clues in two projections, *i.e.*, panorama-view and perspective ceiling-view to recover layout, to build a two-stream network. The floor-ceiling probability map and layout height are predicted from the panorama-view, while 2D floor plan is learned from ceiling-view. The floor-ceiling probability map and 2D floor plan are 2D binary mask maps, and the layout height is a scalar value. DuLa-Net fuses the features of two projections via the E2P conversion module (*similar to the E2C module in BiFuse [237]*), which transforms ERP features to perspective ceiling-view format. Finally, DuLa-Net optimizes the floor plan according to the Manhattan assumption. As the size of 2D probability maps or floor plans is $O(HW)$, HorizonNet [218] proposes a novel efficient representation specifically tailored for room layout estimation, namely three 1D vectors (the output size= $O(3 \times W)$), that predicts the boundary positions of floor-wall and ceiling-wall,

and the existence of wall-wall boundary (See Fig. 24(c)). Especially, to capture global information and model long-term dependencies for geometric patterns, bidirectional LSTM [161] is employed to process the feature embeddings compressed along the vertical axis. Besides efficiency, horizontal features implicitly handle the distortions of spherical images along the rows. After obtaining the compact three representations, HorizonNet adds the Manhattan world constraint, that the ground has been aligned orthogonally to the y-axis (horizontal ground), to obtain the closed layout. This horizontal representation strategy is also employed in both HoHoNet [219] and SSLayout [231]. In particular, HoHoNet proposes an efficient height compression (EHC) module to reduce the feature height to 1 and replace the Bi-LSTM in HorizonNet with a more efficient and effective multi-head self-attention module. SSLayout is the first semi-supervised approach to use a combination of labeled and unlabeled data for improved layout estimation. In SSLayout, HorizonNet is employed as a stochastic predictor with the dual role of being both the student and teacher and leverages the exponential moving average (EMA) [127] to achieve semi-supervised learning. Furthermore, LED²-Net [238] formulate the task of ODI-based layout estimation as predicting depth along the horizon line of a panorama (target output size = $O(W)$). Specifically, LED²-Net encodes the room layout as a set of rays, called horizon-depth representation, which are equiangularly sampled from longitude on the floor-plane (Fig. 24(d)). Based on this, the 3D layout is obtained under the assumption of the gravity-aligned camera with approximately known height, and Manhattan World constraints. By contrast, LGT-Net [109] proposes a transformer-based framework to predict the horizon depth and room height simultaneously. To better model the enclosed layout, the authors computed the normal and gradient errors calculated from horizon depth to constrain the planar geometry. Also predicting the room height and horizon depth with the Manhattan World assumption, Shen *et al.* [202] proposed two improvements: 1) producing two 1D representations from the semantics of two disentangled orthogonal planes; 2) adaptively integrating shallow and deep features with

distortion awareness. The former can address the ambiguous interpretability from the compression procedure, while the latter can enhance the feature representation.

In particular, some works follow the cuboid-shaped or Atlanta World assumption. Single-Shot Cuboids [341] is one of the representative works for cuboid-shaped layout estimation. Without any post-processing, Single-Shot Cuboids predicts geodesic heatmaps to regress corner coordinates and constrains the geometry to a cuboid. Due to the Atlanta World assumption not requiring vertical walls to be orthogonal to other layout elements, it is more lenient than the Manhattan World assumption, while also increasing the difficulty of layout recovery. The first work based on Atlanta World assumption is AtlantaNet [177], which takes the above-camera view and below-camera view of the original gravity-aligned panorama as the input rather than the whole panorama. This strategy can avoid noise from furniture and occlusions. With the estimated floor plan and ceiling plan, AtlantaNet infers the room height and recovers the 3D layout based on the Atlanta World constraints

Some approaches explore the potential to reconstruct 3D layouts from panoramas without relying on these complex structural assumptions. For instance, CFL [69] only considers the floor-ceiling parallelism and recovers the room layouts according to the predicted heatmaps of corners and edges. By leveraging distortion-aware spherical convolutions, CFL can generalize better to camera position variations especially when the input panoramas are not gravity-aligned. In contrast, Deep3DLayout [178] adopts a different approach by building a graph convolutional network to infer the room structure as a 3D mesh. It progressively deforms a graph-encoded tessellated sphere until the final 3D layout is achieved, without explicitly predicting any layout clue. Jia *et al.* [102] proposed a pipeline based on HorizonNet to predict an extra surface normal feature for adaptive post-processing to reconstruct layouts of arbitrary shapes. Seg2Reg [220] adapts NeRF techniques to formulate the 2D layout representation as a density field and employs flattened volume rendering to regress 1D layout depth and generate the floor-plan polygon.

All of the methods mentioned above are based on a single input panorama. However, in reality, due to the presence of many large and complex rooms, a single panoramic image is often insufficient to accurately estimate the layout of the house. Therefore, some works use two panoramas to reconstruct the house layout. Wang *et al.* [241] proposed PSMNet, a joint pose-layout network to predict 2D room layout and refine a noisy 3 DOF relative camera pose simultaneously. The input of PSMNet is the two panoramas captured with different viewpoints and converted ceiling-view images using the

E2P module in DuLa-Net. Notably, the key block of PSMNet for camera pose alignment is based on the two converted ceiling-view images. The geometrical clues for layout estimation are generated by the view fusion. Finally, with Atlanta World constraints, the output mask is post-processed to generate the layout polygon. Similarly, GPR-Net [213] explores the end-to-end supervised room layout estimation from two panoramas. Compared with PSMNet, GPR-Net avoids the initial registration and presents two transformers for 1D layout horizon feature extraction and relative pose regression.

Discussion: From the analysis, it can be observed that, compared to other tasks, room layout estimation based on ODIs and perspective images are quite different. ODI can provide complete ceiling and floor information, which also offers more clues to recover the complete layout. Moreover, from existing methods, we can see that most of the current methods rely on horizontal features for prediction, which imposes high requirements on the accuracy of post-processing. In contrast, Deep3DLayout proposes a promising research direction by directly recovering room layouts from the perspective of 3D meshes, enabling many existing 3D generation methods to be applied to room layout estimation. Specifically, most existing methods focus on central panoramas, while non-central panoramas allow for the recovery of the environment scale. Therefore, [15, 16] adopt layout estimation models for central panoramas to extract structural lines from non-central input panoramas and propose linear solvers to jointly obtain the room height and vertical walls location for reconstructing the scaled layout of the room. More methods targeting non-central panoramas should be developed in the future.

5.3.4 Simultaneous Localization And Mapping

Simultaneous Localization and Mapping (SLAM) leverages sequential RGB and depth data captured by a mobile agent to concurrently estimate the agent’s position within its environment and reconstruct the surrounding 3D structure in real time. Compared to perspective images, omnidirectional images provide more structural information per movement, enabling more efficient and cost-effective SLAM. Caruso *et al.* [23] adapted the monocular perspective SLAM pipeline, LSDSLAM [65], for omnidirectional cameras, and utilized a spherical coordinate system for tracking and depth estimation. In the domain of visual odometry, ROVO [195] introduced an omnidirectional stereo rig using four fisheye cameras, achieving robust and accurate ego-motion estimation by incorporating spherical imaging characteristics and the positional parameters of multiple cameras. Several other works [160], [196], [100], [248], [247], [294], [283], [255] leverage multi-camera systems to achieve omnidirec-

tional perception. These approaches utilize each wide-FoV camera’s observations for pose estimation, key-point matching, and motion tracking within constrained spaces. Subsequently, the parameters of the entire multi-camera system are utilized for omnidirectional loop-closing, resulting in a consistent global solution for localization, tracking, and mapping.

In contrast, [95], [119] focus on utilizing single 360° cameras to capture scenes. These approaches exploit pixel and depth information from adjacent panoramas recorded during the agent’s movement to perform localization and mapping. Compared to multi-camera systems, these methods reduce alignment overhead and associated costs but face challenges in handling the increased semantic complexity inherent in 360° data. Generally, current omnidirectional SLAM research primarily focuses on omnidirectional perception systems constructed from multiple fisheye cameras. With the commercialization of 360° cameras, developing omnidirectional SLAM systems that leverage a single 360° camera for high-precision localization and mapping presents substantial practical value. For example, 360Loc [96] proposes to combine a single 360° camera and LiDAR for precise visual localization that supports the reference images with different FoVs. Furthermore, integrating advanced 3D reconstruction techniques, such as NeRFs [164] or 3D Gaussian splatting [114], into the omnidirectional SLAM pipeline offers promising avenues for future exploration.

6 Application

6.1 AR and VR

With the advancement of techniques and the growing demand for interactive scenarios, AR and VR have seen rapid development in recent years. VR aims to simulate real or imaginary environments, where a participant can obtain immersive experiences and personalized content by perceiving and interacting with the environment. With the advantage of capturing the entire surrounding environment, 360 VR/AR facilitates the development of immersive experiences. [122] gives a detailed SWOT (namely strengths, weaknesses, opportunities, and threats) analysis of 360 VR to make sure that it is suitable to leverage 360 VR to develop athletes’ decision-making skills. Understanding human behaviors is crucial for the application of 360 VR. [249] proposes a preference-aware framework for viewport prediction, and [267] combined the history scan path with image contents for gaze prediction. In addition, to enhance the immersive experience, Kim *et al.* [117] proposed a novel pipeline to estimate room acoustic for plausible reproduction of spatial audio with 360° cameras. Importantly,

obtaining high-quality and editable panoramas can provide users with a better viewing experience with VR/AR devices. Therefore, panoramic image generation methods, *e.g.*, PanoDiffusion [250], Text2Light [37], are very helpful for VR/AR. Meanwhile, depth data is strongly desired in VR/AR to provide a sense of 3D. However, previous consumer-level depth sensors can only capture perspective depth maps, and panoramic depths need time-consuming stitching technologies. Therefore, accurate monocular depth estimation techniques, *e.g.*, UniFuse [105] and PanoFormer [201], are promising.

6.2 Robot Navigation

For the related applications of ODI/ODV in robot navigation, it includes the telepresence system, surveillance, and DL-based optimization methods. The telepresence system aims to overcome space constraints to enable people to remotely visit and interact with each other. ODI/ODV is gaining popularity by providing a more realistic and natural scene, especially in outdoor activities with open environments [85]. [306] proposes a prototype of an ODV-based telepresence system to support more natural interactions and remote environment exploration, where real walking in the remote environment can simultaneously control the relevant movement of the robot platform. Surveillance aims to replace humans for security purposes, in which the calibration is vital for sensitive data. Accordingly, Pudics *et al.* [181] proposed a safe navigation system tailored for obstacle detection and avoidance with a calibration design to obtain the proper distance and direction. Compared with NFoV images, ODIs can reduce the computational cost significantly by providing complete FoV in a single shot. Moreover, Ran *et al.* [186] proposed a lightweight framework based on the uncalibrated 360° cameras. The framework can accurately estimate the heading direction by formulating it into a series of classification tasks and avoid redundant computation by saving the calibration and correction processes. To address dark environments, *e.g.*, underground mine, Mansouri *et al.* [159] utilized online heading rate commands to avoid collision in the tunnels and calculated scene depth information online.

6.3 Autonomous Driving

It requires a full understanding of the surrounding environment, which omnidirectional vision excels at. Some works focus on setting up 360° platform for autonomous driving [14]. Specifically, [14] introduced a multi-modal 360° perception proposal based on visual and LiDAR scanners for 3D object detection and tracking. In addition to the platform, the emergence of public omnidirectional datasets for autonomous driving is crucial for the application of DL methods. Caesar *et al.* [19] were

the first to introduce the relevant dataset which carries six cameras, five radars, and one LiDAR. All devices are with 360° FoV. Recently, OpenMP dataset [311] is captured by six cameras and four LiDARs, which contains scenes in a complex environment, *e.g.*, urban areas with overexposure or darkness.

7 Discussion and New Perspectives

Cons. of Projection Formats. ERP is the most prevalent projection format due to its wide FoV in a planar format. The main challenge for ERP is the increasing stretching distortion towards poles. Therefore, many works were proposed to design specific convolution filters against the distortion [45, 214]. By contrast, CP and tangent images are distortion-less projection formats by projecting a spherical surface into multiple planes. They are similar to the perspective images and therefore can make full use of many pre-trained models and datasets in the planar domain [140]. However, CP and tangent images suffer from the challenges of higher computational cost, discrepancy, and discontinuity.

We summarize two potential directions for utilizing CP and tangent images: (i) Redundant computational costs are resulted from large overlapping regions between projection planes. However, the pixel density varies among different sampling positions. The computation can be more efficient by allocating more resources for dense regions (*e.g.*, equator) and fewer resources for sparse regions (*e.g.*, poles) with reinforcement learning [58]. (ii) Currently, different projection planes are often processed in parallel, which lacks global consistency. To overcome the discrepancy among different local planes, it is effective to explore an additional branch with ERP as the input [237] or attention-based transformers to construct non-local dependencies [140]. However, these constraints are mainly added to the feature maps, instead of the predictions. Moreover, the discrepancy can be also solved from the distribution consistency of predictions, *e.g.*, the consistent depth range among different planes and the consistent uncertainty scores for the same edges and large gradient regions.

Data-efficient Learning. A challenge for DL methods is the need for large-scale datasets with high-quality annotations. However, for omnidirectional vision, constructing large-scale datasets is expensive and tedious. Therefore, it is necessary to explore more data-efficient methods. One promising direction is to transfer the knowledge learned from models trained on the labeled 2D dataset to models to be trained on the unlabeled panoramic dataset. Specifically, domain adaptation approaches can be applied to narrow the gap between perspective images and ODIs [157]. KD is also an effective solution by transferring learned feature information

from a cumbersome perspective DNN model to a compact DNN model learning ODI data [276]. Finally, recent success of self-supervised methods, *e.g.*, [270], demonstrates the effectiveness and necessity of pre-training models, which is still a blank for omnidirectional vision.

Optical aberrations. With the growing demand for wearable devices, panoramic imaging systems face increasing requirements for lightweight and compact designs. While building minimalist panoramic imaging systems, how to correct optical aberrations and improve imaging quality remains a significant challenge. Recent efforts in computational aberration correction for panoramic imaging have focused on Panoramic Annular Lenses (PALs)[180]. ACI [107] introduced a learning-based framework that leverages physical priors and a physics-informed engine [13] to correct panoramic optical aberrations. More recently, based on the Point Spread Function, Jiang [106] proposed a transformer-based architecture, trained on synthetic datasets from simulation, to achieve accurate aberration correction in minimalist panoramic imaging systems. Despite its practical importance, research on computational methods for panoramic aberration correction remains limited compared to perspective imaging. Leveraging knowledge transfer strategies to utilize the abundant data from perspective images presents a promising direction to address the scarcity of real-world panoramic datasets.

Multi-modal Omnidirectional Vision. It refers to the process of learning representations from different types of modalities (*e.g.*, text-image for visual question answering, audio-visual scene understanding) and aligning them. This is a promising yet practical direction for omnidirectional vision. For instance, [14] introduces a multi-modal perception framework based on the visual and LiDAR information for 3D object detection and tracking. However, existing works in this direction treat ODIs as the perspective images and ignore the inherent distortion in the ODIs. Future works may explore how to utilize the advantage of ODIs, *e.g.*, complete FoV, to assist the representation of other modalities. Importantly, with the success of large-scale language models and vision models, it is desired to explore how to adapt these large-scale model on spherical imaging ODI data.

Potential for Adversarial Attacks. There exist few studies focusing on adversarial attacks towards omnidirectional vision models. Zhang *et al.* [316] proposed the first and representative attack approach to fool DNN models by perturbing only one tangent image rendered from the ODI. The proposed attack is sparse as it disturbs only a small part of the input ODI. Therefore, they further proposed a position searching method to search for the tangent point on the spherical surface. There are numerous promising yet challenging research

problems in this direction, *e.g.*, analyzing the generalization capacity of attacks among different DNN models for ODIs, white-box attacks for network architectures and training methods, and defenses against attacks.

Connections to Fisheye Images. Both ODIs and fisheye images are with wide field-of-views (FoVs), but they differ in scope. ODIs capture a full 360° spherical view of the surrounding environment, providing a complete and continuous representation of the scene. In contrast, fisheye images capture a wide but limited FoV, typically up to 200°. While fisheye cameras are more compact and straightforward in design, they are constrained by significant distortion and a partial view of the scene. Nowadays, fisheye images are commonly used in multi-camera systems to create surround-view systems for urban driving applications. Notably, there are several reviews and introductions [97, 182, 207] for fisheye images. Readers are encouraged to refer to these studies for further exploration.

8 Conclusion

In this survey, we comprehensively reviewed and analyzed the recent progress of DL methods for omnidirectional vision. We first introduced the principle of omnidirectional image acquisition, diverse projections, and datasets. We then presented a analytical explanation for distinctive representation learning and described the development of popular optimization strategies for omnidirectional vision. We further provided a hierarchical and structural taxonomy of the DL methods. For each task in the taxonomy, we summarized the current research status and compared existing algorithms, so that researchers can quickly understand the existing research directions. After constructing connections among current approaches via reviewing the practical applications, we discussed the pivotal problems to be solved and indicated promising future research opportunities. We hope this work can promote progress in the community.

Data Availability Statement

Data availability is not applicable to this article as no new data were created or analyzed in this study

References

1. Yasser Abdelaziz, Dahou Djilali, Tarun Krishna, Kevin McGuinness, and Noel E. O'Connor. Rethinking^o 360 image visual attention modelling with unsupervised learning. *ICCV*, 2021.
2. Hao Ai, Zidong Cao, Yan-Pei Cao, Ying Shan, and Lin Wang. Hrdfuse: Monocular 360 depth estimation by collaboratively learning holistic-with-regional depth distributions. In *CVPR*, 2023.
3. Hao Ai, Zidong Cao, H. Lu, Chen Chen, Jiancang Ma, Pengyuan Zhou, Tae-Kyun Kim, Pan Hui, and Lin Wang. Dream360: Diverse and immersive outdoor virtual scene creation via transformer-based 360 image outpainting. *TVCG*, 2024.
4. Naofumi Akimoto, Seito Kasai, Masaki Hayashi, and Yoshimitsu Aoki. 360-degree image completion by two-stage conditional gans. In *ICIP*, 2019.
5. Naofumi Akimoto, Yuhi Matsuo, and Yoshimitsu Aoki. Diverse plausible 360-degree image outpainting for efficient 3d background creation. *CVPR*, 2022.
6. Georgios Albanis, Nikolaos Zioulis, Petros Drakoulis, V. Gkitsas, Vladimiro Sterzentsenko, et al. Pano3d: A holistic benchmark and a solid baseline for 360° depth estimation. *CVPR Workshop*, 2021.
7. André Apitzsch, Roman Seidel, and Gangolf Hirtz. Cubes3d: Neural network based optical flow in omnidirectional image scenes. *arXiv preprint arXiv:1804.09004*, 2018.
8. Iro Armeni, Sasha Sax, Amir R Zamir, and Silvio Savarese. Joint 2d-3d-semantic data for indoor scene understanding. *ArXiv*, 2017.
9. Charles-Olivier Artizzu, Haozhou Zhang, Guillaume Allibert, and Cédric Demonceaux. Omniflownet: a perspective neural network adaptation for optical flow estimation in omnidirectional images. *ICPR*, 2021.
10. Jiayang Bai, Shuichang Lai, Haoyu Qin, Jie Guo, and Yanwen Guo. Gplanodepth: Global-to-local panoramic depth estimation. *arXiv*, 2022.
11. Yixuan Ban, Yuanxing Zhang, Haodan Zhang, Xinggong Zhang, and Zongming Guo. Ma360: Multi-agent deep reinforcement learning based live 360-degree video streaming on edge. *ICME*, pages 1–6, 2020.
12. Omer Bar-Tal, Lior Yariv, Yaron Lipman, and Tali Dekel. Multidiffusion: Fusing diffusion paths for controlled image generation. In *ICML*, 2023.
13. George Barbastathis, Aydogan Ozcan, and Guohai Situ. On the use of deep learning for computational imaging. *Optica*, 6(8):921–943, 2019.
14. Jorge Beltrán, Carlos Guindel, Irene Cortés, Alejandro Barrera, Armando Astudillo, Jesús Urdiales, Mario Álvarez, Farid Bekka, Vicente Milanés, and Fernando García. Towards autonomous driving: a multi-modal 360° perception proposal. In *ITSC*, 2020.
15. Bruno Berenguel-Baeta, Jesus Bermudez-Cameo, and Jose J Guerrero. Scaled 360 layouts: Revisiting non-central panoramas. In *CVPR*, 2021.
16. Bruno Berenguel-Baeta, Jesus Bermudez-Cameo, and Jose J Guerrero. Atlanta scaled layouts from non-central panoramas. *PR*, 2022.
17. Keshav Bhandari, Bin Duan, Gaowen Liu, Hugo Latapie, Ziliang Zong, and Yan Yan. Learning omnidirectional flow in 360° video via siamese representation. In *ECCV*, 2022.
18. Keshav Bhandari, Ziliang Zong, and Yan Yan. Revisiting optical flow estimation in 360 videos. In *2020 25th International Conference on Pattern Recognition (ICPR)*, pages 8196–8203. IEEE, 2021.
19. Holger Caesar, Varun Bankiti, Alex H Lang, Sourabh Vora, Venice Erin Liong, Qiang Xu, Anush Krishnan, Yu Pan, Giancarlo Baldan, and Oscar Beijbom. nuscenes: A multi-modal dataset for autonomous driving. In *CVPR*, 2020.
20. Miao Cao, Satoshi Ikehata, and Kiyoharu Aizawa. Field-of-view iou for object detection in 360° images. *IEEE TIP*, 2022.
21. Ming Cao, Chong Mou, Fang Yu, et al. Ntire 2023 challenge on 360° omnidirectional image and video super-resolution: Datasets, methods and results. *CVPR Workshop*, 2023.

22. Zidong Cao, Hao Ai, Yan-Pei Cao, Ying Shan, Xiaohu Qie, and Lin Wang. Omnizoomer: Learning to move and zoom in on sphere at high-resolution. In *ICCV*, 2023.
23. David Caruso, Jakob J. Engel, and Daniel Cremers. Large-scale direct slam for omnidirectional cameras. *IROS*, 2015.
24. Xiongli Chai and Feng Shao. Blind quality assessment of omnidirectional videos using spatio-temporal convolutional neural networks. *Optik*, 2021.
25. Angel Chang, Angela Dai, Thomas Funkhouser, Maciej Halber, Matthias Niessner, Manolis Savva, Shuran Song, Andy Zeng, and Yinda Zhang. Matterport3d: Learning from rgb-d data in indoor environments. *ArXiv*, 2017.
26. Shih-Hsiu Chang, Ching-Ya Chiu, Chia-Sheng Chang, et al. Generating 360 outdoor panorama dataset with reliable sun position estimation. *SIGGRAPH Asia 2018 Posters*, 2018.
27. Wenjie Chang, Yueyi Zhang, and Zhiwei Xiong. Depth estimation from indoor panoramas with neural scene representation. In *Proceedings of the IEEE/CVF Conference on Computer Vision and Pattern Recognition*, pages 899–908, 2023.
28. Dexiong Chen, Leslie O’Bray, and Karsten M. Borgwardt. Structure-aware transformer for graph representation learning. In *International Conference on Machine Learning*, 2022.
29. Dongwen Chen, Chunmei Qing, Xuan Lin, Mengtao Ye, Xiangmin Xu, and Patrick Dickinson. Intra- and inter-reasoning graph convolutional network for saliency prediction on 360° images. *IEEE TCST*, 2022.
30. Dongwen Chen, Chunmei Qing, Xiangmin Xu, and Huan-sheng Zhu. Salbinet360: Saliency prediction on 360° images with local-global bifurcated deep network. *IEEE VR*, 2020.
31. Gang Chen, Feng Shao, Xiongli Chai, Qiuping Jiang, and Yo-Sung Ho. Multi-stage salient object detection in 360° omnidirectional image using complementary object-level semantic information. *IEEE TETCI*, 2024.
32. Hao Chen, Yuqi Hou, Chenyuan Qu, Irene Testini, Xiaohan Hong, and Jianbo Jiao. 360+ x: A panoptic multi-modal scene understanding dataset. In *Proceedings of the IEEE/CVF Conference on Computer Vision and Pattern Recognition*, pages 19373–19382, 2024.
33. Shoufa Chen, Pei Sun, Yibing Song, and Ping Luo. Diffusiondet: Diffusion model for object detection. *ICCV*, 2022.
34. Sijia Chen, Yingxue Zhang, Yiming Li, Zhenzhong Chen, and Zhou Wang. Spherical structural similarity index for objective omnidirectional video quality assessment. *ICME*, 2018.
35. Yinpeng Chen, Xiyang Dai, Mengchen Liu, Dongdong Chen, Lu Yuan, and Zicheng Liu. Dynamic convolution: Attention over convolution kernels. *CVPR*, pages 11027–11036, 2019.
36. Yuzhong Chen, Yu Du, Zhe Xiao, Lin Zhao, Lu Zhang, David Liu, Dajiang Zhu, Tuo Zhang, Xintao Hu, Tianming Liu, and Xi Jiang. A unified and biologically-plausible relational graph representation of vision transformers. *IEEE TNNLS*, 2022.
37. Zhaoxi Chen, Guangcong Wang, and Ziwei Liu. Text2light: Zero-shot text-driven hdr panorama generation. *TOG*, 2022.
38. Zhenzhong Chen, Yiming Li, and Yingxue Zhang. Recent advances in omnidirectional video coding for virtual reality: Projection and evaluation. *Signal Process.*, 2018.
39. Zisong Chen, Chunyu Lin, Nie Lang, Kang Liao, and Yao Zhao. Unsupervised omnimvs: Efficient omnidirectional depth inference via establishing pseudo-stereo supervision. *IROS*, 2023.
40. Hsien-Tzu Cheng, Chun-Hung Chao, Jin-Dong Dong, Hao-Kai Wen, Tyng-Luh Liu, and Min Sun. Cube padding for weakly-supervised saliency prediction in 360 videos. In *CVPR*, 2018.
41. Sungmin Cho, Raehyuk Jung, and Junseok Kwon. Sampling based spherical transformer for 360 degree image classification. *Expert Systems with Applications*, 2024.
42. Shih-Han Chou, Cheng Sun, Wen-Yen Chang, Wan-Ting Hsu, Min Sun, and Jianlong Fu. 360-indoor: towards learning real-world objects in 360deg indoor equirectangular images. In *WACV*, 2020.
43. Taco Cohen, Maurice Weiler, Berkay Kicanaoglu, and Max Welling. Gauge equivariant convolutional networks and the icosahedral cnn. In *ICML*, 2019.
44. Taco Cohen and Max Welling. Group equivariant convolutional networks. In *International conference on machine learning*. PMLR, 2016.
45. Benjamin Coors, Alexandru Paul Condurache, and Andreas Geiger. Spherenet: Learning spherical representations for detection and classification in omnidirectional images. In *ECCV*, 2018.
46. James M. Coughlan and Alan Loddon Yuille. The manhattan world assumption: Regularities in scene statistics which enable bayesian inference. In *NIPS*, 2000.
47. Steve Cruz, Will Hutchcroft, Yuguang Li, Naji Khosravan, Ivaylo Boyadzhiev, and Sing Bing Kang. Zillow indoor dataset: Annotated floor plans with 360deg panoramas and 3d room layouts. In *CVPR*, 2021.
48. Thiago L. T. da Silveira, Paulo G. L. Pinto, Jeffri Murrugarra-Llerena, and Cl’audio Rosito Jung. 3d scene geometry estimation from 360° imagery: A survey. *ACM CSUR*, 2022.
49. Feng Dai, Youqiang Zhang, Yike Ma, Hongliang Li, and Qiang Zhao. Dilated convolutional neural networks for panoramic image saliency prediction. *ICASSP*, 2020.
50. Mohammad Reza Karimi Dastjerdi, Yannick Hold-Geoffroy, Jonathan Eisenmann, Siavash Khodadadeh, and Jean-François Lalonde. Guided co-modulated gan for 360° field of view extrapolation. *3DV*, 2022.
51. Mohammad Reza Karimi Dastjerdi, Yannick Hold-Geoffroy, Jonathan Eisenmann, and Jean-François Lalonde. Everlight: Indoor-outdoor editable hdr lighting estimation. *ICCV*, 2023.
52. Roberto Gerson de Albuquerque Azevedo, Neil Birkbeck, Ivan Janatra, Balu Adsumilli, and Pascal Frossard. A viewport-driven multi-metric fusion approach for 360-degree video quality assessment. *ICME*, 2020.
53. Bhisma Dedhia, Jui-Chiu Chiang, and Yi-Fan Char. Saliency prediction for omnidirectional images considering optimization on sphere domain. *ICASSP*, 2019.
54. Michaël Defferrard, Martino Milani, Frédéric Gussat, and Nathanaël Perraudin. DeepSphere: a graph-based spherical cnn. In *ICLR*, 2020.
55. Li Deng. The mnist database of handwritten digit images for machine learning research. *IEEE Signal Processing Magazine*, 29(6):141–142, 2012.
56. Liuyuan Deng, Ming Yang, Hao Li, Tianyi Li, Bing Hu, and Chunxiang Wang. Restricted deformable convolution-based road scene semantic segmentation using surround view cameras. *IEEE TITS*, 2020.
57. Liuyuan Deng, Ming Yang, Yeqiang Qian, Chunxiang Wang, and Bing Wang. Cnn based semantic segmentation for urban traffic scenes using fisheye camera. *IV*, 2017.
58. Xin Deng, Hao Wang, Mai Xu, Yichen Guo, Yuhang Song, and Li Yang. Lau-net: Latitude adaptive upscaling network for omnidirectional image super-resolution. *CVPR*, 2021.

59. Ibrahim Djemai, Sid Ahmed Fezza, Wassim Hamidouche, and Olivier Déforges. Extending 2d saliency models for head movement prediction in 360-degree images using cnn-based fusion. *ISCAS*, 2020.
60. Yuan Dong, Chuangjie Fang, Zilong Dong, Liefeng Bo, and Ping Tan. Panocontext-former: Panoramic total scene understanding with a transformer. *ArXiv*, 2023.
61. Alexey Dosovitskiy, Lucas Beyer, Alexander Kolesnikov, Dirk Weissenborn, Xiaohua Zhai, Thomas Unterthiner, Mostafa Dehghani, Matthias Minderer, Georg Heigold, Sylvain Gelly, et al. An image is worth 16x16 words: Transformers for image recognition at scale. *ICLR*, 2020.
62. Huiyu Duan, Guangtao Zhai, Xiongkuo Min, Yucheng Zhu, Yi Fang, and Xiaokang Yang. Perceptual quality assessment of omnidirectional images. *ISCAS*, 2018.
63. Marc Eder, Pierre Moulon, and Li Guan. Pano popups: Indoor 3d reconstruction with a plane-aware network. In *3DV*, 2019.
64. Marc Eder, Mykhailo Shvets, John Lim, and Jan-Michael Frahm. Tangent images for mitigating spherical distortion. In *CVPR*, 2020.
65. Jakob J. Engel, Thomas Schöps, and Daniel Cremers. Lsdslam: Large-scale direct monocular slam. In *European Conference on Computer Vision*, 2014.
66. Patrick Esser, Robin Rombach, and Björn Ommer. Taming transformers for high-resolution image synthesis. *CVPR*, 2020.
67. Brandon Yushan Feng, Wangjue Yao, Zheyuan Liu, and Amitabh Varshney. Deep depth estimation on 360 images with a double quaternion loss. In *3DV*, 2020.
68. Qi Feng, Hubert PH Shum, and Shigeo Morishima. 360 depth estimation in the wild-the depth360 dataset and the segfuse network. In *VR*, 2022.
69. Clara Fernandez-Labrador, José M. Fácil, Alejandro Pérez-Yus, Cédric Demonceaux, Javier Civera, and Josechu J. Guerrero. Corners for layout: End-to-end layout recovery from 360 images. *RAL*, 2020.
70. Clara Fernandez-Labrador, Alejandro Perez-Yus, Gonzalo Lopez-Nicolas, and Jose J Guerrero. Layouts from panoramic images with geometry and deep learning. *RAL*, 2018.
71. María Flores, David Valiente, Adrián Peidró, Oscar Reinoso, and Luis Payá. Generating a full spherical view by modeling the relation between two fisheye images. *The Visual Computer*, pages 1–26, 2024.
72. Jun Fu, Chengbin Hou, Wei Zhou, Jiahua Xu, and Zhibo Chen. Adaptive hypergraph convolutional network for no-reference 360-degree image quality assessment. *ACM MM*, 2021.
73. Pan Gao, Pengwei Zhang, and Aljosa Smolic. Quality assessment for omnidirectional video: A spatio-temporal distortion modeling approach. *TMM*, 2022.
74. Shaohua Gao, Kailun Yang, Hao Shi, Kaiwei Wang, and Jian Bai. Review on panoramic imaging and its applications in scene understanding. *IEEE Transactions on Instrumentation and Measurement*, 71:1–34, 2022.
75. Marc-André Gardner, Yannick Hold-Geoffroy, Kalyan Sunkavalli, Christian Gagné, and Jean-François Lalonde. Deep parametric indoor lighting estimation. *ICCV*, 2019.
76. Marc-André Gardner, Kalyan Sunkavalli, Ersin Yumer, Xiaohui Shen, Emiliano Gambaretto, Christian Gagné, and Jean-François Lalonde. Learning to predict indoor illumination from a single image. *TOG*, 2017.
77. Mathieu Garon, Kalyan Sunkavalli, Sunil Hadap, Nathan A. Carr, and Jean-François Lalonde. Fast spatially-varying indoor lighting estimation. *CVPR*, 2019.
78. Ian Goodfellow, Jean Pouget-Abadie, Mehdi Mirza, Bing Xu, David Warde-Farley, Sherjil Ozair, Aaron Courville, and Yoshua Bengio. Generative adversarial nets. *NIPS*, 2014.
79. Krzysztof M. Gorski, Eric Hivon, A. J. Banday, Benjamin Dan Wandelt, Frode K. Hansen, Martin Reinecke, and M. Bartelman. Healpix: A framework for high-resolution discretization and fast analysis of data distributed on the sphere. *The Astrophysical Journal*, 2005.
80. Byeong-Ju Han and Jae-Young Sim. Zero-shot learning for reflection removal of single 360-degree image. In *European Conference on Computer Vision*, pages 533–548. Springer, 2022.
81. Seo Woo Han and Doug Young Suh. Piinet: A 360-degree panoramic image inpainting network using a cube map. *arXiv*, 2020.
82. Takayuki Hara and Tatsuya Harada. Enhancement of novel view synthesis using omnidirectional image completion. *ArXiv*, 2022.
83. Takayuki Hara, Yusuke Mukuta, and Tatsuya Harada. Spherical image generation from a single image by considering scene symmetry. In *AAAI*, 2021.
84. Kaiming He, X. Zhang, Shaoqing Ren, and Jian Sun. Deep residual learning for image recognition. *CVPR*, 2016.
85. Yasamin Heshmat, Brennan Jones, Xiaoxuan Xiong, Carman Neustaedter, Anthony Tang, Bernhard E. Riecke, and Lillian Yang. Geocaching with a beam: Shared outdoor activities through a telepresence robot with 360 degree viewing. *CHI*, 2018.
86. Jonathan Ho and Stefano Ermon. Generative adversarial imitation learning. In *NIPS*, 2016.
87. Yannick Hold-Geoffroy, Akshaya Athawale, and Jean-François Lalonde. Deep sky modeling for single image outdoor lighting estimation. In *CVPR*, 2019.
88. Yannick Hold-Geoffroy, Kalyan Sunkavalli, Sunil Hadap, Emiliano Gambaretto, and Jean-François Lalonde. Deep outdoor illumination estimation. *CVPR*, 2017.
89. Yuchen Hong, Qian Zheng, Lingran Zhao, Xudong Jiang, Alex C Kot, and Boxin Shi. Panoramic image reflection removal. In *Proceedings of the IEEE/CVF Conference on Computer Vision and Pattern Recognition*, pages 7762–7771, 2021.
90. Yuchen Hong, Qian Zheng, Lingran Zhao, Xudong Jiang, Alex C Kot, and Boxin Shi. Par 2 net: End-to-end panoramic image reflection removal. *IEEE Transactions on Pattern Analysis and Machine Intelligence*, 45(10):12192–12205, 2023.
91. Alain Horé and Djemel Ziou. Image quality metrics: Psnr vs. ssim. *ICPR*, 2010.
92. C. Y. Hsu, Cheng Sun, and Hwann-Tzong Chen. Moving in a 360 world: Synthesizing panoramic parallaxes from a single panorama. *ArXiv*, 2021.
93. Edward J Hu, yelong shen, Phillip Wallis, Zeyuan Allen-Zhu, Yuanzhi Li, Shean Wang, Lu Wang, and Weizhu Chen. LoRA: Low-rank adaptation of large language models. In *ICLR*, 2022.
94. Zongyao Hu, Lixiong Liu, and Qingbing Sang. Omnidirectional video quality assessment with causal intervention. *IEEE T-OB*, 2024.
95. Hu Huang and Sai-Kit Yeung. 360vo: Visual odometry using a single 360 camera. *2022 International Conference on Robotics and Automation (ICRA)*, pages 5594–5600, 2022.
96. Huajian Huang, Changkum Liu, Yipeng Zhu, Hui Cheng, Tristan Braud, and Sai-Kit Yeung. 360loc: A dataset and benchmark for omnidirectional visual localization with cross-device queries. In *Proceedings of the IEEE/CVF*

- Conference on Computer Vision and Pattern Recognition*, pages 22314–22324, 2024.
97. Daniel Jakab, Brian Michael Deegan, Sushil Sharma, Eoin Martino Grua, Jonathan Horgan, Enda Ward, Pepijn Van De Ven, Anthony Scanlan, and Ciarán Eising. Surround-view fisheye optics in computer vision and simulation: Survey and challenges. *IEEE Transactions on Intelligent Transportation Systems*, 2024.
 98. Alexander Jaus, Kailun Yang, and Rainer Stiefelwagen. Panoramic panoptic segmentation: Towards complete surrounding understanding via unsupervised contrastive learning. In *2021 IEEE Intelligent Vehicles Symposium (IV)*, pages 1421–1427. IEEE, 2021.
 99. Alexander Jaus, Kailun Yang, and Rainer Stiefelwagen. Panoramic panoptic segmentation: Insights into surrounding parsing for mobile agents via unsupervised contrastive learning. *IEEE Transactions on Intelligent Transportation Systems*, 24(4):4438–4453, 2023.
 100. Maleen Jayasuriya, Ravindra Ranasinghe, and Gamini Dissanayake. Active perception for outdoor localisation with an omnidirectional camera. *2020 IEEE/RSJ International Conference on Intelligent Robots and Systems (IROS)*, pages 4567–4574, 2020.
 101. Shunping Ji, Zijie Qin, Jie Shan, and Meng Lu. Panoramic slam from a multiple fisheye camera rig. *ISPRS Journal of Photogrammetry and Remote Sensing*, 159:169–183, 2020.
 102. Haijing Jia, Hong Yi, Hirochika Fujiki, Hengzhi Zhang, Wei Wang, and Makoto Odamaki. 3d room layout recovery generalizing across manhattan and non-manhattan worlds. *CVPR Workshop*, 2022.
 103. Chiyu Max Jiang, Jingwei Huang, Karthik Kashinath, Prabhat, Philip Marcus, and Matthias Niessner. Spherical cnns on unstructured grids. In *ICLR*, 2019.
 104. Hao Jiang, Gang yi Jiang, Mei Yu, Yun Zhang, You Yang, Zongju Peng, Fen Chen, and Qingbo Zhang. Cubemap-based perception-driven blind quality assessment for 360-degree images. *TIP*, 2021.
 105. Hualie Jiang, Zhe Sheng, Siyu Zhu, Zilong Dong, and Rui Huang. Unifuse: Unidirectional fusion for 360 panorama depth estimation. *RAL*, 2021.
 106. Qi Jiang, Shaohua Gao, Yao Gao, Kailun Yang, Zhonghua Yi, Hao Shi, Lei Sun, and Kaiwei Wang. Minimalist and high-quality panoramic imaging with psf-aware transformers. *IEEE Transactions on Image Processing*, 2024.
 107. Qi Jiang, Hao Shi, Lei Sun, Shaohua Gao, Kailun Yang, and Kaiwei Wang. Annular computational imaging: Capture clear panoramic images through simple lens. *IEEE Transactions on Computational Imaging*, 8:1250–1264, 2022.
 108. San Jiang, Yaxin Li, Duojie Weng, Kan You, and Wu Chen. 3d reconstruction of spherical images: A review of techniques, applications, and prospects. *ArXiv*, 2023.
 109. Zhigang Jiang, Zhongzheng Xiang, Jinhua Xu, and Ming Zhao. Lgt-net: Indoor panoramic room layout estimation with geometry-aware transformer network. In *CVPR*, 2022.
 110. Zhiqian Jiang, Xu Zhang, Yiling Xu, Zhan Ma, Jun Sun, and Yunfei Zhang. Reinforcement learning based rate adaptation for 360-degree video streaming. *IEEE T-OB*, 2020.
 111. Lei Jin, Yanyu Xu, Jia Zheng, Junfei Zhang, Rui Tang, Shugong Xu, Jingyi Yu, and Shenghua Gao. Geometric structure based and regularized depth estimation from 360 indoor imagery. In *CVPR*, 2020.
 112. Nuowen Kan, Junni Zou, Chenglin Li, Wenrui Dai, and Hongkai Xiong. Rapt360: Reinforcement learning-based rate adaptation for 360-degree video streaming with adaptive prediction and tiling. *IEEE TCSVT*, 2021.
 113. Benjamin Keinert, Matthias Innmann, Michael Sanger, and Marc Stamminger. Spherical fibonacci mapping. *TOG*, 2015.
 114. Bernhard Kerbl, Georgios Kopanas, Thomas Leimkuehler, and George Drettakis. 3d gaussian splatting for real-time radiance field rendering. *ACM Transactions on Graphics (TOG)*, 42:1 – 14, 2023.
 115. Renata Khasanova and Pascal Frossard. Geometry aware convolutional filters for omnidirectional images representation. In *ICML*, 2019.
 116. Hak Gu Kim, Heoun taek Lim, and Yong Man Ro. Deep virtual reality image quality assessment with human perception guider for omnidirectional image. *IEEE TCSVT*, 2020.
 117. Hansung Kim, Luca Hernaggi, Philip J. B. Jackson, and Adrian Hilton. Immersive spatial audio reproduction for VR/AR using room acoustic modelling from 360° images. In *VR*, 2019.
 118. Hansung Kim and Adrian Hilton. 3d scene reconstruction from multiple spherical stereo pairs. *IJCV*, 2013.
 119. Junho Kim, Eungbean Lee, and Y. Kim. Calibrating panoramic depth estimation for practical localization and mapping. *2023 IEEE/CVF International Conference on Computer Vision (ICCV)*, pages 8796–8806, 2023.
 120. Christian Kinzig, Henning Miller, Martin Lauer, and Christoph Stiller. Panoptic segmentation from stitched panoramic view for automated driving. In *2024 IEEE Intelligent Vehicles Symposium (IV)*, pages 3342–3347. IEEE, 2024.
 121. Alexander Kirillov, Eric Mintun, Nikhila Ravi, Hanzi Mao, Chloe Rolland, Laura Gustafson, Tete Xiao, Spencer Whitehead, Alexander C Berg, Wan-Yen Lo, et al. Segment anything. In *Proceedings of the IEEE/CVF International Conference on Computer Vision*, pages 4015–4026, 2023.
 122. Aden Kittel, Paul Larkin, Ian Cunningham, and Michael Spittle. 360 virtual reality: A swot analysis in comparison to virtual reality. *Frontiers in Psychology*, 2020.
 123. A. Krizhevsky and G. Hinton. Learning multiple layers of features from tiny images. *Master’s thesis, Department of Computer Science, University of Toronto*, 2009.
 124. Bernd Krolla, Maximilian Diebold, Bastian Goldlücke, and Didier Stricker. Spherical light fields. In *BMVC*, 2014.
 125. Shreyas Kulkarni, Peng Yin, and Sebastian A. Scherer. 360fusionnerf: Panoramic neural radiance fields with joint guidance. *2023 IEEE/RSJ International Conference on Intelligent Robots and Systems (IROS)*, pages 7202–7209, 2022.
 126. Po Kong Lai, Shuang Xie, Jochen Lang, and Robert Laganière. Real-time panoramic depth maps from omnidirectional stereo images for 6 dof videos in virtual reality. In *2019 IEEE Conference on Virtual Reality and 3D User Interfaces (VR)*, pages 405–412. IEEE, 2019.
 127. Samuli Laine and Timo Aila. Temporal ensembling for semi-supervised learning. In *ICLR*, 2017.
 128. Jaewoo Lee, Dae Hyuck Park, Dongwook Lee, and Daehyun Ji. Semi-supervised 360° depth estimation from multiple fisheye cameras with pixel-level selective loss. *ICASSP*, 2022.
 129. Yeonkun Lee, Jaeseok Jeong, Jong Seob Yun, Wonjune Cho, and Kuk jin Yoon. Spherephd: Applying cnns on a spherical polyhedron representation of 360° images. *CVPR*, 2019.
 130. Chen Li, Mai Xu, Lai Jiang, Shanyi Zhang, and Xiaoming Tao. Viewport proposal cnn for 360° video quality assessment. *CVPR*, 2019.
 131. Jia Li, Yifan Zhao, Weihua Ye, Kaiwen Yu, and Shiming Ge. Attentive deep stitching and quality assessment for

- 360° omnidirectional images. *IEEE Journal of Selected Topics in Signal Processing*, 14(1):209–221, 2019.
132. Jialu Li and Mohit Bansal. Panogen: Text-conditioned panoramic environment generation for vision-and-language navigation. *Advances in Neural Information Processing Systems*, 36:21878–21894, 2023.
 133. Junnan Li, Dongxu Li, Silvio Savarese, and Steven Hoi. Blip-2: Bootstrapping language-image pre-training with frozen image encoders and large language models. In *International conference on machine learning*, pages 19730–19742. PMLR, 2023.
 134. Meng Li, Senbo Wang, Weihao Yuan, Weichao Shen, Zhe Sheng, and Zilong Dong. S2net: Accurate panorama depth estimation on spherical surface. *IEEE RAL*, 2023.
 135. Ming Li, Xueqian Jin, Xuejiao Hu, Jingzhao Dai, Sidan Du, and Yang Li. Mode: Multi-view omnidirectional depth estimation with 360° cameras. In *ECCV*, 2022.
 136. Shigang Li and Kiyotaka Fukumori. Spherical stereo for the construction of immersive vr environment. In *IEEE VR*, 2005.
 137. Shigang Li and Kiyotaka Fukumori. Spherical stereo for the construction of immersive vr environment. In *IEEE Proceedings. VR 2005. Virtual Reality, 2005.*, pages 217–222. IEEE, 2005.
 138. Xuewei Li, Tao Wu, Zhongang Qi, Gaoang Wang, Ying Shan, and Xi Li. Sgat4pass: Spherical geometry-aware transformer for panoramic semantic segmentation. In *IJCAI*, 2023.
 139. Yiheng Li, Connelly Barnes, Kun Huang, and Fang-Lue Zhang. Deep 360° optical flow estimation based on multi-projection fusion. In *European Conference on Computer Vision*, pages 336–352. Springer, 2022.
 140. Yuyan Li, Yuliang Guo, Zhixin Yan, Xinyu Huang, Ye Duan, and Liu Ren. Omnifusion: 360 monocular depth estimation via geometry-aware fusion. *CVPR*, 2022.
 141. Zhengqin Li, Mohammad Shafiei, Ravi Ramamoorthi, Kalyan Sunkavalli, and Manmohan Chandraker. Inverse rendering for complex indoor scenes: Shape, spatially-varying lighting and svbrdf from a single image. *CVPR*, 2020.
 142. Zhijun Li, Yumei Wang, and Yu Liu. Sad360: Spherical viewport-aware dynamic tiling for 360-degree video streaming. *VCIP*, 2022.
 143. Kang Liao, Xiangyu Xu, Chunyu Lin, Wenqi Ren, Yunchao Wei, and Yao Zhao. Cylin-painting: Seamless 360° panoramic image outpainting and beyond. *IEEE TIP*, 2022.
 144. Zhixin Ling, Zhen Xing, Xiangdong Zhou, Manliang Cao, and Guichun Zhou. Panoswin: A pano-style swin transformer for panorama understanding. In *CVPR*, 2023.
 145. Mengyi Liu, Shuhui Wang, Yulan Guo, Yuan He, and Hui Xue. Pano-sfmlearner: Self-supervised multi-task learning of depth and semantics in panoramic videos. *IEEE SPL*, 2021.
 146. Min Liu, Fupin Yao, Chiho Choi, Ayan Sinha, and Karthik Ramani. Deep learning 3d shapes using alt-az anisotropic 2-sphere convolution. In *ICLR*, 2018.
 147. Ruyi Liu, Guodao Zhang, Jiangming Wang, and Shuwen Zhao. Cross-modal 360° depth completion and reconstruction for large-scale indoor environment. *IEEE TITS*, 2022.
 148. Xinyuan Liu, Hang Xu, Bin Chen, Qiang Zhao, Yike Ma, Chenggang Clarence Yan, and Feng Dai. Sph2pob: Boosting object detection on spherical images with planar oriented boxes methods. In *IJCAI*, 2023.
 149. Xuelin Liu, Jiebin Yan, Liping Huang, Yuming Fang, Zheng Wan, and Yang Liu. Perceptual quality assessment of omnidirectional images: A benchmark and computational model. *ACM TOMM*, 2024.
 150. Ze Liu, Yutong Lin, Yue Cao, Han Hu, Yixuan Wei, Zheng Zhang, Stephen Lin, and Baining Guo. Swin transformer: Hierarchical vision transformer using shifted windows. *ICCV*, 2021.
 151. I-chan Lo, Kuang-tsu Shih, and Homer H Chen. Image stitching for dual fisheye cameras. In *2018 25th IEEE International Conference on Image Processing (ICIP)*, pages 3164–3168. IEEE, 2018.
 152. I-Chan Lo, Kuang-Tsu Shih, and Homer H Chen. Efficient and accurate stitching for 360° dual-fisheye images and videos. *IEEE Transactions on Image Processing*, 31:251–262, 2021.
 153. I-Chan Lo, Kuang-Tsu Shih, Gwo-Hwa Ju, and Homer H Chen. Photometric consistency for dual fisheye cameras. In *2020 IEEE International Conference on Image Processing (ICIP)*, pages 261–265. IEEE, 2020.
 154. Zhuqiang Lu, Kun Hu, Chaoyue Wang, Lei Bai, and Zhiyong Wang. Autoregressive omni-aware outpainting for open-vocabulary 360-degree image generation. *AAAI*, 2024.
 155. Bruce D Lucas and Takeo Kanade. An iterative image registration technique with an application to stereo vision. In *IJCAI’81: 7th international joint conference on Artificial intelligence*, volume 2, pages 674–679, 1981.
 156. Haoran Lv, Qin Yang, Chenglin Li, Wenrui Dai, Junni Zou, and Hongkai Xiong. Salgen: Saliency prediction for 360-degree images based on spherical graph convolutional networks. *ACM MM*, 2020.
 157. Chaoxiang Ma, Jiaming Zhang, Kailun Yang, Alina Roitberg, and Rainer Stiefelhagen. Densepass: Dense panoramic semantic segmentation via unsupervised domain adaptation with attention-augmented context exchange. *ITSC*, 2021.
 158. Pantelis Maniotis and Nikolaos Thomos. Viewport-aware deep reinforcement learning approach for 360° video caching. *TMM*, 2020.
 159. Sina Sharif Mansouri, Petros S. Karvelis, Christoforos Kanellakis, Dariusz Kominiak, and George Nikolakopoulos. Vision-based mav navigation in underground mine using convolutional neural network. *IECON*, 2019.
 160. Hidenobu Matsuki, Lukas von Stumberg, Vladyslav C. Usenko, J. Stückler, and Daniel Cremers. Omnidirectional dso: Direct sparse odometry with fisheye cameras. *IEEE Robotics and Automation Letters*, 3:3693–3700, 2018.
 161. Larry R Medsker and LC Jain. Recurrent neural networks. *Design and Applications*, 2001.
 162. Jieru Mei, Alex Zihao Zhu, Xinchun Yan, Hang Yan, Siyuan Qiao, Liang-Chieh Chen, and Henrik Kretzschmar. Waymo open dataset: Panoramic video panoptic segmentation. In *European Conference on Computer Vision*, pages 53–72. Springer, 2022.
 163. Andreas Meuleman, Hyeonjoong Jang, Daniel S. Jeon, and Min H. Kim. Real-time sphere sweeping stereo from multiview fisheye images. *CVPR*, 2021.
 164. Ben Mildenhall, Pratul P Srinivasan, Matthew Tancik, Jonathan T Barron, Ravi Ramamoorthi, and Ren Ng. Nerf: Representing scenes as neural radiance fields for view synthesis. *Communications of the ACM*, 65(1):99–106, 2021.
 165. Mehdi Mirza and Simon Osindero. Conditional generative adversarial nets. *ArXiv*, abs/1411.1784, 2014.
 166. Rafael Monroy, Sebastian Lutz, Tejo Chalasani, and Aljoscha Smolic. Salnet360: Saliency maps for omnidirectional images with cnn. *Signal Process. Image Commun.*, 2017.
 167. Anh Nguyen, Zhisheng Yan, and Klara Nahrstedt. Your attention is unique: Detecting 360-degree video saliency

- in head-mounted display for head movement prediction. *ACM MM*, 2018.
168. TH O’Beirne. Introduction to geometry. *Physics Bulletin*, 1962.
 169. Jeremy Ocampo, Matthew A. Price, and Jason D. McEwen. Scalable and equivariant spherical cnns by discrete-continuous convolutions. In *ICLR*, 2023.
 170. Changgyoon Oh, Wonjune Cho, Daehee Park, Yujeong Chae, Lin Wang, and Kuk-Jin Yoon. Bips: Bi-modal indoor panorama synthesis via residual depth-aided adversarial learning. *ArXiv*, 2021.
 171. Cagri Ozcinar, Julián Cabrera, and Aljosa Smolic. Visual attention-aware omnidirectional video streaming using optimal tiles for virtual reality. *IEEE JETCAS*, 2019.
 172. Cagri Ozcinar, Aakanksha Rana, and Aljosa Smolic. Super-resolution of omnidirectional images using adversarial learning. In *MMSP*, 2019.
 173. Jonghyuk Park, Hyeona Kim, Eunpil Park, and Jae-Young Sim. Fully-automatic reflection removal for 360-degree images. In *Proceedings of the IEEE/CVF Winter Conference on Applications of Computer Vision*, pages 1609–1617, 2024.
 174. Sohee Park, Minh Hoai, Arani Bhaacharya, and Samir R Das. Adaptive streaming of 360-degree videos with reinforcement learning. *WACV*, 2021.
 175. Shmuel Peleg and Moshe Ben-Ezra. Stereo panorama with a single camera. *CVPR*, 1999.
 176. Chi-Han Peng and Jiayao Zhang. High-resolution depth estimation for 360deg panoramas through perspective and panoramic depth images registration. In *Proceedings of the IEEE/CVF Winter Conference on Applications of Computer Vision*, pages 3116–3125, 2023.
 177. Giovanni Pintore, Marco Agus, and E. Gobbetti. Atlantantet: Inferring the 3d indoor layout from a single 360° image beyond the manhattan world assumption. In *ECCV*, 2020.
 178. Giovanni Pintore, Eva Almansa, Marco Agus, and Enrico Gobbetti. Deep3dlayout: 3d reconstruction of an indoor layout from a spherical panoramic image. *TOG*, 2021.
 179. Giovanni Pintore, Eva Almansa, and Jens Schneider. Slicenet: deep dense depth estimation from a single indoor panorama using a slice-based representation. *CVPR*, 2021.
 180. Ian Powell. Panoramic lens. *Applied Optics*, 33(31):7356–7361, 1994.
 181. Gyula Pudics, Miklos Zsolt Szabo-Resch, and Zoltán Vámosy. Safe robot navigation using an omnidirectional camera. *CINTI*, 2015.
 182. Ye qiang Qian, Ming Yang, and John M Dolan. Survey on fish-eye cameras and their applications in intelligent vehicles. *IEEE Transactions on Intelligent Transportation Systems*, 23(12):22755–22771, 2022.
 183. Minglang Qiao, Mai Xu, Zulin Wang, and Ali Borji. Viewport-dependent saliency prediction in 360° video. *TMM*, 2021.
 184. Alec Radford, Jong Wook Kim, Chris Hallacy, Aditya Ramesh, Gabriel Goh, Sandhini Agarwal, Girish Sastry, Amanda Askell, Pamela Mishkin, Jack Clark, Gretchen Krueger, and Ilya Sutskever. Learning transferable visual models from natural language supervision. In *ICML*, 2021.
 185. Yashas Rai, Jesús Gutiérrez, and Patrick Le Callet. A dataset of head and eye movements for 360 degree images. In *ACM MMSys*, 2017.
 186. Lingyan Ran, Yanning Zhang, Qilin Zhang, and Tao Yang. Convolutional neural network-based robot navigation using uncalibrated spherical images †. *Sensors*, 2017.
 187. René Ranftl, Alexey Bochkovskiy, and Vladlen Koltun. Vision transformers for dense prediction. In *ICCV*, 2021.
 188. Shaoqing Ren, Kaiming He, Ross B. Girshick, and Jian Sun. Faster r-cnn: Towards real-time object detection with region proposal networks. *IEEE T-PAMI*, 2015.
 189. Manuel Rey-Area, Mingze Yuan, and Christian Richardt. 360monodepth: High-resolution 360° monocular depth estimation. *CVPR*, 2022.
 190. Rafael Roberto, Daniel Perazzo, João Paulo Lima, Veronica Teichrieb, Jonysberg Peixoto Quintino, Fabio QB da Silva, Andre LM Santos, and Helder Pinho. Using local refinements on 360 stitching from dual-fisheye cameras. In *VISIGRAPP (5: VISAPP)*, pages 17–26, 2020.
 191. Jannick P Rolland and Hong Hua. Head-mounted display systems. *Encyclopedia of optical engineering*, 2005.
 192. Robin Rombach, A. Blattmann, Dominik Lorenz, Patrick Esser, and Björn Ommer. High-resolution image synthesis with latent diffusion models. *CVPR*, 2021.
 193. Grant Schindler and Frank Dellaert. Atlanta world: an expectation maximization framework for simultaneous low-level edge grouping and camera calibration in complex man-made environments. In *CVPR*, 2004.
 194. Roman Seidel, André Apitzsch, and Gangolf Hirtz. Omniflow: Human omnidirectional optical flow. *CVPR Workshops*, 2021.
 195. Hochang Seok and Jongwoo Lim. Rovo: Robust omnidirectional visual odometry for wide-baseline wide-fov camera systems. *2019 International Conference on Robotics and Automation (ICRA)*, pages 6344–6350, 2019.
 196. Hochang Seok and Jongwoo Lim. Rovins: Robust omnidirectional visual inertial navigation system. *IEEE Robotics and Automation Letters*, 5:6225–6232, 2020.
 197. Mehran Shakerinava and Siamak Ravanbakhsh. Equivariant networks for pixelized spheres. In *ICML*, 2021.
 198. Zhuoyi Shang, Yanwei Liu, Guoyi Li, Yunjian Zhang, Jingbo Miao, Jinxia Liu, and Liming Wang. Viewport-oriented panoramic image inpainting. In *ICIP*, 2022.
 199. Qing-Yang Shen, Tian-Guo Huang, Pengxin Ding, and Jiantao He. Training real-time panoramic object detectors with virtual dataset. *ICASSP*, 2021.
 200. Zhengyang Shen, Tiancheng Shen, Zhouchen Lin, and Jinwen Ma. Pdo-es2cnns: Partial differential operator based equivariant spherical cnns. In *AAAI*, 2021.
 201. Zhijie Shen, Chunyu Lin, Kang Liao, Lang Nie, Zishuo Zheng, and Yao Zhao. Panoflormer: Panorama transformer for indoor 360° depth estimation. In *ECCV*, 2022.
 202. Zhijie Shen, Zishuo Zheng, Chunyu Lin, Lang Nie, Kang Liao, Shuai Zheng, and Yao Zhao. Disentangling orthogonal planes for indoor panoramic room layout estimation with cross-scale distortion awareness. In *CVPR*, 2023.
 203. Hao Shi, Yifan Zhou, Kailun Yang, Xiaoting Yin, Ze Wang, Yaozu Ye, Zhe Yin, Shi Meng, Peng Li, and Kaiwei Wang. Panoflow: Learning 360° optical flow for surrounding temporal understanding. *IEEE Transactions on Intelligent Transportation Systems*, 24(5):5570–5585, 2023.
 204. Xingjian Shi, Zhourong Chen, Hao Wang, Dit-Yan Yeung, Wai-Kin Wong, and Wang-chun Woo. Convolutional lstm network: A machine learning approach for precipitation nowcasting. *NIPS*, 2015.
 205. Kashun Shum, Hong-Wing Pang, Binh-Son Hua, Duc Thanh Nguyen, and Sai-Kit Yeung. Conditional 360-degree image synthesis for immersive indoor scene decoration. *ICCV*, pages 4455–4465, 2023.
 206. Karen Simonyan and Andrew Zisserman. Very deep convolutional networks for large-scale image recognition. *ArXiv*, 2014.

207. Apoorv Singh. An overview of multi-view fisheye for vision-first autonomous driving. *Authorea Preprints*, 2024.
208. Vincent Sitzmann, Ana Serrano, Amy Pavel, Maneesh Agrawala, Diego Gutierrez, Belen Masia, and Gordon Wetzstein. Saliency in vr: How do people explore virtual environments? *TVCG*, 2018.
209. Kihyuk Sohn, Honglak Lee, and Xinchen Yan. Learning structured output representation using deep conditional generative models. In *NIPS*, 2015.
210. Gowri Somanath and Daniel Kurz. Hdr environment map estimation for real-time augmented reality. *CVPR*, 2021.
211. Shuran Song and Thomas A. Funkhouser. Neural illumination: Lighting prediction for indoor environments. *CVPR*, pages 6911–6919, 2019.
212. Julian Straub, Thomas Whelan, Lingni Ma, Yufan Chen, Erik Wijmans, Simon Green, Jakob J Engel, Raul Mur-Artal, Carl Ren, Shobhit Verma, et al. The replica dataset: A digital replica of indoor spaces. *ArXiv*, 2019.
213. Jheng-Wei Su, Chi-Han Peng, Peter Wonka, and Hung-Kuo Chu. Gpr-net: Multi-view layout estimation via a geometry-aware panorama registration network. In *CVPR*, 2023.
214. Yu-Chuan Su and Kristen Grauman. Learning spherical convolution for fast features from 360° imagery. In *NIPS*, 2017.
215. Yu-Chuan Su and Kristen Grauman. Kernel transformer networks for compact spherical convolution. *CVPR*, 2019.
216. Yu-Chuan Su and Kristen Grauman. Learning spherical convolution for 360 recognition. *TPAMI*, 2021.
217. Xiangjie Sui, Hanwei Zhu, Xuelin Liu, Yuming Fang, Shiqi Wang, and Zhou Wang. Perceptual quality assessment of 360° images based on generative scanpath representation. *ArXiv*, 2023.
218. Cheng Sun, Chi-Wei Hsiao, Min Sun, and Hwann-Tzong Chen. Horizonnet: Learning room layout with 1d representation and pano stretch data augmentation. *CVPR*, 2019.
219. Cheng Sun, Min Sun, and Hwann-Tzong Chen. Hohonet: 360 indoor holistic understanding with latent horizontal features. In *CVPR*, 2021.
220. Cheng Sun, Wei-En Tai, Yu-Lin Shih, Kuan-Wei Chen, Yong-Jing Syu, Kent Selwyn The, Yu-Chiang Frank Wang, and Hwann-Tzong Chen. Seg2reg: Differentiable 2d segmentation to 1d regression rendering for 360 room layout reconstruction. *ArXiv*, 2023.
221. Wei Sun, Ke Gu, Guangtao Zhai, Siwei Ma, Weisi Lin, and Patrick Le Callet. Cviqd: Subjective quality evaluation of compressed virtual reality images. *ICIP*, 2017.
222. Wei Sun, Xiongkuo Min, Guangtao Zhai, Ke Gu, Huiyu Duan, and Siwei Ma. Mc360iqa: A multi-channel cnn for blind 360-degree image quality assessment. *IEEE J-STSP*, 2020.
223. Yule Sun, Ang Lu, and Lu Yu. Weighted-to-spherically-uniform quality evaluation for omnidirectional video. *IEEE SPL*, 2017.
224. Tatsuya Suzuki and Takao Yamanaka. Saliency map estimation for omni-directional image considering prior distributions. *SMC*, 2018.
225. Heoun taek Lim, Hak Gu Kim, and Yong Man Ro. Vr iqa net: Deep virtual reality image quality assessment using adversarial learning. *ICASSP*, 2018.
226. Keisuke Tateno, Nassir Navab, and Federico Tombari. Distortion-aware convolutional filters for dense prediction in panoramic images. In *ECCV*, 2018.
227. Chongzhen Tian, Feng Shao, Xiongli Chai, Qiuping Jiang, Long Xu, and Yo-Sung Ho. Viewport-sphere-branch network for blind quality assessment of stitched 360° omnidirectional images. *IEEE TCSVT*, 2023.
228. Nafiseh Jabbari Tofghi, Mohamed Hedi Elfkir, Nevrez Imamoglu, Cagri Ozcinar, Erkut Erdem, and Aykut Erdem. St360iq: No-reference omnidirectional image quality assessment with spherical vision transformers. *ICASSP*, 2023.
229. Guofeng Tong, Huairong Chen, Yong Li, Xiance Du, and Qingchun Zhang. Object detection for panoramic images based on ms-rpn structure in traffic road scenes. *IET Comput. Vis.*, 2019.
230. Guilherme Luz Tortorella, João Ascenso, Catarina Brites, and Fernando Pereira. Saliency-driven omnidirectional imaging adaptive coding: Modeling and assessment. *MMSP*, 2017.
231. Phi Vu Tran. Sslayout360: Semi-supervised indoor layout estimation from 360° panorama. *CVPR*, 2021.
232. Hayat Ullah, Osama Zia, Jun Ho Kim, Kyungjin Han, and Jong Weon Lee. Automatic 360 mono-stereo panorama generation using a cost-effective multi-camera system. *Sensors*, 20(11):3097, 2020.
233. Evgeniy Upenik, Martin Rerábek, and Touradj Ebrahimi. Testbed for subjective evaluation of omnidirectional visual content. *PCS*, 2016.
234. Tran Thi Hai Uyen, Oh-Jin Kwon, Seungcheol Choi, and Ikram Hussain. Subjective assessment of 360° image projection formats. *IEEE Access*, 2020.
235. Rafael Grompone Von Gioi, Jeremie Jakubowicz, Jean-Michel Morel, and Gregory Randall. Lsd: A fast line segment detector with a false detection control. *PAMI*, 2008.
236. Fu-En Wang, Hou-Ning Hu, Hsien-Tzu Cheng, Juan-Ting Lin, Shang-Ta Yang, Meng-Li Shih, Hung-Kuo Chu, and Min Sun. Self-supervised learning of depth and camera motion from 360° videos. In *ACCV*, 2018.
237. Fu-En Wang, Yu-Hsuan Yeh, Min Sun, Wei-Chen Chiu, and Yi-Hsuan Tsai. Bifuse: Monocular 360 depth estimation via bi-projection fusion. In *CVPR*, 2020.
238. Fu-En Wang, Yu-Hsuan Yeh, Min Sun, Wei-Chen Chiu, and Yi-Hsuan Tsai. Led2-net: Monocular 360° layout estimation via differentiable depth rendering. *CVPR*, 2021.
239. Guangcong Wang, Yinuo Yang, Chen Change Loy, and Ziwei Liu. Stylelight: Hdr panorama generation for lighting estimation and editing. In *ECCV*, 2022.
240. Hai Wang, Xiaoyu Xiang, Yuchen Fan, and Jing-Hao Xue. Customizing 360-degree panoramas through text-to-image diffusion models. In *WACV*, 2024.
241. Haiyan Wang, Will Hutchcroft, Yuguang Li, Zhiqiang Wan, Ivaylo Boyadzhiev, Yingli Tian, and Sing Bing Kang. Psmnet: Position-aware stereo merging network for room layout estimation. In *CVPR*, 2022.
242. Jiong-Qi Wang, Ziyu Chen, Jun Ling, Rong Xie, and Li Song. 360-degree panorama generation from few unregistered nfov images. *ACM MM*, 2023.
243. Kuan-Hsun Wang and Shang-Hong Lai. Object detection in curved space for 360-degree camera. In *ICASSP*, 2019.
244. Ning-Hsu Wang, Bolivar Solarte, Yi-Hsuan Tsai, Wei-Chen Chiu, and Min Sun. 360sd-net: 360 stereo depth estimation with learnable cost volume. In *2020 IEEE International Conference on Robotics and Automation (ICRA)*, pages 582–588. IEEE, 2020.
245. Peng Wang, An Yang, Rui Men, Junyang Lin, Shuai Bai, Zhikang Li, Jianxin Ma, Chang Zhou, Jingren Zhou, and Hongxia Yang. Ofa: Unifying architectures, tasks, and modalities through a simple sequence-to-sequence learning framework. In *ICML*, 2022.
246. Qian Wang, Weiqi Li, Chong Mou, Xinhua Cheng, and Jian Zhang. 360dvd: Controllable panorama video generation with 360-degree video diffusion model. *ArXiv*, 2024.

247. Ze Wang, Kailun Yang, Haowen Shi, and Kaiwei Wang. Lf-vio: A visual-inertial-odometry framework for large field-of-view cameras with negative plane. *2022 IEEE/RSJ International Conference on Intelligent Robots and Systems (IROS)*, pages 4423–4430, 2022.
248. Changhee Won, Hochang Seok, Zhaopeng Cui, Marc Pollefeys, and Jongwoo Lim. Omnislam: Omnidirectional localization and dense mapping for wide-baseline multi-camera systems. *2020 IEEE International Conference on Robotics and Automation (ICRA)*, pages 559–566, 2020.
249. Chenglei Wu, Ruixiao Zhang, Zhi Wang, and Lifeng Sun. A spherical convolution approach for learning long term viewport prediction in 360 immersive video. In *AAAI*, 2020.
250. Tianhao Wu, Chuanxia Zheng, and Tat-Jen Cham. Panodiffusion: 360-degree panorama outpainting via diffusion. In *ICLR*, 2024.
251. Tianhe Wu, Shuwei Shi, Haoming Cai, Mingdeng Cao, Jing Xiao, Yinqiang Zheng, and Yujiu Yang. Assessor360: Multi-sequence network for blind omnidirectional image quality assessment. In *NIPS*, 2023.
252. Fei Xia, Amir R. Zamir, Zhiyang He, Alexander Sax, Jitendra Malik, and Silvio Savarese. Gibson Env: real-world perception for embodied agents. In *CVPR*, 2018.
253. Jianxiong Xiao, Krista A. Ehinger, Aude Oliva, and Antonio Torralba. Recognizing scene viewpoint using panoramic place representation. *CVPR*, 2012.
254. Shuang Xie, Po Kong Lai, Robert Laganieri, and Jochen Lang. Effective convolutional neural network layers in flow estimation for omnidirectional images. In *2019 International Conference on 3D Vision (3DV)*, pages 671–680. IEEE, 2019.
255. Weijian Xie, Guanyi Chu, Quanhao Qian, Yihao Yu, Shangjin Zhai, Danpeng Chen, Nan Wang, Hujun Bao, and Guofeng Zhang. Omnidirectional dense slam for back-to-back fisheye cameras. *2024 IEEE International Conference on Robotics and Automation (ICRA)*, pages 1653–1660, 2024.
256. Hang Xu, Xinyuan Liu, Qiang Zhao, Yike Ma, Chenggang Clarence Yan, and Feng Dai. Gaussian label distribution learning for spherical image object detection. *CVPR*, pages 1033–1042, 2023.
257. Hang Xu, Qiang Zhao, Yike Ma, Xiao-Di Li, Peng Yuan, Bailan Feng, Chenggang Clarence Yan, and Feng Dai. Pandora: A panoramic detection dataset for object with orientation. In *European Conference on Computer Vision*, 2022.
258. Jiahua Xu, Wei Zhou, and Zhibo Chen. Blind omnidirectional image quality assessment with viewport oriented graph convolutional networks. *IEEE TCSVT*, 2020.
259. Mai Xu, Lai Jiang, Chen Li, Zulin Wang, and Xiaoming Tao. Viewport-based cnn: A multi-task approach for assessing 360° video quality. *TPAMI*, 2020.
260. Mai Xu, Chen Li, Zhenzhong Chen, Zulin Wang, and Zhenyu Guan. Assessing visual quality of omnidirectional videos. *IEEE TCSVT*, 2019.
261. Mai Xu, Chen Li, Shanyi Zhang, and Patrick Le Callet. State-of-the-art in 360° video/image processing: Perception, assessment and compression. *IEEE J-STSP*, 2020.
262. Mai Xu, Yuhang Song, Jianyi Wang, MingLang Qiao, Liangyu Huo, and Zulin Wang. Predicting head movement in panoramic video: A deep reinforcement learning approach. *IEEE T-PAMI*, 2018.
263. Mai Xu, Yuhang Song, Jianyi Wang, Minglang Qiao, Liangyu Huo, and Zulin Wang. Predicting head movement in panoramic video: A deep reinforcement learning approach. *TPAMI*, 2019.
264. Mai Xu, Li Yang, Xiaoming Tao, Yiping Duan, and Zulin Wang. Saliency prediction on omnidirectional image with generative adversarial imitation learning. *IEEE TIP*, 2019.
265. Mai Xu, Li Yang, Xiaoming Tao, Yiping Duan, and Zulin Wang. Saliency prediction on omnidirectional image with generative adversarial imitation learning. *IEEE TIP*, 2021.
266. Mai Xu, Li Yang, Xiaoming Tao, Yiping Duan, and Zulin Wang. Saliency prediction on omnidirectional image with generative adversarial imitation learning. *IEEE TIP*, 2021.
267. Yanyu Xu, Yanbing Dong, Junru Wu, Zhengzhong Sun, Zhiru Shi, Jingyi Yu, and Shenghua Gao. Gaze prediction in dynamic 360° immersive videos. *CVPR*, 2018.
268. Ni Yan, Yupeng Mei, Ling Xu, Huihui Yu, Bo Sun, Zimao Wang, and Yingyi Chen. Deep learning on image stitching with multi-viewpoint images: A survey. *Neural Processing Letters*, 55:3863–3898, 2023.
269. Zhiqiang Yan, Xiang Li, Kun Wang, Shuo Chen, Jun Li, and Jian Yang. Distortion and uncertainty aware loss for panoramic depth completion. In *International Conference on Machine Learning*, pages 39099–39109. PMLR, 2023.
270. Zhiqiang Yan, Xiang Li, Kun Wang, Zhenyu Zhang, Jun Li, and Jian Yang. Multi-modal masked pre-training for monocular panoramic depth completion. In *European Conference on Computer Vision*, pages 378–395. Springer, 2022.
271. Kailun Yang, Xinxin Hu, Luis M Bergasa, Eduardo Romera, Xiao Huang, Dongming Sun, and Kaiwei Wang. Can we pass beyond the field of view? panoramic annular semantic segmentation for real-world surrounding perception. In *IV*, 2019.
272. Kailun Yang, Xinxin Hu, Luis Miguel Bergasa, Eduardo Romera, and Kaiwei Wang. Pass: Panoramic annular semantic segmentation. *IEEE TITS*, 2020.
273. Kailun Yang, Xinxin Hu, Hao Chen, Kaito Xiang, Kaiwei Wang, and Rainer Stiefelwagen. Ds-pass: Detail-sensitive panoramic annular semantic segmentation through swaff-net for surrounding sensing. *IV*, 2019.
274. Kailun Yang, Xinxin Hu, Yicheng Fang, Kaiwei Wang, and Rainer Stiefelwagen. Omnisupervised omnidirectional semantic segmentation. *IEEE TITS*, 2020.
275. Kailun Yang, Xinxin Hu, and Rainer Stiefelwagen. Is context-aware cnn ready for the surroundings? panoramic semantic segmentation in the wild. *IEEE TIP*, 2021.
276. Kailun Yang, Jiaming Zhang, Simon Reiß, Xinxin Hu, and Rainer Stiefelwagen. Capturing omni-range context for omnidirectional segmentation. *CVPR*, 2021.
277. Li Yang, Mai Xu, Xin Deng, and Bo Feng. Spatial attention-based non-reference perceptual quality prediction network for omnidirectional images. *ICME*, 2021.
278. Li Yang, Mai Xu, Tie Liu, Liangyu Huo, and Xinbo Gao. Tvformer: Trajectory-guided visual quality assessment on 360° images with transformers. *ACM MM*, 2022.
279. Qin Yang, Chenglin Li, Wenrui Dai, Junni Zou, Guo-Jun Qi, and Hongkai Xiong. Rotation equivariant graph convolutional network for spherical image classification. *CVPR*, 2020.
280. Shang-Ta Yang, Fu-En Wang, Chi-Han Peng, Peter Wonka, Min Sun, and Hung kuo Chu. Dula-net: A dual-projection network for estimating room layouts from a single rgb panorama. *CVPR*, 2019.
281. Shuai Yang, Liming Jiang, Ziwei Liu, and Chen Change Loy. Pastiche master: Exemplar-based high-resolution portrait style transfer. *CVPR*, 2022.
282. Wenyan Yang, Yanlin Qian, Joni-Kristian Kämäräinen, Francesco Cricri, and Lixin Fan. Object detection in equirectangular panorama. In *ICPR*, 2018.

283. Yi Yang, Miaoxin Pan, Di Tang, Tao Wang, Yufeng Yue, Tong Liu, and Mengyin Fu. Mcov-slam: A multicamera omnidirectional visual slam system. *IEEE/ASME Transactions on Mechatronics*, 29:3556–3567, 2024.
284. Yiwei Yang, Yucheng Zhu, Zhongpai Gao, and Guangtao Zhai. Salgfcn: Graph based fully convolutional network for panoramic saliency prediction. *VCIP*, 2021.
285. Abid Yaqoob, Ting Bi, and Gabriel-Miro Muntean. A survey on adaptive 360 video streaming: solutions, challenges and opportunities. *IEEE Commun. Surv. Tutor.*, 2020.
286. Youngho Yoon, Inchul Chung, Lin Wang, and Kuk-Jin Yoon. Spheresr. *CVPR*, 2022.
287. Dawen Yu and Shunping Ji. Grid based spherical cnn for object detection from panoramic images. *Sensors*, 2019.
288. Fanghua Yu, Xintao Wang, Mingdeng Cao, Gen Li, Ying Shan, and Chao Dong. Osrt: Omnidirectional image super-resolution with distortion-aware transformer. In *CVPR*, 2023.
289. Haozheng Yu, Lu He, Bing Jian, Weiwei Feng, and Shan Liu. Panelnet: Understanding 360 indoor environment via panel representation. In *CVPR*, 2023.
290. Jingrui Yu, Ana Pérez Grassi, and Gangolf Hirtz. Applications of deep learning for top-view omnidirectional imaging: A survey. *CVPR Workshop*, 2023.
291. Li Yu, Yanjun Gao, Farhad Pakdaman, and Moncef Gabouj. Panoramic image inpainting with gated convolution and contextual reconstruction loss. *ArXiv*, 2024.
292. Matt C. Yu, Haricharan Lakshman, and Bernd Girod. A framework to evaluate omnidirectional video coding schemes. *ISMAR*, 2015.
293. Mingze Yuan and Christian Richardt. 360 optical flow using tangent images. In *British Machine Vision Conference:(BMVC)*. Christian Richardt, 2021.
294. Ze yuan Wang, Kailun Yang, Hao miao Shi, Peng Li, Fei Gao, Jian Bai, and Kaiwei Wang. Lf-vislam: A slam framework for large field-of-view cameras with negative imaging plane on mobile agents. *IEEE Transactions on Automation Science and Engineering*, 21:6321–6335, 2022.
295. Il Dong Yun, Hyuk-Jae Lee, and Chae-Eun Rhee. Improving 360 monocular depth estimation via non-local dense prediction transformer and joint supervised and self-supervised learning. In *AAAI*, 2021.
296. Ilwi Yun, Chanyong Shin, Hyunku Lee, Hyuk-Jae Lee, and Chae Eun Rhee. Egformer: Equirectangular geometry-biased transformer for 360 depth estimation. In *ICCV*, 2023.
297. Vladyslav Zakharchenko, Kwang Pyo Choi, and Jeonghoon Park. Quality metric for spherical panoramic video. In *Optical Engineering + Applications*, 2016.
298. Fangneng Zhan, Yingchen Yu, Rongliang Wu, Changgong Zhang, Shijian Lu, Ling Shao, Feiying Ma, and Xuansong Xie. Gmlight: Lighting estimation via geometric distribution approximation. *IEEE TIP*, 2021.
299. Fangneng Zhan, Changgong Zhang, Yingchen Yu, Yuan Chang, Shijian Lu, Feiying Ma, and Xuansong Xie. Em-light: Lighting estimation via spherical distribution approximation. *ArXiv*, 2020.
300. Chao Zhang, Stephan Liwicki, Sen He, William H. B. Smith, and Roberto Cipolla. Hexnet: An orientation-aware deep learning framework for omni-directional input. *TPAMI*, 2023.
301. Chao Zhang, Stephan Liwicki, William Smith, and Roberto Cipolla. Orientation-aware semantic segmentation on icosahedron spheres. In *ICCV*, 2019.
302. Cheng Zhang, Zhaopeng Cui, Cai Chen, Shuaicheng Liu, Bing Zeng, Hujun Bao, and Yinda Zhang. Deeppanocontext: Panoramic 3d scene understanding with holistic scene context graph and relation-based optimization. *ICCV*, 2021.
303. Jiaming Zhang, Chaoxiang Ma, Kailun Yang, Alina Roitberg, Kunyu Peng, and Rainer Stiefelhagen. Transfer beyond the field of view: Dense panoramic semantic segmentation via unsupervised domain adaptation. *IEEE TITS*, 2021.
304. Jiaming Zhang, Kailun Yang, Chaoxiang Ma, Simon Reiß, Kunyu Peng, and Rainer Stiefelhagen. Bending reality: Distortion-aware transformers for adapting to panoramic semantic segmentation. *CVPR*, 2022.
305. Jiaming Zhang, Kailun Yang, Haowen Shi, Simon Reiß, Kunyu Peng, Chaoxiang Ma, Haodong Fu, Kaiwei Wang, and Rainer Stiefelhagen. Behind every domain there is a shift: Adapting distortion-aware vision transformers for panoramic semantic segmentation. *ArXiv*, 2022.
306. Jingxin Zhang. A 360° video-based robot platform for telepresent redirected walking. In *VAM-HRI*, 2018.
307. Jinsong Zhang, Kalyan Sunkavalli, Yannick Hold-Geoffroy, Sunil Hadap, Jonathan Eisenmann, and Jean-François Lalonde. All-weather deep outdoor lighting estimation. *CVPR*, pages 10150–10158, 2019.
308. Lvmin Zhang, Anyi Rao, and Maneesh Agrawala. Adding conditional control to text-to-image diffusion models. *ICCV*, 2023.
309. Pan Zhang, Bo Zhang, Ting Zhang, Dong Chen, Yong Wang, and Fang Wen. Prototypical pseudo label denoising and target structure learning for domain adaptive semantic segmentation. *CVPR*, 2021.
310. Weiming Zhang, Yexin Liu, Xu Zheng, and Lin Wang. Goodsam: Bridging domain and capacity gaps via segment anything model for distortion-aware panoramic semantic segmentation. In *2024 IEEE/CVF Conference on Computer Vision and Pattern Recognition (CVPR)*, pages 28264–28273, 2024.
311. Xinyu Zhang, Zhiwei Li, Yan Gong, Dafeng Jin, Jun Li, Li Wang, Yanzhang Zhu, and Huaping Liu. Openmpd: An open multimodal perception dataset for autonomous driving. *IEEE TVT*, 2022.
312. Yinda Zhang, Shuran Song, Ping Tan, and Jianxiang Xiao. Panocontext: A whole-room 3d context model for panoramic scene understanding. In *ECCV*, 2014.
313. Yuanxing Zhang, Pengyu Zhao, Kaigui Bian, Yunxin Liu, Lingyang Song, and Xiaoming Li. Drl360: 360-degree video streaming with deep reinforcement learning. *INFOCOM*, pages 1252–1260, 2019.
314. Yulun Zhang, Kungpeng Li, Kai Li, Lichen Wang, Bineng Zhong, and Yun Fu. Image super-resolution using very deep residual channel attention networks. In *Proceedings of the European conference on computer vision (ECCV)*, pages 286–301, 2018.
315. Yunjian Zhang, Yanwei Liu, Jinxia Liu, Jingbo Miao, Antonios Argyriou, Liming Wang, and Zhen Xu. 360-attack: Distortion-aware perturbations from perspective-views. In *CVPR*, 2022.
316. Yunjian Zhang, Yanwei Liu, Jinxia Liu, Pengwei Zhan, Liming Wang, and Zhen Xu. Sp attack: Single-perspective attack for generating adversarial omnidirectional images. In *ICASSP*, 2022.
317. Ziheng Zhang, Yanyu Xu, Jingyi Yu, and Shenghua Gao. Saliency detection in 360° videos. In *ECCV*, 2018.
318. Pengyu Zhao, Ansheng You, Yuanxing Zhang, Jiaying Liu, Kaigui Bian, and Yunhai Tong. Spherical criteria for fast and accurate 360 object detection. In *AAAI*, 2020.
319. Qiang Zhao, Bin Chen, Hang Xu, Yike Ma, Xiao-Di Li, Bailan Feng, Chenggang Clarence Yan, and Feng Dai.

- Unbiased iou for spherical image object detection. In *AAAI*, 2021.
320. Qiang Zhao, Wei Feng, Liang Wan, and Jiawan Zhang. Sphorb: A fast and robust binary feature on the sphere. *IJCV*, 113:143 – 159, 2014.
 321. Shengyu Zhao, Jonathan Cui, Yilun Sheng, Yue Dong, Xiao Liang, Eric I-Chao Chang, and Yan Xu. Large scale image completion via co-modulated generative adversarial networks. In *ICLR*, 2021.
 322. Jia Zheng, Junfei Zhang, Jing Li, Rui Tang, Shenghua Gao, and Zihan Zhou. Structured3d: A large photo-realistic dataset for structured 3d modeling. In *ECCV*, 2020.
 323. Xu Zheng, Pengyuan Zhou, Athanasios V Vasilakos, and Lin Wang. Semantics distortion and style matter: Towards source-free uda for panoramic segmentation. In *Proceedings of the IEEE/CVF Conference on Computer Vision and Pattern Recognition*, pages 27885–27895, 2024.
 324. Xu Zheng, Jinjing Zhu, Yexin Liu, Zidong Cao, Chong Fu, and Lin Wang. Both style and distortion matter: Dual-path unsupervised domain adaptation for panoramic semantic segmentation. In *CVPR*, 2023.
 325. Xueye Zheng, Tianbo Pan, Yuan Luo, and Lin Wang. Look at the neighbor: Distortion-aware unsupervised domain adaptation for panoramic semantic segmentation. *ICCV*, 2023.
 326. Bolei Zhou, Aditya Khosla, Àgata Lapedriza, Aude Oliva, and Antonio Torralba. Learning deep features for discriminative localization. *CVPR*, 2016.
 327. Wei Zhou, Jiahua Xu, Qiuping Jiang, and Zhibo Chen. No-reference quality assessment for 360-degree images by analysis of multifrequency information and local-global naturalness. *IEEE TCSVT*, 2021.
 328. Yu Zhou, Yanjing Sun, Leida Li, Ke Gu, and Yuming Fang. Omnidirectional image quality assessment by distortion discrimination assisted multi-stream network. *IEEE TCSVT*, 2022.
 329. Yufeng Zhou, Mei Yu, Hualin Ma, Hua Shao, and Gangyi Jiang. Weighted-to-spherically-uniform ssim objective quality evaluation for panoramic video. *ICSP*, 2018.
 330. Dandan Zhu, Yongqing Chen, Tian Han, Defang Zhao, Yucheng Zhu, Qiangqiang Zhou, Guangtao Zhai, and Xiaokang Yang. Ransp: Ranking attention network for saliency prediction on omnidirectional images. *ICME*, 2020.
 331. Dandan Zhu, Yongqing Chen, Defang Zhao, Xiongkuo Min, Qiangqiang Zhou, Shaobo Yu, Guangtao Zhai, and Xiaokang Yang. A lightweight saliency prediction model for omnidirectional images. *ICME*, 2021.
 332. Dandan Zhu, Kaiwei Zhang, Guokai Zhang, Qiangqiang Zhou, Xiongkuo Min, Guangtao Zhai, and Xiaokang Yang. Decoupled dynamic group equivariant filter for saliency prediction on omnidirectional image. *Neurocomputing*, 2022.
 333. Wenhao Zhu, Tianyu Wen, Guojie Song, Xiaojun Ma, and Liang Wang. Hierarchical transformer for scalable graph learning. *ArXiv*, 2023.
 334. Yongjie Zhu, Yinda Zhang, Si Li, and Boxin Shi. Spatially-varying outdoor lighting estimation from intrinsics. *CVPR*, 2021.
 335. Yucheng Zhu, Guangtao Zhai, Xiongkuo Min, and Jiantao Zhou. The prediction of saliency map for head and eye movements in 360 degree images. *TMM*, 2020.
 336. Yucheng Zhu, Guangtao Zhai, Yiwei Yang, Huiyu Duan, Xiongkuo Min, and Xiaokang Yang. Viewing behavior supported visual saliency predictor for 360 degree videos. *IEEE TCSVT*, 2021.
 337. Chuanqing Zhuang, Zhengda Lu, Yiqun Wang, Jun Xiao, and Ying Wang. Acdnet: Adaptively combined dilated convolution for monocular panorama depth estimation. In *AAAI*, 2022.
 338. Chuanqing Zhuang, Zhengda Lu, Yiqun Wang, Jun Xiao, and Ying Wang. Spdet: Edge-aware self-supervised panoramic depth estimation transformer with spherical geometry. *IEEE Transactions on Pattern Analysis and Machine Intelligence*, 45(10):12474–12489, 2023.
 339. Osama Zia, Jun-Ho Kim, Kyungjin Han, and Jong Weon Lee. 360 panorama generation using drone mounted fish-eye cameras. In *2019 IEEE International Conference on Consumer Electronics (ICCE)*, pages 1–3. IEEE, 2019.
 340. Michael Zink, Ramesh K. Sitaraman, and Klara Nahrstedt. Scalable 360° video stream delivery: Challenges, solutions, and opportunities. *Proceedings of the IEEE*, 2019.
 341. Nikolaos Zioulis, Federico Álvarez, Dimitrios Zarpalas, and Petros Daras. Single-shot cuboids: Geodesics-based end-to-end manhattan aligned layout estimation from spherical panoramas. *Image Vis. Comput.*, 2021.
 342. Nikolaos Zioulis, Antonis Karakottas, Dimitrios Zarpalas, Federico Alvarez, and Petros Daras. Spherical view synthesis for self-supervised 360 depth estimation. In *3DV*, 2019.
 343. Nikolaos Zioulis, Antonis Karakottas, Dimitrios Zarpalas, Federico Álvarez, and Petros Daras. Spherical view synthesis for self-supervised 360° depth estimation. *3DV*, 2019.
 344. Nikolaos Zioulis, Antonis Karakottas, Dimitrios Zarpalas, and Petros Daras. Omnidepth: Dense depth estimation for indoors spherical panoramas. In *ECCV*, 2018.
 345. Chuhang Zou, Alex Colburn, Qi Shan, and Derek Hoiem. Layoutnet: Reconstructing the 3d room layout from a single rgb image. *CVPR*, 2018.
 346. Chuhang Zou, Jheng-Wei Su, Chi-Han Peng, Alex Colburn, Qi Shan, Peter Wonka, Hung kuo Chu, and Derek Hoiem. Manhattan room layout reconstruction from a single 360° image: A comparative study of state-of-the-art methods. *IJCV*, 2021.